CHARACTERIZATION OF DISULFIDE CONSTRAINED NATURAL PEPTIDES

by

Mickelene F. Hoggard

A Dissertation Submitted to the Faculty of

The Charles E. Schmidt College of Science

In Partial Fulfillment of the Requirements for the Degree of

Doctor of Philosophy

Florida Atlantic University

Boca Raton, FL

May 2018

CHARACTERIZATION OF DISULFIDE CONSTRAINED NATURAL PEPTIDES

by

Mickelene F. Hoggard

This dissertation was prepared under the direction of the candidate's dissertation advisor, Dr. Mare Cudic, Department of Chemistry and Biochemistry, and has been approved by the members of her supervisory committee. It was submitted to the faculty of the Charles E. Schmidt College of Science and was accepted in partial fulfillment of the requirements for the degree of Doctor of Philosophy.

SUPERVISORY COMMITTEE:

Mare Cudic, Ph.D.
Dissertation Advisor

Frank Marí, Ph.D.

Tanja Godenschwege, Ph.D.

Lyndon West, Ph.D.

Gregg Fields, Ph.D.
Chair, Department of Chemistry and Biochemistry

Deguo Du, Ph.D.

Ata Sarajedini, Ph.D.
Dean, Charles E. Schmidt College of Science

Deborah L. Floyd, Ed.D.
Dean, Graduate College

March 27, 2018
Date

ACKNOWLEDGEMENTS

I would like to extend my extreme gratitude to Dr. Frank Marí for taking a chance on a graduate student who came to a snail lab wanting to work with plants. I grew as a scientist under his tutelage. He also provided me with amazing opportunities to explore other scientific fields and to interact with world-renowned scientists.

I am also incredibly grateful for Dr. Mare Cudic and the Department of Chemistry and Biochemistry for their patience and understanding during a time of uncertainty in my degree progress.

Thank you, Dr. Tanja Godenschwege for your time and guidance in all things *Drosophila*. Your expertise and acceptance allowed me to pursue an interdisciplinary project, for which, I am very thankful. I would also like to thank Dr. Deguo Du and Dr. Lyndon West for serving on my committee and for their advice and guidance throughout my project.

A special thank you goes out to all the people I met at FAU. Thank you for your support, for letting me vent to you, and for being my outlets during the stressful days.

Thank you to all of my family for your encouragement, patience, and support throughout this project. I love all of you!

Most importantly, I would like to thank my personal cheerleader and therapist, Kalyn, for always being my rock and for pepping me up when things got hard. You are the best, thanks for being in my corner!

ABSTRACT

Author: Mickelene F. Hoggard

Title: Characterization of Disulfide Constrained Natural Peptides

Institution: Florida Atlantic University

Dissertation Advisor: Dr. Mare Cudic

Degree: Doctor of Philosophy

Year: 2018

The use of peptide drugs has gained popularity recently. Peptides are attractive drug targets due to their high specificity and potency towards their biological targets. A drawback for peptide drugs is a lack of stability for oral delivery. Two classes of disulfide-rich peptides, conotoxins and cyclotides, have been shown to have higher stability than linear peptides thanks to their disulfide connectivity. Conotoxins are present in the venom of cone snails, a carnivorous marine mollusk that preys upon fish, worms, or other mollusks. Conotoxins are promising drugs leads with great prospects in the treatment of diseases and disorders such as chronic pain, multiple sclerosis and Parkinson's and Alzheimer's diseases. Cyclotides, which are cyclic cysteine knot containing peptides, isolated from the Violaceae (violet), Rubiaceae (coffee), and Cucurbitaceae (cucurbit) families and they have a wide range of biological activities, such as anti-HIV, uterotonic, and antimicrobial. P-superfamily framework IX conotoxins (C-C- C-CXC- C) contain the same cysteine framework, homologous sequences, and similar 3D structures to cyclotides.

The knot containing conotoxins have been identified in several *Conus* species, but this work focuses on those from *Conus brunneus, Conus purpurascens,* and *Conus gloriamaris.* The cysteine knot motif of cyclotides and P-superfamily conotoxins is characterized by a cyclic backbone and six-conserved cysteine residues that form the three-disulfide bridges of the "knot". This motif provides cyclotides and conotoxins with superior stability against thermal, chemical, and enzymatic degradation; marking them as potential frameworks for peptide drug delivery. Presented are details on the isolation of conotoxins and cyclotides, from *Viola tricolor*, and the characterization of their activity in the well-characterized *Drosophila melanogaster* giant fiber system (GFS) neuronal circuit, which contains GAP, acetylcholine, and glutamate synapses.

The transcriptomes of two *Conus brunneus* specimens were assembled and mined for P-superfamily framework IX conotoxins. Eleven mature P-superfamily framework IX conotoxins were identified in the crude venom.

CHARACTERIZATION OF DISULFIDE CONSTRAINED NATURAL PEPTIDES

List of Figures xii

List of Tables xiv

Chapter 1: Background and significance 1

1.1 Cone snails and their venom 1

1.2 Cyclotides 3

1.3 Peptides as drugs 4

1.4 Drosophila GFS 6

1.5 Cone snail venomics 8

Chapter 2: Evaluation of P-superfamily conotoxins of *Conus brunneus* for neuronal activity in *Drosphila melanogaster* 11

2.1 Introduction 11

2.2 Materials and Methods 13

2.2.1 Specimen collection 13

2.2.2 Dissected venom extraction 14

2.2.3 Extract purification and conotoxin isolation 14

2.2.4 Identification and quantification of conotoxins 15

2.2.5 Fly stocks 15

2.2.6 *Drosophila* GFS bioassay 16

2.3 Results 16

2.3.1 Size exclusion chromatography 16

2.3.2 Isolation and identification of bru9b 17
2.3.3 Isolation and identification of bru9a 20
2.3.4 *In vivo Drosophila* GFS bioassay 21
2.4 Discussion 22
Chapter 3: Evaluation of cyclic peptides from *Viola tricolor* neuronal activity in *Drosophila melanogaster* 24
3.1 Introduction 24
3.2 Materials and Methods 26
3.2.1 Specimen Collection 26
3.2.2 Cyclotide Extraction 26
3.2.3 Extract fractionation and cyclotide isolation 26
3.2.4 Identification and quantification of cyclotides 27
3.2.5 Fly stocks 28
3.2.6 Establishing a DMSO control 28
3.2.7 *Drosophila* GFS bioassay 28
3.3 Results 29
3.3.1 Extraction of cyclotides from *V. tricolor* 29
3.3.2 Isolation of cyclotides from crude extract 29
3.3.3 *In vivo D. melanogaster* GFS assay 30
3.4 Discussion 32
Chapter 4: Evaluation of the neuronal activity of a *Conus gloriamaris* P-superfamily conotoxin in *Drosophila melanogaster* 34
4.1 Introduction 34

4.2 Materials and Methods 36
4.2.1 Peptide synthesis 36
4.2.2 Quantification 36
4.2.3 Fly stocks 36
4.2.4 *D. melanogaster* GFS bioassay 36
4.2.5 *In vivo* patch clamping 37
4.3 Results 38
4.3.1 Quantification 38
4.3.2 *In vivo D. melanogaster* GFS assay 38
4.3.3 *In vivo* patch clamp of GF neuron 40
4.4 Discussion 42
Chapter 5: Evaluating α-conotoxins in the *Drosophila melanogaster* GFS 44
5.1 Introduction 44
5.2 Materials and Methods 46
5.2.1 Conotoxin extraction 46
5.2.2 Isolation of conotoxins by RP-HPLC 46
5.2.3 *In vivo* electrophysiology in the *D. melanogaster* GFS 48
5.2.4 *In vitro* electrophysiology in *Xenopus oocytes* expressing nAChRs 49
5.2.5 Homology modeling of PIA and PIC bound to the Dα7 nAChR 50
5.2.6 Transcriptome of the *C. purpurascens* venom duct 50
5.3 Results 51
5.3.1 Isolation and sequencing of PIA, PIC, and PIC[O7] 51

5.3.2 In vitro electrophysiology activity of PIC and PIC[O7] in the *D. melanogaster* GFS 51
5.3.3 In vitro electrophysiology activity of PIC and PIC[O7] at the heterologously expressed nAChRs in Xenopus oocytes 53
5.3.4 Molecular interaction of PIA and PIC with Dα7 nAChR 54
5.4 Discussion 56
Chapter 6: Interrogation of two *Conus brunneus* transcriptomes for P-superfamily conotoxins 60
6.1 Introduction 60
6.2 Materials and Methods 62
6.2.1 Specimen collection 62
6.2.2 RNA preparation and sequencing 62
6.2.3 Mining the transcriptome 63
6.2.4 Dissected venom extraction 66
6.2.5 Size-exclusion HPLC of the dissected venom 66
6.2.6 Reduction/alkylation and trypsin digest of fractions 66
6.2.7 Identification of P-superfamily conotoxins using high-resolution mass spectrometry 67
6.3 Results 68
6.3.1 RNA preparation and sequencing 68
6.3.2 Mining the transcriptome 68
6.3.3 Size-exclusion HPLC of crude venom 72
6.3.4 LC-MS/MS of size exclusion fractions 73

6.3.5 Identification of P-superfamily conotoxins in the crude venom 74

6.4 Discussion 75

Chapter 7: Conclusions 77

References 83

LIST OF FIGURES

Figure 1. The cyclotide cyclic cysteine knot 3

Figure 2. Model of the aligned backbone of a conotoxin and cyclotide. 6

Figure 3. Neuronal schematic of the *Drosophila* giant fiber system 8

Figure 4. Size-exclusion HPLC of *C. brunneus* crude venom extract 17

Figure 5. Semi-preparative HPLC separation and mass spectrometry of bru9b 18

Figure 6. Analytical HPLC separation and mass spectrometry of bru9b 19

Figure 7. Semi-preparative RP-HPLC separation of bru9a 20

Figure 8. Analytical HPLC purification and mass spectra of bru9a 21

Figure 9. Effects of bru9a and bru9b on the *D. melanogaster* GFS 22

Figure 10. Cyclotide backbone structure showing the disulfide connectivity 25

Figure 11. Semi-preparative and analytical HPLC isolations of cyclotides 30

Figure 12. Effects of isolated cyclotides on the *Drosophila* GFS 31

Figure 13. Targeted DLM recording injection site and the effects of isolated cyclotides on the DLM 32

Figure 14. Shell of cone snail *Conus gloriamaris* 34

Figure 15. *In vivo* patch clamp mount 38

Figure 16. Effect of 220pmol of gm9a on the GFS 39

Figure 17. Effects of gm9a on the DLM with the targeted experiment 40

Figure 18. Current clamp steps of giant fiber 41

Figure 19. Percent changes of membrane input resistance. 42

Figure 20. *D. melanogaster* giant fiber system 45

Figure 21. RP-HPLC isolation of PIA, PIC, and PIC[O7] from injected venom of *C. purpurascens* 47

Figure 22. PIC precursor protein from transcriptome. 51

Figure 23. Functional characterization of PIA, PIC, and PIC[O7] in the GFS 53

Figure 24. Activity of PIC and PIC[O7] at rodent and human nAChR subtypes 54

Figure 25. PIA and PIC modeled binding to the Dα7 nAChR 56

Figure 26. Structure of a conotoxin precursor protein 61

Figure 27. Size-exclusion HPLC of crude *C. brunneus* venom 73

Figure 28. LC-MS/MS chromatograms of the SE-HPLC peptide fractions of *C. brunneus.* 74

LIST OF TABLES

Table 1. Conotoxin neuropharmacological classification..... 12

Table 2. Isolated P-superfamily conotoxins of *C. brunneus*..... 13

Table 3. Aligned sequences of cyclotides isolated from *V. tricolor*..... 29

Table 4. Properties of gm9a. 36

Table 5. Sequences and nAChR selectivity of *C. purpurascens* α-conotoxins 48

Table 6. P-superfamily conotoxins on Conoserver..... 65

Table 7. P-superfamily precursor protein sequence mined from the transcriptomes 70

Table 8. Mature conotoxin sequences of the P-superfamily precursor proteins..... 71

Table 9. Signal sequence homology among the P-superfamily precursor proteins..... 72

Table 10. LC-MS/MS results for reduced and alkylated peptide fractions 74

Table 11. Confirmed P-superfamily conotoxins present in *C. brunneus* venom..... 75

CHAPTER 1: BACKGROUND AND SIGNIFICANCE

1.1 Cone snails and their venom

Cone snails are venomous marine mollusks of the genus *Conus* that are categorized into subgroups based upon their diet, hunting either fish (piscivorous), worms (vermivorous), or other mollusks (molluscivorous). There are more than 750 species of cone snails producing more than 5,500 components in the injected venom, and only a fraction of those components have been characterized [1, 2]. The disparity of the functional characterization of conotoxins is due, in part, to the limited quantities occurring in the venom, making it difficult to isolate enough native peptide to evaluate their neuropharmacological activity. This work focuses, primarily on, the venom of the Eastern Pacific cone snail, *Conus brunneus*, but also on *Conus purpurascens* and *Conus gloriamaris*.

Cone snails utilize their venom for predation and defense and it is composed of proteins, peptides, and small molecules. The venom is produce within their venom gland and along the venom duct. The snails employ either the “hook and line” or the “net engulfment” methods of prey-capture [3]. The hook and line strategy is implemented when the snail physically injects its venom into the prey, rapidly immobilizing it, and then pulls the prey into its mouth. The net engulfment strategy is different because the venom is not directly injected into the prey, but ejaculated towards the prey, sedating it, and allowing the snail to open its mouth to engulf the prey.

The venom peptides are of particular research interest. They can be classified into either non-cysteine-rich (≤ 2 cysteine residues) conopeptides and cysteine rich (> 2 cysteine residues) conotoxins based on their primary amino acid sequence [4]. The venom has a diverse range of molecular targets, from ion channels (Na^+, Ca^{2+}, K^+), to receptors (nAChR, GABA, NMDA), to transporters.

The general structure of a conotoxin precursor proteins translated from mRNA is the signal sequence, a pre-peptide region, the mature peptide, and sometimes a post-peptide region. The signal sequence is at the N-terminus of the precursor and contains mostly hydrophobic amino acids that serve as a "signal" for transport [5]. The pre and post peptide regions are thought to aid in mature peptide folding and are cleaved off leaving the properly folded mature peptide [6].

Conotoxins are categorized through a hierarchy of classifications. First into one of 27 gene superfamilies based upon their signal sequences. The cysteine connectivity further classifies the mature conotoxins into one of 26 cysteine frameworks. Lastly, the conotoxins are categorized by their pharmacological activity. To date, there have been 12 pharmacological families identified [7].

A synthetic peptide modeled after ω-conotoxin, MVIIA isolated from the venom of *Conus magus* has been FDA approved for the treatment of chronic pain, Ziconotide. Ziconotide is attractive as an analgesic due to its unique mechanism of action. The peptide is an antagonist against N-type calcium channels present in the nervous system [8-10]. Binding of the peptide causes a reduction of neurotransmitters released in part of the pain transmission pathway. Since the peptide targets ion channels and not an opioid receptor, the risk of developing a tolerance is decreased [11].

1.2 Cyclotides

During a Red Cross relief project to Republic of Congo in 1960, a Norwegian anesthesiologist, Lorents Gran, noticed pregnant women utilizing a native plant, *Oldenlandia affinis*, to make a tea to be drunk during childbirth. In 1973, Gran discovered that the active component in the tea was a cyclic peptide, Kalata B1, which induced uterine contractions [12, 13]. These peptides have since been classified as "cyclotides", disulfide-rich head-to-tail cyclic peptides. Cyclotides have been found in the *Rubiaceae, Cucurbitaceae, Fabaceae, Solanaceae, Apocynaceae*, and every studied species in the *Violaceae* families [14]. The primary structure of the peptides consists of ~30 amino acids, six of those being cysteines that form three stabilizing disulfide bonds. The three disulfide bonds create a cyclic cysteine knot (CCK) motif that makes the peptide stable to proteolytic degradation [15] (Figure 1).

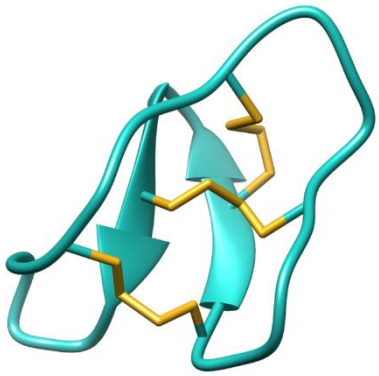

Figure 1. The cyclotide cyclic cysteine knot. Head-to-tail cyclized peptide backbone (teal) with disulfide bonds (yellow) demonstrating the knot.

The current thought is that the plants are producing these peptides as a defense against pest and pathogens [16]. Cyclotides are biosynthesized from ribosomally produced precursor proteins [17]. The precursor protein contains a signal sequence that directs them to the endoplasmic reticulum for processing. The exact mechanism of cyclization is not yet

understood, but is thought to occur after the formation of the disulfide bonds. Cyclotides are produced in all tissues of the plant (roots, stems, leaves, flowers) and some species can produce well over 100 different cyclotides [18]. It has been estimated that over 100,000 unique cyclotides exist in nature [19]. Cyclotides have been shown to stunt larval growth and therefore preventing the breeding of future generations of the insect [20].

Cyclotides have a distinct hydrophobic patch of amino acids in their primary structure, which is thought to be responsible for their biological activity. The hydrophobic patch aids in the peptide's ability to insert into and disrupt cell membranes [21, 22]. There are currently 314 cyclotide entries on the CyBase (cybase.org.au) database and none have been evaluated in an *in vivo* neurological assay before [23, 24].

1.3 Peptides as drugs

In recent years, peptides have gained prominence as natural product drug design and delivery due to their selectivity and potency towards their targets [25-27]. Peptides have multiple roles endogenously in humans. They can act as neurotransmitters, hormones, ion channel modulators, growth factors, or as defense against foreign invaders. In 2016 peptide therapeutics were valued at $21.5 billion globally [28]. Peptides are often more potent than small molecules that act upon the same receptors. There have been 68 approved therapeutic peptides and are currently 155 in clinical development, 25 of those have achieved Phase III clinical trial status [29]. One drawback of peptide-drugs is their limited bioavailability due to their quick degradation by proteases, but the market is projected to increase in value to $48.04 billion by 2025 due to the growing demand for rapid and efficient treatments for cancer, pathogenic diseases, metabolic disorders, and heart disease [28, 29].

There are currently six FDA approved medication derived from venoms for the treatment of hypertension, pain, stroke, and diabetes [30]. One of these is the cone snail venom derived mentioned previously. Conotoxins are intriguing due to their disulfide constrained tertiary structure and their potent and specific binding to membrane receptors and ion channels [31]. These characteristics make conotoxins attractive as neuronal probes and drug candidates. Several conotoxins contain the cysteine knot motif; two disulfide bonds create a ring in the peptides structure and a third disulfide bond is threaded through between the peptide backbone created by the first two. The conotoxins bru9a and bru9b of *Conus brunneus* and gm9a of *Conus gloriamaris* are framework IX conotoxins with the cysteine connectivity of Cys(I-IV), Cys(II-V), and Cys(III-VI) [32].

Some of the same characteristics that make conotoxins such attractive leads are also found in cyclotides. Cyclotides also have the disulfide constrained tertiary structure that stabilizes them but also the head-to-tail cyclization that adds further stability to proteolytic and thermal degradation. In fact, some conotoxins and Cyclotides have quite similar three-dimensional structures (Figure 2). Cyclotides have also been shown to be tolerant to modification and grafting of active peptide sequences into their stable backbone [25, 33, 34]. Previously in the Marí lab, it has been shown that cyclizing conotoxins to make them look more like cyclotides increases their stability and has no effect on their potency towards their target [35].

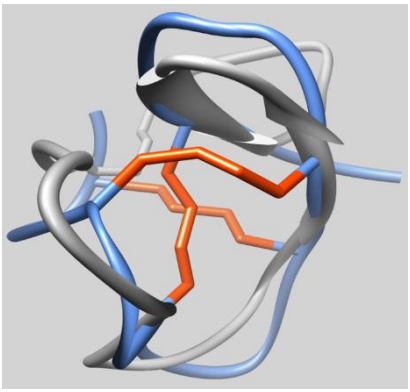

Figure 2. Model of the aligned backbone of a conotoxin and cyclotide. Conotoxin bru9a (blue) backbone structure stacked on top of the quintessential cyclotide kalata B1. The backbones of the two peptides are spatially similar to one another.

1.4 Drosophila GFS

The fruit fly, *Drosophila melanogaster,* is considered a model organism especially in the field of neuroscience thanks to its well-defined genome, easy maintenance, and small size. It was the first sequenced genome of a complex organism [36]. Fruit flies are genetically suited for modeling human diseases. Seventy-five percent of all human disease-related genes have *Drosophila* homologues [37, 38]. There is also verily high homology between human and fly proteins, especially in ligand binding regions. The fly is superior to other models organisms like *C. elegans*, because the worm has poorer gene homology and is missing key physiological aspects that the fly and humans contain. Since the genome of the fruit fly has been so well studied, creating genetic mutants has become easier. Flies are easy to maintain and propagate. They require little maintenance other than food source renewal, and a mating pair can rapidly reproduce hundreds of genetically identical progeny in just 10 days.

The fly is well suited for *in vivo* experimentation and has several delivery methods available for experimental design. The fly's robust system allows compounds to be administrated as vapor, food, dropped onto an exposed nerve, injected directly into a nerve

cord, or injected into the head or abdomen where the compound quickly diffuses throughout the fly's hemolymph [39-43].

It is a good system to model the effects of various disease states. It has been used as a model for Alzheimer's disease [44], Parkinson's disease [45], Huntington's disease [46], learning and memory [47, 48], and various psychiatric disorders of the central nervous system [49]. Flies are valuable for evaluated neurological disorders since they possess several of the same neurotransmitters found in humans, such as glutamate, dopamine, acetylcholine, GABA, and serotonin.

The *D. melanogaster* giant fiber system (GFS) is composed of four neurons terminating on two muscles, the tergo trochanteral muscle (TTM) and the dorsal longitudinal muscle (DLM), mediating the fly's jump and flight responses, respectively. The GFS contains various types of synapses between the four neurons and two muscles. The Giant Fiber (GF) branches and terminates to both muscle pathways. The DLM pathway has a gap junction between the GF and the peripherally synapsing interneuron (PSI) that has a α7 nicotinic acetylcholine receptor (nAChR) dependent synapse to the dorsal longitudinal motor neuron (DLMn) which has a glutamate synapse to the DLM. The TTM pathway has a mixed electrical (GAP) and chemical (α7 nAChR) synapse between the GF and the tergo trochanteral motor neuron (TTMn) which synapses with the TTM via a glutamate synapse (Figure 3) [50]. There are also several types of ion channels present in the fly's nervous system including, voltage-gated calcium and sodium, ligand-gated calcium, potassium, and chloride channels.

Figure 3. Neuronal schematic of the Drosophila giant fiber system. The giant fiber system is responsible for the fly's escape response showing the variation in the types of synapses in the circuit and between the two muscles.

Due to the limited expression of the peptides in the venom, an assay that requires minimal peptide would be ideal. *D. melanogaster* requires small amounts of compound to elicit a response, making it an advantageous model organism to evaluate conotoxins. One such assay includes the neuronal pathway responsible for the fly's escape response, the GFS [51], and allows for the simultaneous stimulation and recording of responses during injection of conotoxin [43, 50, 52]. This assay takes advantage of the fly's small size and well-defined neuronal escape response. It is a good starting point to get a general target for novel components and it is an excellent assay for evaluating nAChR activity since only one of the muscle pathways contains a synapse solely dependent upon nAChRs.

1.5 Cone snail venomics

There are two different approaches to peptide and protein sequencing through mass spectrometry, top-down and bottom-up [53]. Top-down relies on the mass spectrometer to fragment the native peptide or protein for fragmentation. The bottom-up technique uses chemical reactions to disrupt the sequence into more manageable smaller fragments.

Bottom-up often chemically reduces the disulfide bonds then blocks them from reforming then, depending on the method, those now linear peptides are enzymatically digested. Both of these methods are limited by the resolution of the mass spectrometer used to obtain the fragmentation used for sequencing. The top-down method can be further constrained by the dynamic range of the native sample where the bottom-up approach normalizes the sample to smaller and more similar in size fragments.

Recent advances in liquid-chromatography coupled with tandem mass spectrometry (LC-MS/MS) and next-generation sequencing have allowed the venom-studies community to dig deeper into the composition of venoms. The once a laborious task to sequence peptides and proteins has become easier with the use of RNA-seq, a high-throughput DNA sequencing from RNA method, and transcriptomic databases. The transcriptome represents all transcripts present in a tissue, including low components in low abundance. RNA-seq is ideal for non-model organisms without a solved genome, and since there is, currently, not a decent cone snail genome the primary database currently in use for cone snail venomics is species-specific transcriptomes in addition to the publically available NCBI and UniProt venoms databases or the Conoserver database [54]. The venom transcriptome of a cone snail is made by extracting the mRNA that is present in the venom gland and reverse transcribing it into cDNA and then sequencing the cDNA [55]. Using the transcriptomes, genomes, and proteomes of a venomous species to study their venom is an emerging field called venomics [56]. These complimentary fields are helping to push the field of venom studies forward.

The transcriptome can be used as a searchable database when paired with a data matching program that takes the parent ion fragmentation spectra and matches it to the sequences of

the database. An advantage of these data matching programs is that they are able to account for posttranslational modifications (PTMs). Since PTMs are added after the peptide has been translated from RNA, the transcriptome will not account for them. Conotoxins have been reported to have as many as 75% of their amino acid sequence post-translationally modified [57]. The most common conotoxin PTMs are disulfide bonds, C-terminal amidation, N-terminal pyroglutamylation, hydroxylation of Pro, carboxylation of Glu, and bromination [58]. The data matching programs take the mass changes of these modifications into account when matching the spectra with the sequence.

This work utilized the model system of *D. melanogaster* to characterize the biological activity of conotoxins and cyclotides. Two new α-conotoxins were found to have selectivity towards neuromuscular subtypes of nAChRs. A P-superfamily conotoxin of *Conus gloriamaris* was found to increase membrane resistance. Two other P-superfamily conotoxins from *Conus brunneus* did not have activity in the *D. melanogaster* GFS. Two transcriptomes for *C. brunneus* were sequenced and assembled and used to find 37 new possible P-superfamily members. The transcriptomes were also used as a database to match LC-MS/MS spectra from the crude venom of *C. brunneus.* Nine new P-superfamily conotoxins were identified in the crude venom.

CHAPTER 2: EVALUATION OF P-SUPERFAMILY CONOTOXINS OF *CONUS BRUNNEUS* FOR NEURONAL ACTIVITY IN *DROSPHILA MELANOGASTER*

2.1 Introduction

Conotoxins are first categorized into superfamilies based on their gene signal sequence, then by their cysteine arrangement or their cysteine framework and finally into families by pharmacological activity [54].

There are currently 12 P-superfamily conotoxins on the Conoserver database from *C. gloriamaris, C. imperialis, C. litteratus, C. pulicarius, C. regius, C. textile,* and *C. victoriae*. The signal sequence varies among the 12 P-superfamily conotoxins, but has the general sequence of MHXXLXXSAVLILXLLXAXXNFXVVQS, where "X" is for a none conserved amino acid [7]. Of the 12 P-superfamily conotoxins on Conoserver, only one does not have the framework IX cysteine arrangement, Vc14.5 that is a member of framework 14. Framework IX conotoxins contain six cysteines with a varying number of amino acids between the cysteines. The typical cysteine connectivity of framework IX conotoxins is Cys (I-IV, II-V, III-VI) [59]. Not only has the pharmacological target of P-superfamily conotoxins not been identified, but the cysteine framework IX has also not been associated with an activity (

Table 1).

Family	Target	Gene Superfamilies	Cysteine Frameworks
α	Nicotinic acetylcholine receptors (nAChRs) [4]	A, D, L, M, S	I, II, III, IV, VI/VII, VII, XIV, XX,
γ	Neuronal pacemaker cation currents [60]	O1, O2	VI/VII, XII, XV
δ	Inhibition of fast inactivation voltage-gated Na^+ channels [61]	O1	VI/VII, XII
ε	Presynaptic Ca^{2+} channels [62]	T	V, X
ι	Na^+ channels by shifting the voltage dependence of activation [63]	I1, M	II, III, IV, VI/VII, XI, XVI
κ	Voltage-gated K^+ channel blocker[64]	A, I2, J, M, O1	I, II, III, IV, VI/VII, XI, XII, XIV,
μ	block Na^+ channels by inhibiting ion flow through the channel [65]	M, O1, T	II, III, IV, V, VI/VII, X, XII, XVI
ρ	Inhibits α1-adrenoceptor (GPCR) [66]	A	I, II, IV, XIV
σ	Serotonin-gated ion channels (5-HT3) [67]	S	VII
τ	Somatostatin receptor blocker [68]	T	V
χ	Noradrenaline transporter [66]	T	V, X
ω	Voltage-gated Ca^{2+} channel blocker [8]	O1	VI/VII, XII

Table 1. Conotoxin neuropharmacological classification. Conotoxins are categorized by their gene superfamilies, then their cysteine frameworks, then finally by their pharmacological activity. This table highlights that a single pharmacological activity can be coded by several different gene superfamilies and have varying cysteine frameworks.

Previously, two framework IX conotoxins have been isolated and sequenced using Edman degradation by previous members of the Marí lab, bru9a [69] and bru9b [70] (

Table 2). bru9a is of particular interest because it is one of the most abundant peptides in the crude venom of *C. brunneus*.

Previously in the Marí lab, an *in vivo* assay was developed to screen conotoxins [43, 52]. The assay utilizes the giant fiber system (GFS) of the *Drosophila melanogaster*. The GFS is the well-characterized neuronal circuit responsible for the jump and flight muscles of the fly's escape response. The GFS consists of four neurons that terminate on

two muscles, the Dorsal Longitudinal muscle (DLM) and the Tergo Trochanteral muscle (TTM). There are three different types of synapses within the GFS, gap junction, nicotinic-acetylcholine receptor, and glutamate. The biological target of a conotoxin can be narrowed down by the effect seen in the electrophysiological recordings.

Conotoxin	Sequence	Monoisotopic Mass Experimental (Da)	Calculated Molar Extinction Coefficient (M^{-1}, cm^{-1})
bru9a	------SCGGS-CFGG--CWOG--CSCYART--CFRD	2531.865	7365
bru9b	SLDKGSNCGQD-CSSDN-COSG--CFCYPRDNVCYVERRKN	4128.634	3355

Table 2. Isolated P-superfamily conotoxins of C. brunneus. Previously identified P-superfamily conotoxins. The molar extinction coefficients were calculated using the Expasy ProtParam tool [71]. The cysteines (red) are aligned to show the framework IX cysteine arrangement.

P-superfamily conotoxins are a class of conotoxins that have not yet had their biological activity assigned. A majority of P-superfamily conotoxins are also framework IX conotoxins with the cysteine arrangement of C-C-C-CXC-C. Of the two P-superfamily conotoxins previously discovered in the Marí lab, bru9a has been evaluated in several biological assays [69], but a definitive target has yet to be identified. This work is the first known evaluation of conotoxin bru9b for biological activity. Conotoxins bru9a and bru9b were isolated from crude venom and evaluated in the *D. melanogaster* giant fiber system *in vivo* assay, which combines simultaneously injecting conotoxin while recording electrorheological recordings.

2.2 Materials and Methods

2.2.1 Specimen collection

Conus brunneus snails were collected from the Pacific coast of Costa Rica and transported alive to Florida Atlantic University. Upon arrival at the lab, the animals were sacrificed and their venom ducts dissected and stored at -80°C for later use.

2.2.2 Dissected venom extraction

The dissected and frozen venom ducts from *C. brunneus* were homogenized with a tissue disrupter in 0.1% trifluoroacetic acid in water on ice. The duct tissue extract was centrifuged at 10,000 rpm at 4°C for 20 minutes to form a tissue pellet. The supernatant was removed and saved. The pellet was washed and re-centrifuged multiple times using the same conditions. The crude extract supernatants were pooled together and lyophilized then stored at -80°C until needed.

2.2.3 Extract purification and conotoxin isolation

Dried crude venom extract was reconstituted in 0.1M ammonium bicarbonate (NH_4HCO_3) (~50mg/5mL) and separated via size-exclusion high-performance liquid chromatography (SE-HPLC) on a Pharmacia Superdex 30 column (2.5cmx100cm) with 0.1M NH_4HCO_3 at 1.5mL/min. Chromatographic fractions were UV-detection monitored at λ= 220 and 280 nm and collected manually over 300 min.

From the SE-HPLC the fraction containing the desired peptides was selected for further fractionation by reverse phase-HPLC (RP-HPLC) on a C18 semi-preparative column (Vydac, 218EV510, 10 x 250 mm; 5 µm particle diameter; 300 Å pore size) equipped with a C18 guard column (Upchurch Scientific, AC-43 4.6 mm) at a flow rate of 3.5 mL/min. The fractions identified as containing the desired peptides were pooled and

further fractionated by analytical RP-HPLC on a Kinetex C8 column (4.6 mm x 50 mm; 2.6 μm particle diameter; 100 Å pore size, Phenomenex, Torrance, CA, USA) at a flow rate of 1 mL/min. All RP-HPLC methods were performed using a linear gradient over 100 min of 100% solution A (0.1% TFA in water) to 100% solution B (0.1% TFA in 60% acetonitrile in water) by a Series 200 LC pump (Perkin Elmer, Waltham, MA, USA). All fractions were collected manually under UV detection at λ= 220 and 280 nm by a SpectroMonitor 5000 Photodiode Array Detector (LDC Inc., Carlsbad, CA, USA). All fractions were lyophilized and stored at -20°C until needed.

2.2.4 Identification and quantification of conotoxins

The fractions were identified by their molecular mass using positive ion matrix assisted laser desorption ionization time-of-flight mass spectrometry (MALDI-TOF MS). The spectra were collected with an Applied Biosystems Voyager-DE PRO mass spectrometer (Framingham, MA, USA) in both linear and reflector modes. Regular calibrations were done using Applied Biosystems/MDS Mass Standards Kits (Calmix 1 and 2) as external calibration standards with a mass tolerance better than 10 ppm. Dry HPLC fractions were reconstituted in 0.1% TFA, 60% acetonitrile and spotted onto an Applied Biosystems 384-well magnetic insert plate with α-cyano-4-hydroxycinnamic acid (CHCA, 20-25 mg/mL in water/acetonitrile/methanol 15:31:54, ACROS Organics, NJ, USA) matrix. A modified two spot method was used where first the matrix was spotted and allowed to dry completely before the sample solution was spotted on top of the matrix. Matrix-fraction spots were allowed to dry before analysis in the 800-5,000 Da range.

Isolated conotoxins were quantified using Beer's Law and the absorbance at λ = 280nm with a BioTek Epoch Microplate Spectrophotometer and the Gen5 Microplate Data Analysis Software. The calculated molar extinction coefficient (

Table 2) was used in calculating the peptide quantities.

2.2.5 Fly stocks

Wild type (w^{118}) flies were obtained from the Bloomington Stock Center (Stock 2 6326) and were kept at room temperature in vials containing standard media. The stocks were transferred to fresh media on a weekly basis and 1-6 day old male flies were selected for the assays.

2.2.6 Drosophila GFS bioassay

The paired electrophysiology-nanoinjection bioassays were performed using the methods first described by [43, 52]. Male flies less than one week old were mounted in dental wax dorsal side up to immobilize the legs and wings. A sharpened tungsten electrode was placed into each eye to deliver the stimulation pulse to the GFS circuit. A tungsten ground electrode was placed into the abdomen of the fly. One sharpened glass electrode back filled with 0.7% NaCl solution was placed into either the DLM or TTM muscle. A baseline recording of the muscle response prior to compound injected was done with 10 trains of 10 stimuli at 100 Hz [50, 72]. Flies whose muscles did not follow >95% at this stimulation were not considered to be wild type and were discarded. The O'Dowds saline control solution (101 mM NaCl, 1 mM $CaCl_2$, 4 mM $MgCl_2$, 3 mM KCl, 5 mM Glucose, 1.25 mM NaH_2PO_4, 20.7 mM $NaHCO_3$, pH=7.2) was designed to mimic the hemolymph of the fly and therefore, should not affect neuronal firing [73]. Flies with wild type muscle response were then injected with either compound or control solution while simultaneously

stimulating and recording muscle responses to a 1 Hz stimulation for up to one minute after injection. Then the GF pathways were monitored every 5 minutes for 20 minutes with 10 trains of 10 stimuli at 100 Hz. An n=10 was used for each data point.

2.3 Results

2.3.1 Size exclusion chromatography

The crude venom extract was first separated by SE-HPLC. The peak with the highest λ = 280nm absorbance is known as the "peptide peak" and is the peak in which most of the conotoxins are found. The peak labeled peak 5 is the SE-HPLC peak that was selected for further chromatographic analysis to purify bru9b (Figure 4). The peptide peak is labeled as peak 6 this is the peak that was selected for further chromatographic analysis to purify bru9a (Figure 4).

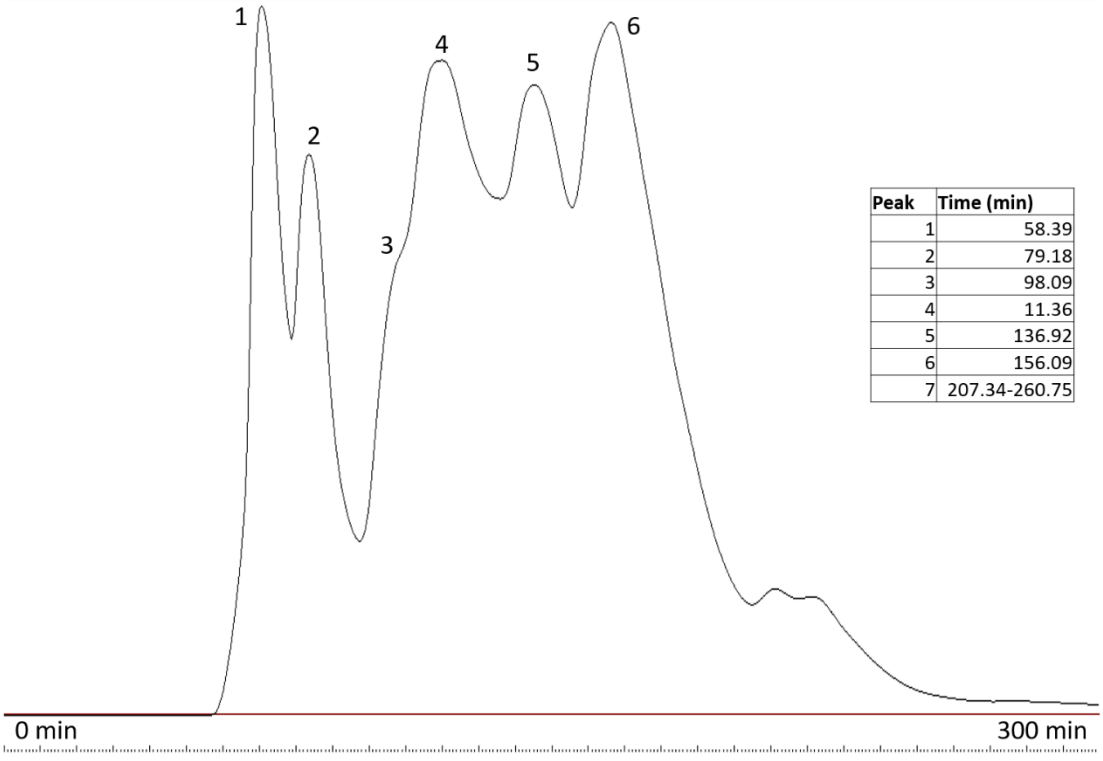

Peak	Time (min)
1	58.39
2	79.18
3	98.09
4	11.36
5	136.92
6	156.09
7	207.34-260.75

Figure 4. Size-exclusion HPLC of C. brunneus crude venom extract. An isocratic gradient with a flow-rate of 1.5 mL/min was used to elute the chromatographic peaks. peak 5 is the

peak that bru9b is more prevalent in. peak 6 is the λ = 280nm peptide peak that contains bru9a.

2.3.2 Isolation and identification of bru9b

Peak 5 from Figure 4 was identified as the fraction containing bru9b and was used in the semi-preparative separation for the purification of bru9b. The absorbance was monitored and the fractions were manually collected. Conotoxin bru9b is not a major component of the venom (Figure 5a) but was identified using MALDI-TOF MS. Five RP-HPLC runs were done and the bru9b containing fractions from each were pooled together to be further purified using the analytical column (Figure 6a). The purified peptide was confirmed with MALDI-TOF MS (Figure 5b and Figure 6b).

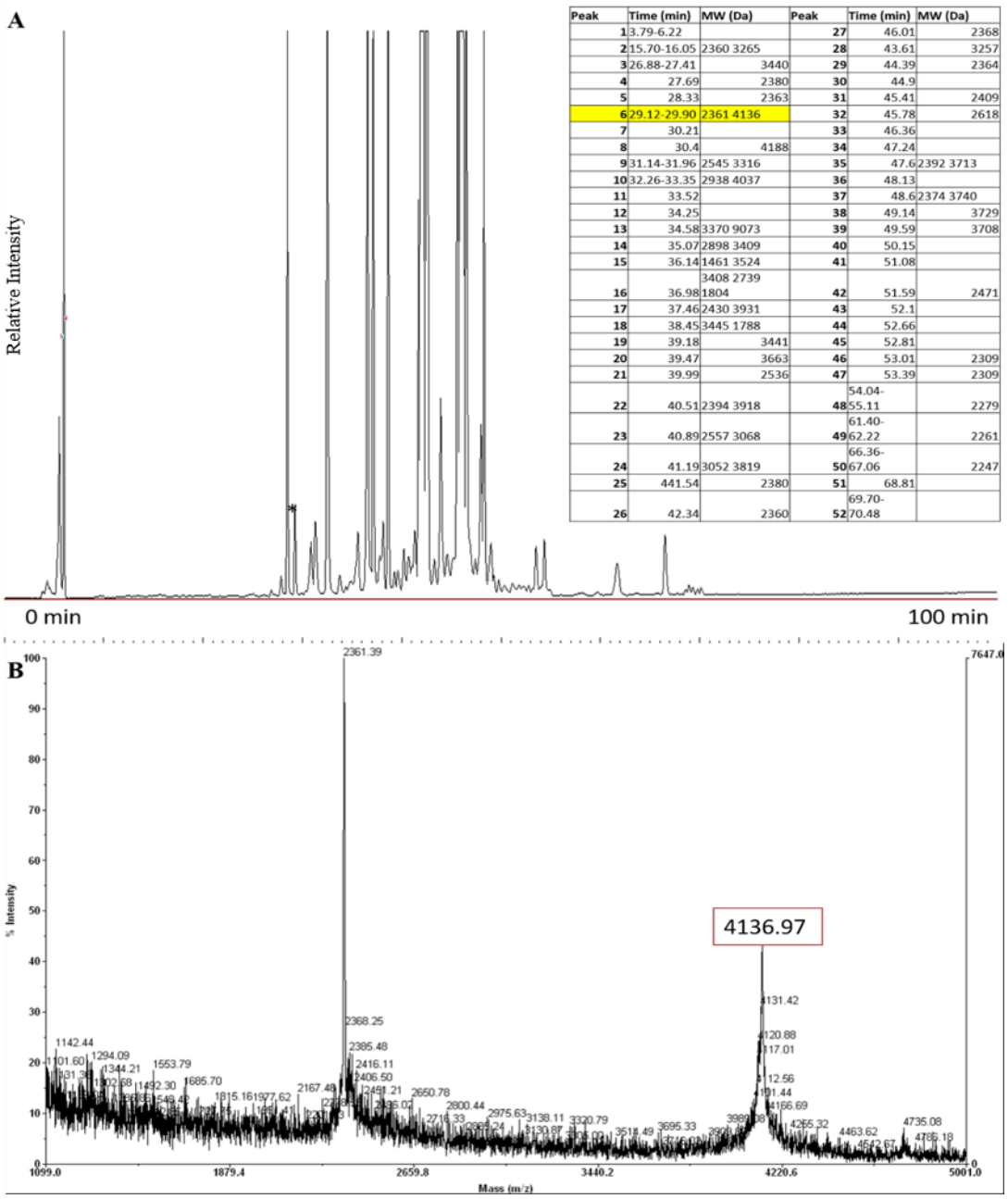

Peak	Time (min)	MW (Da)	Peak	Time (min)	MW (Da)
1	3.79-6.22		27	46.01	2368
2	15.70-16.05	2360 3265	28	43.61	3257
3	26.88-27.41	3440	29	44.39	2364
4	27.69	2380	30	44.9	
5	28.33	2363	31	45.41	2409
6	29.12-29.90	2361 4136	32	45.78	2618
7	30.21		33	46.36	
8	30.4	4188	34	47.24	
9	31.14-31.96	2545 3316	35	47.6	2392 3713
10	32.26-33.35	2938 4037	36	48.13	
11	33.52		37	48.6	2374 3740
12	34.25		38	49.14	3729
13	34.58	3370 9073	39	49.59	3708
14	35.07	2898 3409	40	50.15	
15	36.14	1461 3524	41	51.08	
16	36.98	3408 2739 1804	42	51.59	2471
17	37.46	2430 3931	43	52.1	
18	38.45	3445 1788	44	52.66	
19	39.18	3441	45	52.81	
20	39.47	3663	46	53.01	2309
21	39.99	2536	47	53.39	2309
22	40.51	2394 3918	48	54.04-55.11	2279
23	40.89	2557 3068	49	61.40-62.22	2261
24	41.19	3052 3819	50	66.36-67.06	2247
25	441.54	2380	51	68.81	
26	42.34	2360	52	69.70-70.48	

Figure 5. Semi-preparative HPLC separation and mass spectrometry of bru9b A) Semi-preparative chromatography of SE-the asterisk indicates HPLC Peak 5, bru9b. B) MALDI-TOF MS of the bru9b containing semi-preparative fraction, bru9b (boxed in red) is a minor component

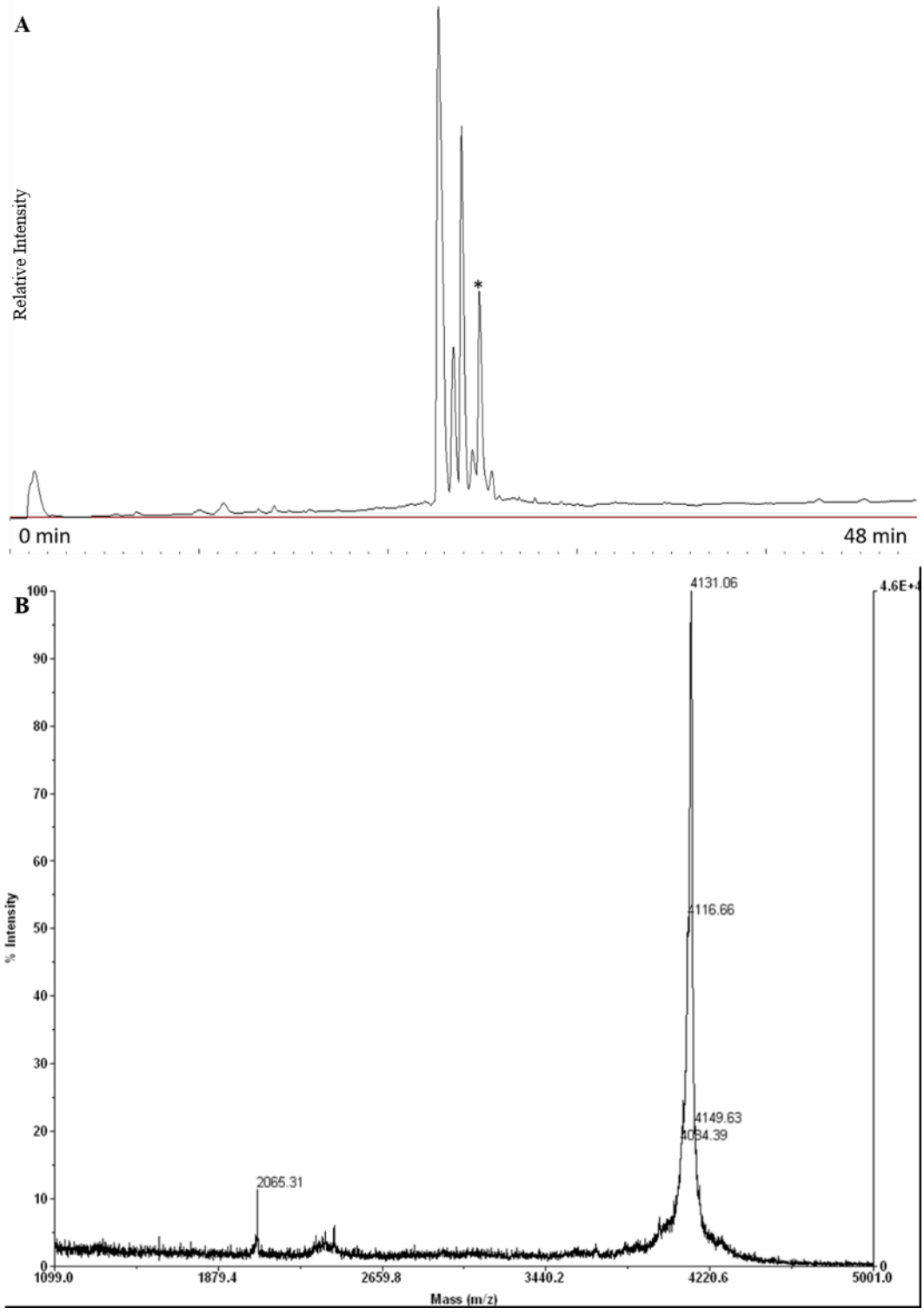

Figure 6. Analytical HPLC separation and mass spectrometry of bru9b A) Analytical chromatography of five-pooled semi-preparative bru9b fractions, bru9b is indicated by the asterisk. B) MALDI-TOF MS of the bru9b containing analytical HPLC fraction, bru9b is the major component of the fraction with a molecular mass of 4131.06.

2.3.3 Isolation and identification of bru9a

Peak 6 from the size-exclusion HPLC (Figure 4) was subjected to semi-preparative RP-HPLC and the fraction containing bru9a was identified using MALDI-TOF MS (Figure 7) and pooled with other bru9a containing fractions from other semi-preparative RP-HPLC runs. The pooled bru9a fractions were re-chromatographed using an analytical column and the brun9a containing fraction was identified by mass spectrometry (Figure 8).

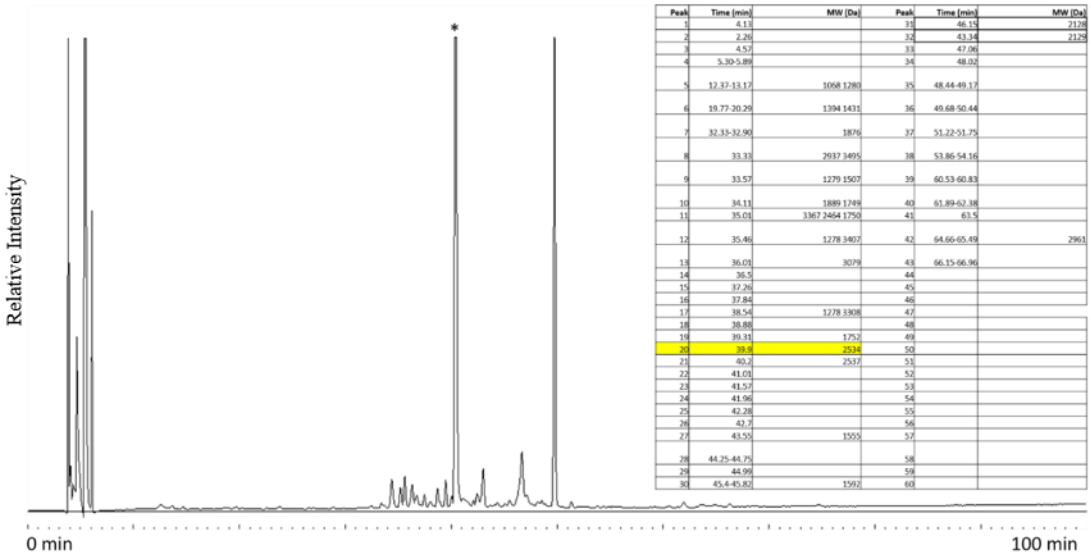

Peak	Time (min)	MW (Da)	Peak	Time (min)	MW (Da)
1	4.13		33	46.15	2128
2	2.26		32	43.34	2129
3	4.57		33	47.06	
4	5.30-5.89		34	48.02	
5	12.37-13.17	1068 1280	35	48.44-49.17	
6	19.77-20.29	1394 1431	36	49.68-50.44	
7	32.33-32.90	1876	37	51.22-51.75	
8	33.33	2937 3495	38	53.86-54.16	
9	33.57	1279 1507	39	60.53-60.83	
10	34.11	1889 1749	40	61.89-62.38	
11	35.01	3367 2464 1750	41	63.5	
12	35.46	1278 3407	42	64.66-65.49	2961
13	36.01	3079	43	66.15-66.96	
14	36.5		44		
15	37.26		45		
16	37.84		46		
17	38.54	1278 3308	47		
18	38.88		48		
19	39.31	1752	49		
20	39.9	2534	50		
21	40.2	2537	51		
22	41.01		52		
23	41.57		53		
24	41.96		54		
25	42.28		55		
26	42.7		56		
27	43.55	1555	57		
28	44.25-44.75		58		
29	44.99		59		
30	45.4-45.82	1592	60		

Figure 7. Semi-preparative RP-HPLC separation of bru9a. The asterisk indicates the bru9a containing fraction and the elution time from the associated retention time and MALDI-TOF MS table is highlighted in yellow.

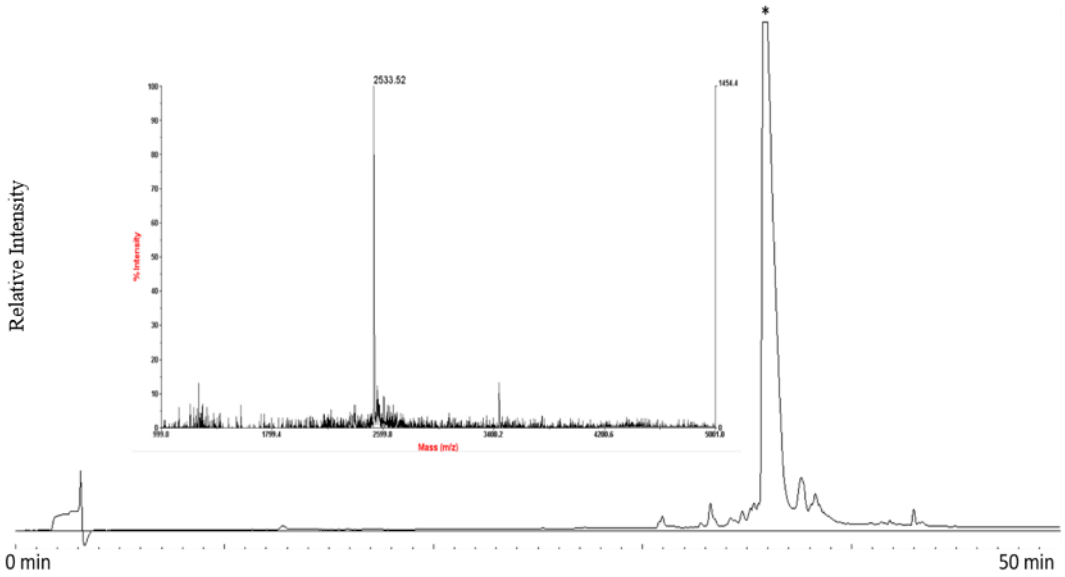

Figure 8. Analytical HPLC purification and mass spectra of bru9a. The bru9a containing fraction is indicated by the asterisk. The mass spectra of bru9a is added as an insert.

2.3.4 In vivo Drosophila GFS bioassay

The 60 picomole of conotoxin was injected into the fly and the DLM and TTM muscle responses were recorded, respectfully. The conotoxin injected flies were compared to the control flies that were injected with 0.7% saline at the same time point. There was no significant effect compared to the control (Figure 9).

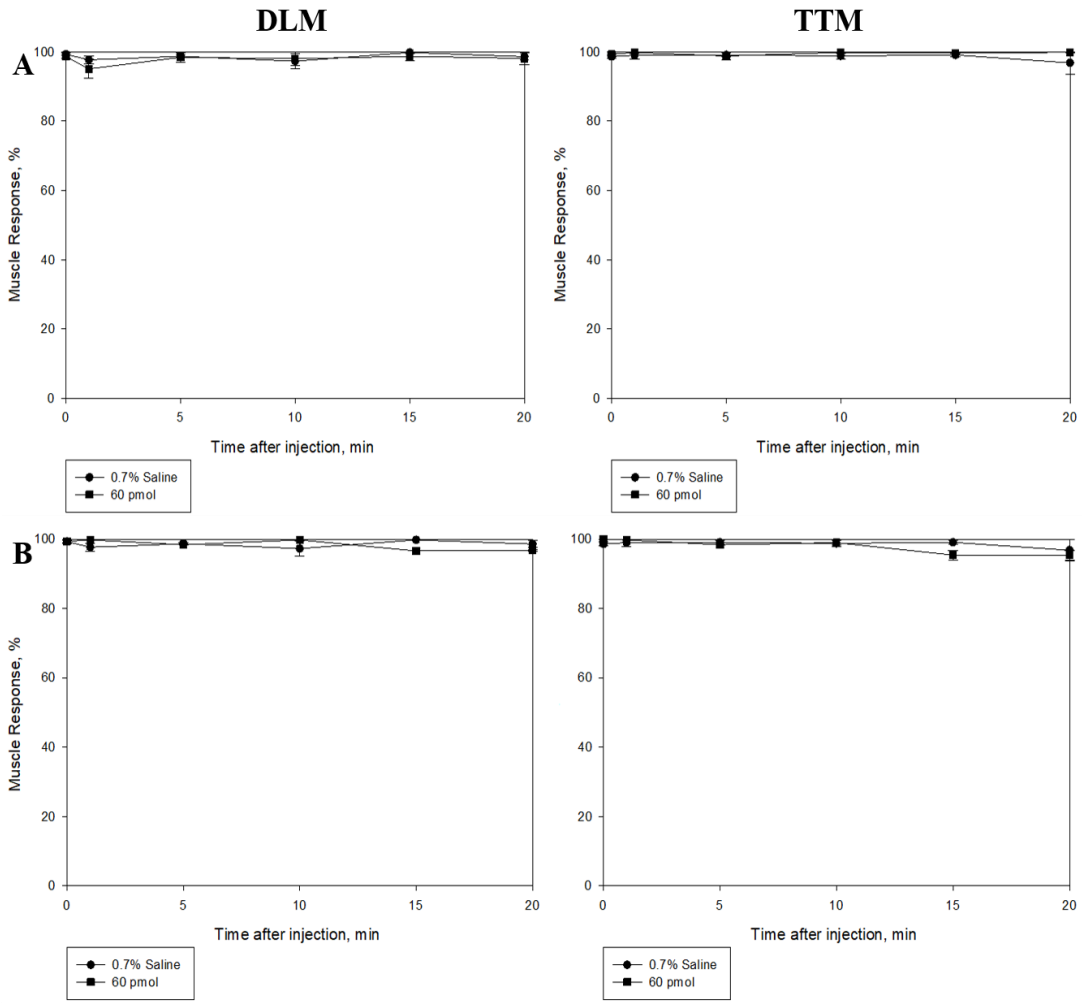

Figure 9. Effects of bru9a and bru9b on the D. melanogaster GFS. A) Effects of 60 pmol of bru9b on the DLM and TTM muscle B) Effects of 60 pmol of bru9a on the DLM and TTM muscle. Results are plotted as mean ± SEM, n=10.

2.4 Discussion

The MALDI-TOF MS of the semi-preparative fraction of bru9b appears to contain a major contaminant with the molecular mass of 2361.39 Da. This could be a real contaminant or it may ionize better than bru9b and therefore seem to be more abundant in the peak. After pooling and re-chromatographing on the analytical column the MALDI-TOF MS shows, that bru9b is the only component in the fraction. This suggests that the contaminant was removed from bru9b. The variation in the molecular mass of bru9b is due

to its large size preventing it from ionizing well in the higher resolution reflector mode of the mass spectrometer. All bru9b fractions were identified in the less accurate linear mode and therefore I was unable to obtain a monoisotopic mass for this conotoxin.

Conotoxin bru9a was isolated from the peptide peak (peak 6 Figure 4) from the size-exclusion HPLC. It was identified using MALDI-TOF MS in linear mode the measured molecular mass is 2533.52 Da which corresponds to the molecular mass previously described [69].

Neither bru9a nor bru9b was active in the *D. melanogaster* GFS (Figure 9). Despite bru9a, being one of the major venom components detected using RP-HPLC and absorbance at $\lambda = 220$nm, which has been tested in several biological assays and a biological target has yet to be determined. It is unlikely that the cone snails would produce this peptide in large quantities without it playing a major role in either predation or defense. They could be working synergistically with another venom component and therefore lose their activity when isolated.

CHAPTER 3: EVALUATION OF CYCLIC PEPTIDES FROM *VIOLA TRICOLOR* NEURONAL ACTIVITY IN *DROSOPHILA MELANOGASTER*

3.1 Introduction

Cyclotides are cyclic cysteine knot containing plant peptides that have been studied for several decades and have many biological activities, such as, insecticidal, uterotonic, anti-HIV, and anti-cancer. Until now, there has not been an investigation into the *in vivo* neuronal activity of these compounds. Cyclotides have the cysteine connectivity of Cys^{I}-Cys^{IV}, Cys^{II}-Cys^{V}, and Cys^{III}-Cys^{VI} where the first two disulfide bonds forming a "ladder" type arrangement for the third disulfide bond to thread through creating a cyclic cysteine knot (Figure 10) resulting in the peptides thermal and enzymatic stability [15, 74]. Due to their extreme stability, cyclotides have become a topic of interest for natural product drug discovery and modification. Cyclotides have been found to have a variety of biological activities ranging from uterotonic [12], to anti-HIV [75], to antimicrobial [13, 76], and to anti-cancer [77]. They are also insecticidal [16, 78] and anthelminthic [79, 80], which are thought to be their intended activities in protecting the plants from pests.

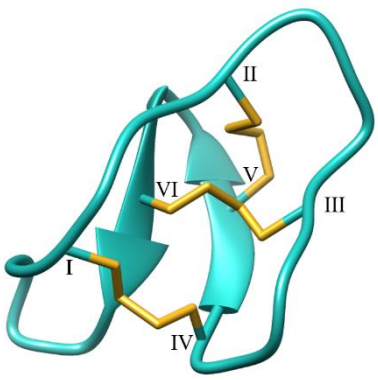

Figure 10. Cyclotide backbone structure showing the disulfide connectivity, Cys^{I}-Cys^{IV}, Cys^{II}-Cys^{V}, and Cys^{III}-Cys^{VI}.

Although, cyclotides have these biological activities and have been evaluated *in vivo* for their bioavailability, they have not yet been studied in an *in vivo* neurological assay. Here, the well-characterized *Drosophila melanogaster* giant fiber system (GFS) is utilized to evaluate directly the *in vivo* effect of injected cyclotides on the fly's nervous system. The four neurons of the GFS contain several different synapses that can be used to screen cyclotides based upon how the muscles respond to the stimulus after injection of the cyclotide.

Cyclotides are notorious for having a hydrophobic patch in the amino acid sequence that causes solubility issues in bioassays [81]. Due to this, DMSO is often added to the peptide to increase solubility, but it has been previously suggested that large quantities of DMSO can affect GFS circuit [82]. It was necessary to determine the minimum DMSO needed to solubilize the cyclotides and then test that amount of DMSO in the bioassay as a negative control. The percentages of DMSO used in this study (9%) may seem high, but the DMSO is diluted by the hemolymph once injected. The average volume of extracted male fly hemolymph is 25nL [83], and if that is the total volume of hemolymph in the fly then the DMSO would be diluted to 5% and should have no effect on the fly.

The cyclotides of *Viola tricolor* were evaluated using the paired nanoinjection of cyclotide with the simultaneous electrophysiological recording from the *D. melanogaster* giant fiber system (GFS). The isolated cyclotides, varv A, varv E, and vitri A, had a dramatic effect on both the tergo trochanteral and dorsal longitudinal muscles within the GFS.

3.2 Materials and Methods

3.2.1 Specimen Collection

Live *V. tricolor* plants were purchased from NuTurf Nursery in Pompano Beach, Florida. The plant, roots, stems, and flowers were used for extraction.

3.2.2 Cyclotide Extraction

Between 250 and 300 grams of wet plant material (flowers, stems, leaves, roots) was used for cyclotide extraction. The plant material was crushed and blended in methanol with an electric blender. The methanol/plant mixture was then transferred to a beaker and equal amounts of dichloromethane was added. The methanol/dichloromethane/plant mixture was left stirring for one day at room temperature [84]. Then a solvent extraction was performed by adding an equal part of water. The organic layer was removed and washed two more times with water. The aqueous layer was saved for tannin removal.

3.2.3 Extract fractionation and cyclotide isolation

The tannins were removed from the aqueous plant extract using Sephadex G10 [85]. The aqueous plant extract was then lyophilized and stored at -20°C until needed for RP-HPLC.

The tannin-free extract was then reconstituted in 0.1% trifluoroacetic acid in water and fractioned by semi-preparative reverse phase-HPLC (RP-HPLC). A C18 semi-

preparative column (Vydac, 218EV510, 10 x 250 mm; 5 µm particle diameter; 300 Å pore size) equipped with a C18 guard column (Upchurch Scientific, AC-43 4.6 mm) at a flow rate of 3.5 mL/min with a linear gradient of 1% incremental change per minute from 100% solution A (0.1% TFA in water) to 100% solution B (0.1% TFA in 60% acetonitrile in water). The fractions identified as containing the desired peptides were then further fractionated by analytical RP-HPLC on a Kinetex C8 column (4.6 mm x 50 mm; 2.6 µm particle diameter; 100 Å pore size, Phenomenex, Torrance, CA, USA) at a flow rate of 1 mL/min. A 100 min linear gradient of 100% solution A (0.1% TFA in water) to 100% solution B (0.1% TFA in 60% acetonitrile in water) by a Series 200 LC pump (Perkin Elmer, Waltham, MA, USA) was used. All fractions were collected manually under UV detection at λ= 220 and 280 nm by a SpectroMonitor 5000 Photodiode Array Detector (LDC Inc., Carlsbad, CA, USA) and lyophilized and stored at -20°C until needed.

3.2.4 Identification and quantification of cyclotides

The fractions containing the cyclotides were identified by their molecular weight using matrix-assisted laser desorption ionization (MALDI) time of flight (TOF) mass spectrometry (MS). The lyophilized fractions collected from RP-HPLC were reconstituted in 50-100 µL of solution B from the RP-HPLC procedure and spotted onto an Applied Biosystems 384-well magnetic insert plate with α-cyano-4-hydroxycinnamic acid (CHCA, 20-25 mg/mL in water/acetonitrile/methanol 15:31:54, ACROS Organics, NJ, USA) matrix. A modified two spot method was used where first the matrix was spotted and allowed to dry completely before the sample solution was spotted on top of the matrix. Matrix-fraction spots were allowed to dry before analysis in the 800-5,000 Da range.

Isolated cyclotides were quantified using Beer's Law and the absorbance at λ = 280nm with a BioTek Epoch Microplate Spectrophotometer and the Gen5 Microplate Data Analysis Software. The molar extinction coefficient was calculated based on the amino acid sequence of the cyclotide using the ExPASy ProtParam Tool [71].

3.2.5 Fly stocks

Wild type (w^{118}) flies were used for experiments. Refer to section 2.2.5 on page 15 for fly husbandry methods.

3.2.6 Establishing a DMSO control

Increasing percentages of dimethyl sulfoxide (DMSO) in O'Dowds saline solution (v/v) were prepared and analyzed in the bioassay to evaluate the effect of higher concentrations of DMSO on the neuronal circuit. The DMSO concentration was increased stepwise to 10% DMSO. Control flies were injected with O'Dowds saline solution (101 mM NaCl, 1 mM $CaCl_2$, 4 mM $MgCl_2$, 3 mM KCl, 5 mM Glucose, 1.25 mM NaH_2PO_4, 20.7 mM $NaHCO_3$, pH=7.2) [73].

3.2.7 Drosophila GFS bioassay

The paired electrophysiology-nanoinjection bioassays were preformed using the methods first described by [43, 52], and full methods can be found in section 2.2.6 on page 16.

In order to visualize the effect the peptides were having on the muscle response, a modified version of the above experiment was performed. Recordings were only taken from the DLM, the more robust of the two muscles, and the peptide was injected into the thorax of the fly instead of the head to observe the immediate effects. The peptides were

injected within the first 30 seconds of the experiment. The GF was stimulated with 1 Hz pulses every 2 seconds for 5 minutes (n=10).

3.3 Results

3.3.1 Extraction of cyclotides from V. tricolor

Four extractions were done, each with ~250 g of wet plant material resulting in approximately 3 grams of crude extract each. The crude extract was stored at -20 °C until further use.

3.3.2 Isolation of cyclotides from crude extract

Cyclotides were late eluting off the column at >70% solution B and relatively low abundance in the extract. (Figure 11) The cyclotide containing fractions from multiple semi-preparative RP-HPLC runs were pooled together then further purified using analytical RP-HPLC. The purification chromatographs showed that the cyclotides were relatively pure. The MALDI-TOF MS of each cyclotide fraction confirmed the molecular weight and therefore identification of each fraction. Using the values in

Table 3 and the absorbance at 280nm, the calculated quantities of the peptides were 300 µg, 360 µg, and 200 µg for varv A, varv E, and vitri A, respectively.

Cyclotide	Sequence	Molecular Mass (Da)	Extinction Coefficient (M^{-1} cm^{-1})
varv A	CGETCVGGTCNTPG--CSCSWPVCTRNGLPV	2877	5875
varv E	CGETCVGGTCNTPG--CSCSWPVCTRNGLPI	2892	5875
vitri A	CGESCVWIPCITSAIGCSCKSKVCYRNGIP	3152	7365

Table 3. Aligned sequences of cyclotides isolated from V. tricolor. Sequence, molecular mass, and calculated extinction coefficient used to calculate quantities of cyclotides from V. tricolor extract. Peptides are cyclic and the "start" and "stop" locations were chosen to show the alignment of the cysteines in the sequence.

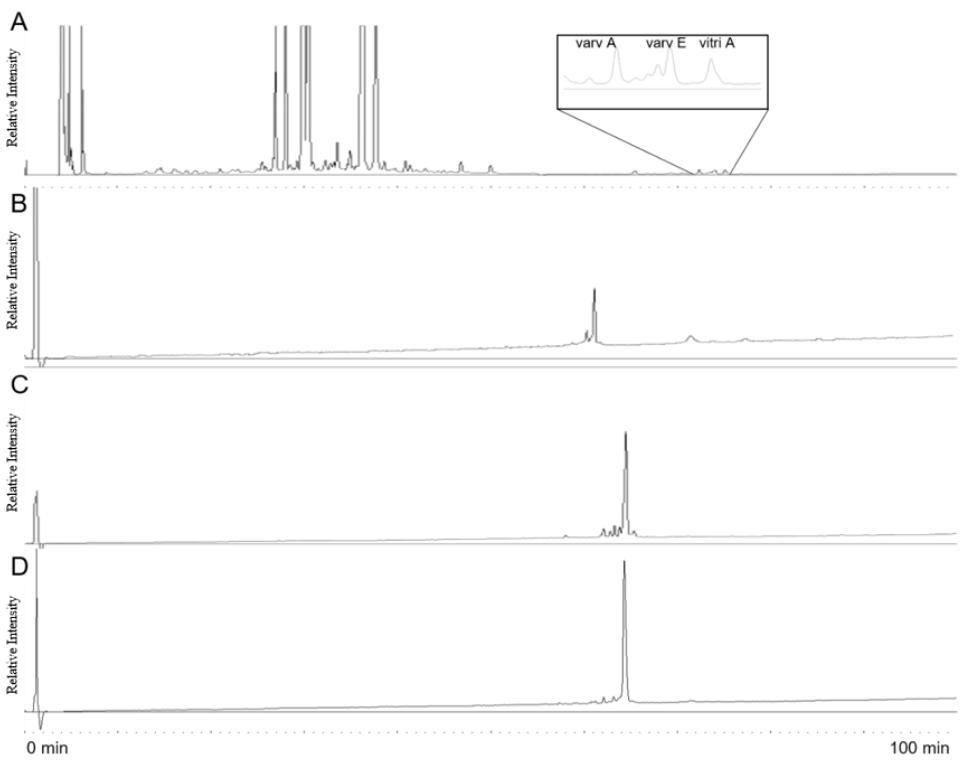

Figure 11. Semi-preparative and analytical HPLC isolations of cyclotides. Reverse-phase high-performance liquid chromatography separation of cyclotides using a linear 100-minute gradient A) Semi-preparative separation of crude tannin-free extract. B-D) Analytical separation of pooled cyclotide containing semi-preparative fractions of varv A, varv E, and vitri A respectively.

3.3.3 In vivo D. melanogaster GFS assay

The three cyclotides isolated from *V. tricolor* were all active in the *D. melanogaster* GFS. Both muscle responses were effected in a non-pathway specific manor (Figure 12). The cyclotides had a dose-dependent response on the muscles, with varv E appearing to have a lesser effect on muscle response when compared to the other two cyclotides tested.

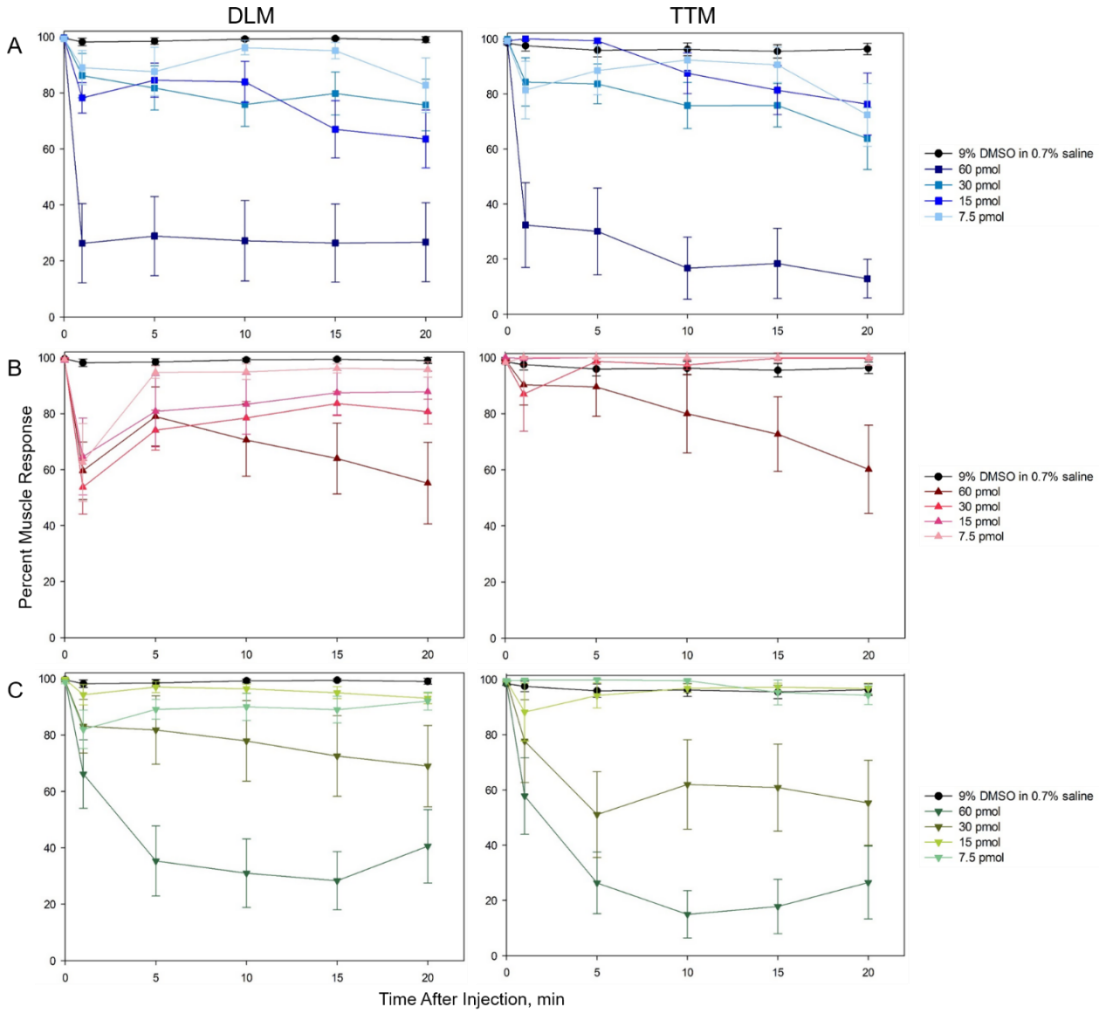

Figure 12. Effects of isolated cyclotides on the Drosophila GFS. A-C show the DLM and TTM responses to increasing amounts of cyclotide injected into the fly for varv A, varv E, and vitri A, respectively. The GF was stimulated with 10 trains of 10 1 Hz stimulation every 5 minutes and the muscle response was measured in the percentage of wild type muscle responses that occurred in the 100 stimulations. Both muscles are affected by the peptides over a 20-minute experiment, plotted at mean ± SEM, n=10.

The thoracic injection of the cyclotides and DLM recordings (Figure 13b-c) show a shift in the latency of the response as well as a change in the shape of the response for varv A and varv E, the changes are not as dramatic with vitri A. The changes in the responses were recorded in 71%, 80%, and 91% of the flies injected with varv A, varv E, and vitri A, respectively.

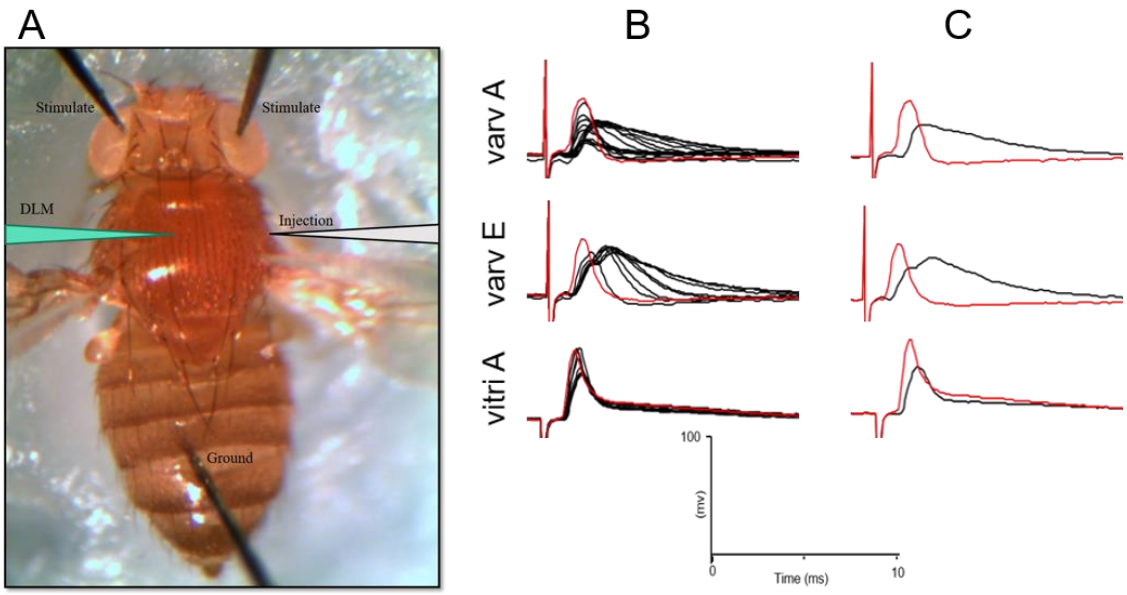

Figure 13. Targeted DLM recording injection site and the effects of isolated cyclotides on the DLM. Effects of cyclotides on DLM muscle response when stimulated with a 1 Hz pulse every 2 seconds for 5 minutes, scale shown below responses. A) Modified recording setup for thoracic injection and DLM recording. Peptide was injected into the thorax of the fly on the side opposite from where the recording electrode is. B) Muscle response traces for every 20th stimulation for 5 minutes. C) The first (red) and the last (black) traces of the experiment, showing the shift in not only latency but also in the shape of the action potential.

3.4 Discussion

The percent of DMSO was increased until a decrease in muscle response when compared to pure saline was witnessed. Muscle response was unaffected by the presence of DMSO until 10% DMSO to saline (v/v) was reached. This concentration of DMSO appears to be the upper limit of DMSO that can be used in a control solution. For this reason, a control solution of 9% DMSO:saline (v/v) was used for the cyclotides. This concentration also provided enough organic solvent to solubilize the cyclotides completely without effecting the integrity of the assay.

The biological effects of cyclotides have been exhaustively studied since their discovery in the early 1970s, but they still do not have a defined biological target. It has

been suggested that their biological effects are due to their ability to disrupt membranes [86]. This is the first reporting of the neuronal *in vivo* evaluation of isolated cyclotides of *V. tricolor*. All three cyclotides caused a disruption of both muscle responses at the highest amount of 60 pmol of peptide injected (Figure 12). When looking at the DLM response using the thoracic injection method, there is a noticeable change in the response latency and shape. This suggests that ion channels responsible for the repolarization of the membrane potential of the neuron are being targeted. The *D. melanogaster* GFS nanoinjection/electrophysiology assay is a good starting point for determining biological activity, and it is especially useful in the identification of a neurological target. This assay has been shown to be well suited for evaluating nAChR activity since only one of the muscle pathways contains nAChR dependent synapses; however, it is clear that the responses elicited by these cyclotides are different from those that inhibit nicotinic receptors.

CHAPTER 4: EVALUATION OF THE NEURONAL ACTIVITY OF A *CONUS GLORIAMARIS* P-SUPERFAMILY CONOTOXIN IN *DROSOPHILA MELANOGASTER*

4.1 Introduction

One of the most sought-after shells of collectors belongs to the cone snail *Conus gloriamaris* [87] (Figure 14). The desirability of this shell stems from the relative rarity of the cone snail due to this cone snail preferring water deeper than 100 meters of the Indo-Pacific region. *C. gloriamaris* became of scientific significance in 1995 when the first biological activity to one of its conotoxins was discovered [88]; the conotoxin, GmVIA was found to influence the voltage-activated sodium currents of *Aplysia* neurons. Since then another biologically active conotoxin, gm9a the spasmodic peptide, has been isolated but no molecular target has been identified [59].

Figure 14. Shell of cone snail Conus gloriamaris, one of the most desired shell among collectors.

The conotoxin gm9a of *C. gloriamaris* has the cysteine framework IX connectivity where Cys(I-IV), Cys(II-V), and Cys(III-VI) form disulfide bonds [32]. It was previously cyclized and shown to have activity in the GFS [35], but the specific biological activity has not been determined [89].

The conotoxin gm9a of *C. gloriamaris*, a cone snail of the Indo-Pacific, was evaluated for its neurological activity in *D. melanogaster*. The conotoxin belongs to the P-superfamily and framework IX for its cysteine arrangement. Two *in vivo D. melanogaster* giant fiber system assay was used to evaluate the biological target of conotoxin gm9a. Both an *in vivo* voltage clamp and patch clamp techniques were used. The *in vivo* voltage clamp assay was previously described as a combination of nanoinjection of the toxin with the simultaneous recording of electrophysiological responses [43]. The conotoxin was injected into the head of *D. melanogaster* while simultaneously recording electrophysiological responses from the dorsal longitudinal muscle and the tergotrochanteral muscle. The conotoxin effected the latency and duration of the muscle responses. The *in vivo* patch-clamp assay to monitor the giant fiber's (GF) intracellular activity was established [90, 91]. The patch clamp assay involves removing the cuticle and muscle of the thorax exposing the giant fiber neuron to a perfusion chamber. The conotoxin was also tested by a collaborator in an *in vivo* patch-clamping assay that determined that gm9a is effecting cellular membrane input resistance. The neuronal activity in *D. melanogaster* of P-superfamily conotoxin gm9a, originally sequenced from *C. gloriamaris* [32] is reported in this work.

4.2 Materials and Methods

4.2.1 Peptide synthesis

Conotoxin gm9a was synthesized, purified, and lyophilized by Olivier Cheneval from David J. Craik's laboratory at the Institute for Molecular Bioscience, The University of Queensland, Brisbane QLD 4072, Australia [35].

4.2.2 Quantification

Conotoxin gm9a was quantified using Beer's Law and the absorbance at λ = 205nm using a molar absorptivity prediction calculator with a plate reader (BioTek Epoch Microplate Spectrophotometer and the Gen5 Microplate Data Analysis Software). The extinction coefficient at λ = 205nm was calculated using the Nick Anthis Protein Parameter Calculator [92] (

Table 4).

Peptide	Monoisotopic Mass (Da)	Sequence	Molar absorptivity at 205nm (M^{-1} cm^{-1})
gm9a	2796.01	SCNNSCQSHSDCASHCICTFRGCGAVN*	100830

*Table 4. Properties of gm9a. Molecular mass, sequence, and calculated molar absorptivity used to calculated concentration for gm9a. *indicates C-terminus amidation*

4.2.3 Fly stocks

Wild type (w^{118}) flies were used for experiments. Refer to section 2.2.5 on page 15 for fly husbandry methods.

4.2.4 D. melanogaster GFS bioassay

Wild type male flies (Stock 46326; Bloomington Stock Center, Bloomington, IN) less than one week old were used in the paired nanoinjection/electrophysiology *D.*

melanogaster bioassay as previously described [43, 52]. Only flies with a following frequency >95% at a stimulation of 10 trains of 10 stimuli at 100 Hz were considered to be wild type and suitable for experimentation. Flies were then either injected with the saline control solution (O'Dowds; 140 mM NaCl, 1 mM $CaCl_2$, 4 mM $MgCl_2$, 3 mM KCl, 5 mM HEPES, pH 7.2) or conotoxin solution [73]. Then the GF pathways were monitored for changes in the following frequency based on a stimulation of 10 trains of 10 stimuli at 100 Hz.

Once established that gm9a had an effect the experiment was modified to better visualize the change in the muscle response action potential. The fly was stimulated with 1 Hz pulses for every 2 seconds for 5 min, 143 pmol (435 ng) of the peptide was injected into the head of the fly during the first 50 sweeps and injection electrode was removed immediately after injection, only the DLM response was monitored due to its large wild type response amplitude compared to the TTM.

4.2.5 In vivo patch clamping

Patch clamp experiments were performed by Dr. Catherine von Reyn at Drexel University School of Biomedical Engineering, Science and Health Systems, Philadelphia, Pennsylvania, USA. Female flies were mounted to the perfusion chamber stage (Figure 15). The cuticle of the head was removed to allow exposure of the brain and the chamber was continuously perfused with extracellular saline (103 mM NaCl, 3 mM KCl, 5 mM N-Tris (hydroxymethyl) methyl-2- aminoethane-sulfonic acid, 8 mM trehalose, 10 mM glucose, 26 mM $NaHCO_3$, 1 mM NaH_2PO_4, 1.5 mM $CaCl_2$, and 4 mM MgCl, bubbled with 95% O2/5% CO_2 at a pH of 7.3 at 22 °C) [93]. A collagenase solution was used to break down the perineural sheath and better expose the giant fiber neuron [90]. Patch clamp

electrodes were filled with intracellular saline (140 mM potassium aspartate, 10 mM HEPES, 1 mM EGTA, 4 mM MgATP, 0.5 mM Na_3GTP, 1 mM KCl, and 20 µM Alexa-568-hydazine-Na at a pH of 7.3) [93]. Recordings were acquired in current clamp mode with a MultiClamp 700B amplifier (Molecular Devices), low-pass filtered at 10 kHz, and digitized (Digidata 1440A, Molecular Devices) at 20 kHz [90]. Current injections were held at zero and traces were not corrected for the liquid junction potential. The perfusion was paused and conotoxin gm9a (34 µM) was applied. Recordings were taken during the period of paused perfusion and after perfusion was started again.

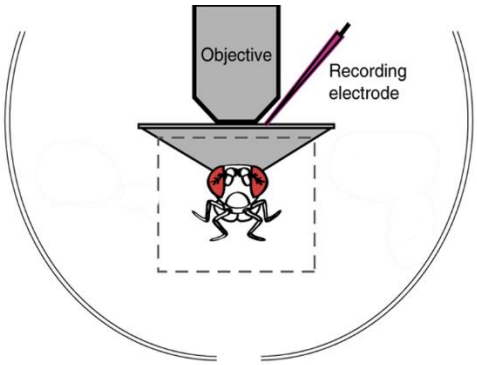

Figure 15. In vivo patch clamp mount. Diagram of how an alive fly is mounted to the perfusion chamber for the in vivo patch clamp assay [90].

4.3 Results

4.3.1 Quantification

An aliquot of the received quantity of gm9a was quantified for the assay using a molar absorptivity estimation at $\lambda = 205$nm since there are no Trp or Tyr residues in the sequence [92]. It was confirmed that there was 2 mg of the synthetic peptide available.

4.3.2 In vivo D. melanogaster GFS assay

gm9a affected both muscle responses, as when 220 pmol of the peptide were injected during the original stimulation experiment (Figure 16) show decreased muscle responses when compared to the saline controls. The DLM's response rate was decreased

to 78% ±11 and the TTM's response was decreased to 62% ±12. The non-muscle-specific effect indicates that the biological target is present in both muscle neuronal pathways.

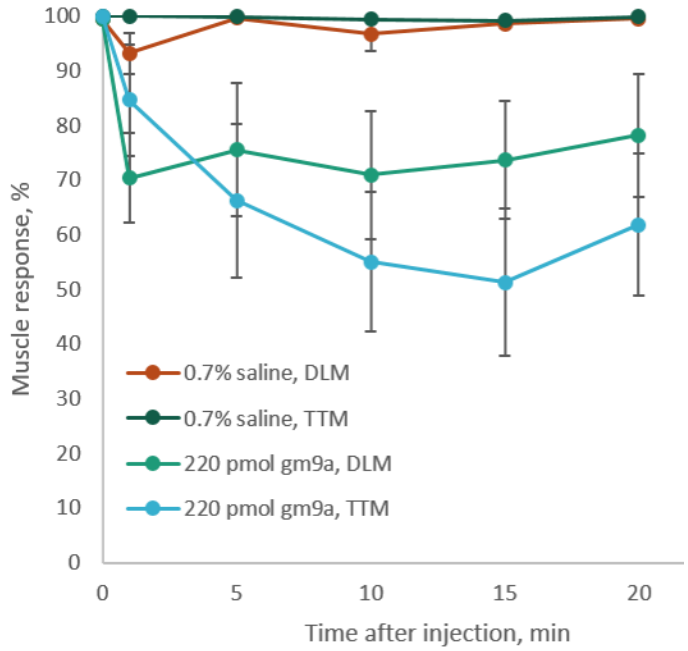

Figure 16. Effect of 220pmol of gm9a on the GFS. Both muscle responses were decreased compared to the saline control, mean ± SEM, n=10

Since a single muscle neuronal pathway could not be eliminated, the DLM pathway was selected for the extended experiment due to its more robust electrical response to stimulation. The DLM muscle response latency was disrupted by the injection of 435 ng of synthetic conotoxin gm9a. There was a distinct shift in the latency of the muscle response to the stimulation, as well as a change in the overall shape of the response (Figure 17). Figure 17 shows the first stimulation in red to emphasize the latency shift throughout the experiment.

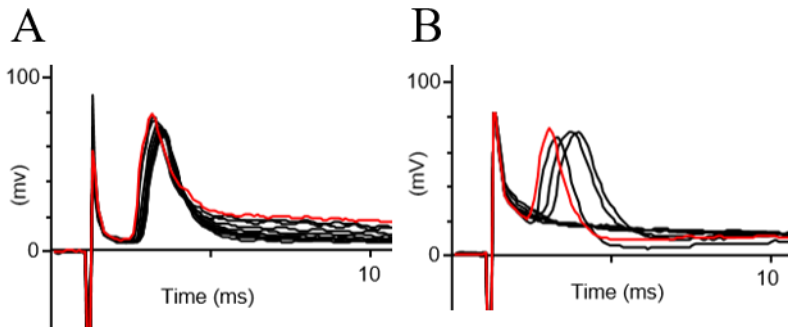

Figure 17. Effects of gm9a on the DLM with the targeted experiment. The muscle responses for stimulations every 40 seconds for 5 minutes. A) Shows the control injection of 0.7% saline and B) shows the injection of 435 ng of gm9a.

4.3.3 In vivo patch clamp of GF neuron

The change in latency and shape of the DLM response hinted towards an ion channel being targeted. The shift in latency in indicative of GAP junctions and the amplitude change can be attributed to an ion channel. To evaluate this, current steps were done while patched onto the GF. When compared to the voltage changes caused by saline the toxin had a greater effect (Figure 18). From this, it was determined that the input resistance of the membrane was affected by the toxin (Figure 19) shown as percent change in membrane resistance between before and after exposure to gm9a. There is a dramatic difference between the saline control and gm9a at 20 minutes after addition.

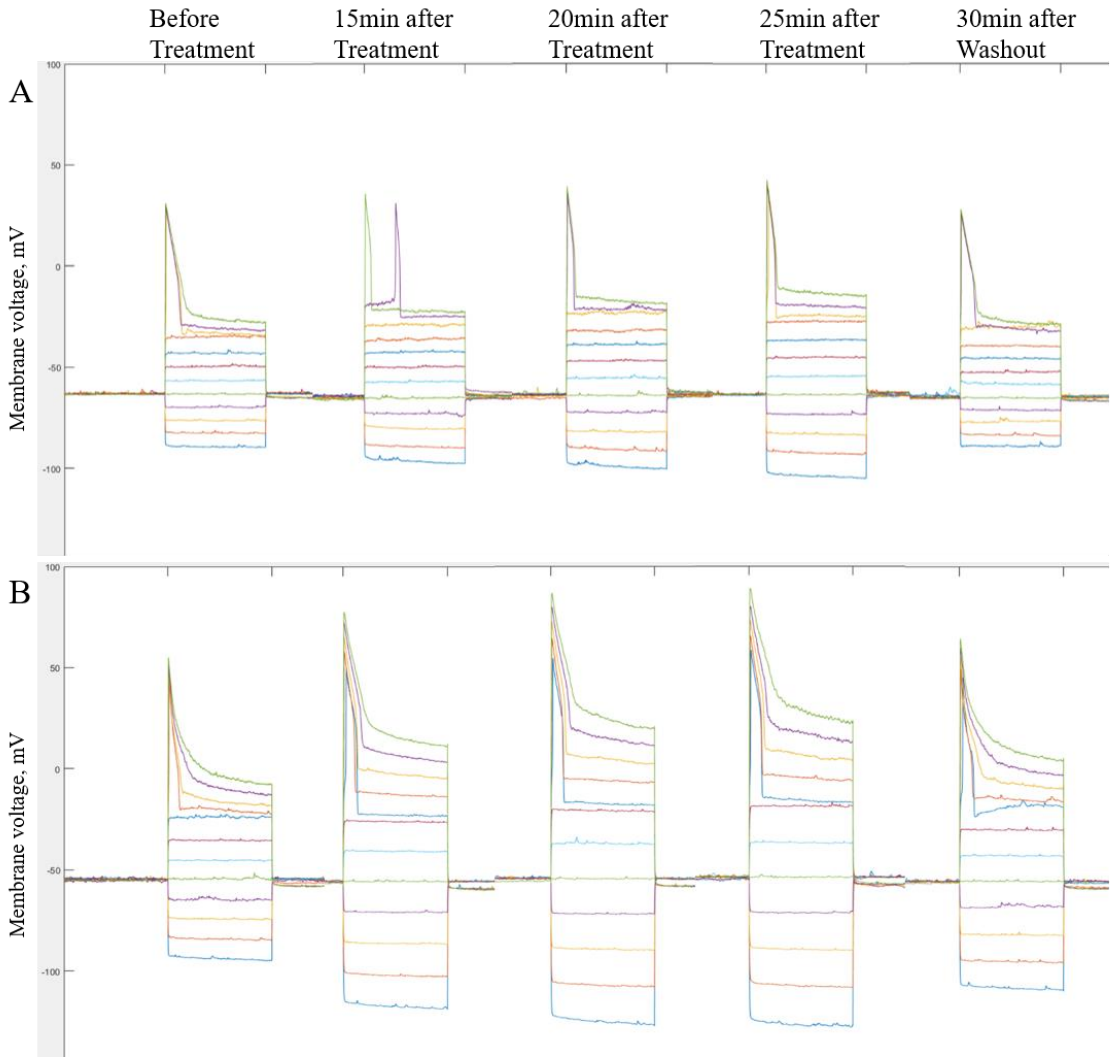

Figure 18. Current clamp steps of giant fiber. There is a difference in the voltage measured when (A) saline is applied compared to (B) when 62ng of gm9a is applied.

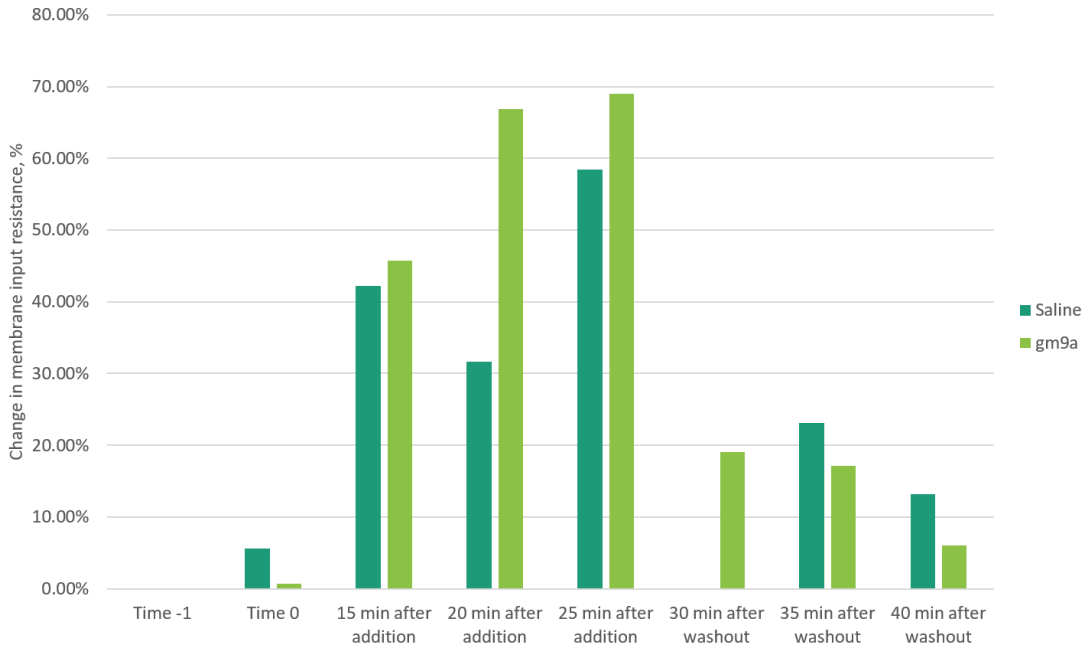

Figure 19. Percent changes of membrane input resistance compared to the initial resistance with an applied current of -200pA. Time points -1 and 0 were resistance measurement time points prior to addition of either saline or gm9a. After 25 minutes, the perfusion bath was started again and toxin or saline was washed out, n=1.

4.4 Discussion

After injection of gm9a, the response latency extended from the stimulation. The relative intensity of the amplitude remained unchanged, but the duration of the response was slightly extended. This led us to focus only on the DLM response and to extend the stimulation experiment. In doing this, we were able to visualize the effect of gm9a on the response over time. Over the extended continuous stimulation experiment, the response latency and duration increased when gm9a was injected. We exhausted the capabilities of this *Drosophila* assay to identify the exact target. Based on the change in latency and duration it was hypothesized that an ion channel was targeted. To evaluate this, gm9a was sent to Dr. Catherine von Reyn at Drexel University to test in her *in vivo* patch clamping

of the *Drosophila* giant fiber. They were able to rule out calcium-activated potassium channels as initially thought, but current clamping steps, as well as an evaluation of the membrane input resistance were measured. The effects of the current steps on the membrane voltage indicated that gm9a was affecting the membrane resistance and the resistance experiments verified this.

An increase in membrane input resistance suggests that the conotoxins is blocking a resting state leak channel, such as a Cl^- or K^+ channels. It is unclear what ion channel may be being inhibited by gm9a during resting and causing a change in membrane resistance, but an increase in membrane resistance causes changes in the responsiveness of neurons to action potentials or other inputs. Due to unexpected and unresolvable circumstances, the experiments at Drexel were halted after the initial testing of gm9a and unfortunately, only a single fly was tested against the addition of saline and gm9a. Without repeatability of this assay, we are not able to make a confident claim as to what the target of gm9a may be.

CHAPTER 5: EVALUATING α-CONOTOXINS IN THE *DROSOPHILA MELANOGASTER* GFS

5.1 Introduction

Cone snail venom components have a variety of molecular targets within their prey such as, K^+ channels, Na^+ channels, Ca^{2+} channels, and nicotinic acetylcholine receptors (nAChRs), among others [94-96]. The venom of each *Conus* species contains over 2000 unique conopeptides spanning over 30 conotoxin gene superfamilies [5, 97]. There are seven classes of conotoxins that target nAChRs [98]; α-conotoxins being the quintessential nAChR inhibitors of the venom of most species of cone snails [94]. These peptides are relatively short peptides, 12-19 amino acids in length with two loops formed by the cysteine arrangement of C1- C3 and C2-C4 forming two disulfide bonds [99]. Several α-conotoxins are used as molecular probes for specific inhibition of certain nAChRs subtypes [100, 101]. Such specificity has greatly advanced our knowledge of cholinergic-mediated mechanisms of neurological conditions such as Alzheimer's disease, schizophrenia, nicotine addiction, and depression disorders [102-104]. One α-conotoxin, Vc1.1, has reached phase IIA clinical trials as a neuropathic pain therapeutic [105, 106].

The fruit fly is an ideal model organism for studying α-conotoxins due to the small amounts of peptide necessary to elicit responses and the extensive number of studies that have been carried out on the neurobiology of these flies. The *D. melanogaster* GFS has been shown to be particularly beneficially to evaluate the

activity of α-conotoxins [43, 52, 101, 107]. The synapse between the PSI and Dorsal Longitudinal motor neuron (DLMn) is solely dependent upon the *Drosophila* α7 nAChR (Figure 20) [101], a homolog of the human α7 nAChR [108], whereas the motor neurons use glutamate as a neurotransmitter.

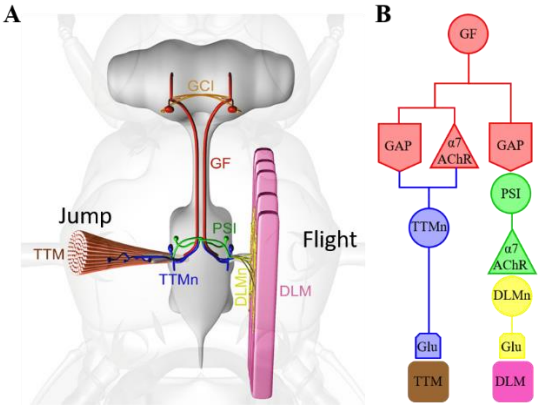

Figure 20. D. melanogaster giant fiber system. A) Shows the orientation of the neurons in the fly and B) shows the types of synapses within the circuit. The DLM pathway contains a synapse solely dependent upon the Dα7 nAChR.

This chapter focus on the isolation of one known α-conotoxin (PIA) and two novel α-conotoxins (PIC and PIC[O7]) and their direct *in vivo* characterization in the *D. melanogaster* GFS. Collaborators from the Illawarra Health and Medical Research Institute at the University of Wollongong assisted in determining the activity of PIC and PIC[O7] at rodent and human nAChR subtypes and PIA at human α7 nAChRs expressed in *Xenopus laevis* oocytes. All three α-conotoxins were isolated from the injected venom of a single specimen of *Conus purpurascens*, the only fish-hunting cone snail species found in the tropical Eastern Pacific region. The α-conotoxins of *C. purpurascens* act synergistically with other paralytic components (the motor cabal) to produce a flaccid paralysis as part of the mechanism of envenomation used to secure the prey. The disruption of cholinergic

pathways is central to the mechanism of envenomation used by cone snails.

5.2 Materials and Methods

5.2.1 Conotoxin extraction

The injected venom was "milked" from a single live *C. purpurascens* individual using the protocol established previously [109]. Briefly, the snail was enticed with a feeder gold fish until the proboscis was extended, and then the fish was replaced with a "trap" made from a microcentrifuge tube with the opening covered in latex and a fish tail. The snail was able to sense the fish tail and sting the trap, injecting its venom into the microcentrifuge tube. The care and maintenance of the gold fish followed the Institutional Animal Care and Use Committee (IACUC) guidelines established at Florida Atlantic University. The injected venom was collected once a week with an average volume of 10 μL and stored at $-80\ ^{o}C$ until needed.

5.2.2 Isolation of conotoxins by RP-HPLC

PIA, PIC, and PIC[O7] were isolated by RP-HPLC from the injected venom of a single *C. purpurascens* individual (Figure 21) by pooling the venom from several "milkings" to obtain a total volume of 50 μL. The venom was then diluted with 0.1% TFA (trifluoroacetic acid) in water in preparation for RP-HPLC analysis by a Series 200 LC pump (Perkin Elmer, Waltham, MA, USA) coupled to a SpectroMonitor 5000 Photodiode Array Detector (LDC Inc., Carlsbad, CA, USA). Venom was separated on a 4.6 mm 50 mm, 2.6 mm-particle diameter, 100 Å-pore size Kinetex C8 column (Phenomenex, Torrance, CA, USA) using an incremental linear gradient of 100% solution A (0.1% TFA, 99.9% H_2O) to 100% solution B (60% acetonitrile in 0.1% TFA) over 100 min with a flow rate of 1.0 mL/min. Chromatography was monitored using

PeakSimple 4.35 system (SRI Instruments, Torrance, CA, USA). Fractions were manually collected under UV monitoring at λ=205, 220, and 280 nm. Fractions were dried and stored at 20^{o}C until needed. The molecular masses of the conotoxins were determined by MALDI-TOF MS, Applied Biosystems Voyager-DE PRO mass spectrometer (Framingham, MA, USA) (

Table 5)[2]. The sequences of PIC and PIC[O7] were solved using Edman degradation by a previous student in the Marí lab [110].

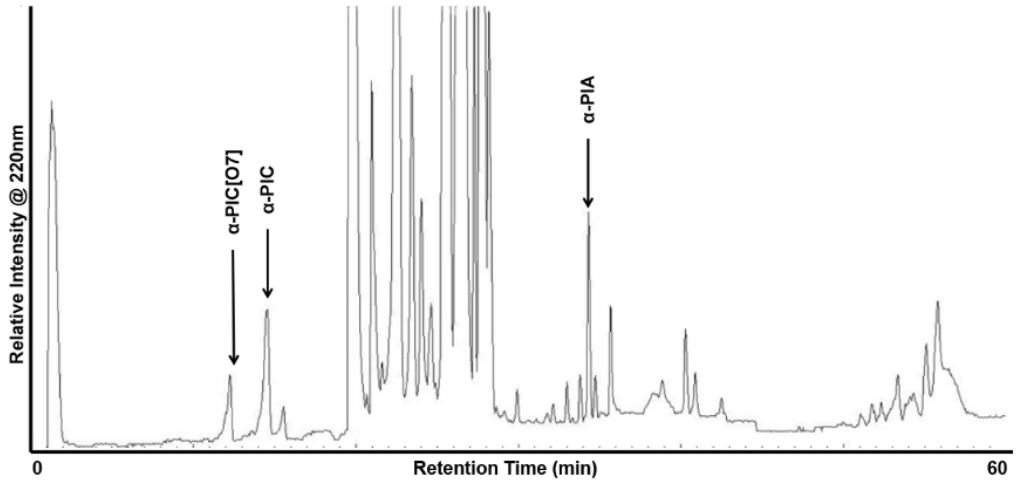

Figure 21. RP-HPLC isolation of PIA, PIC, and PIC[O7] from injected venom of C. purpurascens

Conotoxin	Sequence	Molecular Mass (Da)	nAChR Selectivity
PIA [111, 112]	RDP-**CC**SNPV**C**TVHNPQI**C***	1980.94	rα6/α3β2 ≥ rα6/α3β3 > rα6/α3β4 > rα3β2 > rα3β4 >> rα4β2, r α4β4 hα6/α3β2β3 > hα6/α3β4 >> hα1β1δε
PIB [113]	ZSOG**CC**WNPA**C**-VKNR--**C***	(not in this study)	rα1β1δε, rα1β1γδ >> rα3β2, rα3β4, rα7
PIC [114]	SG--**CC**KHPA**C**-GKNR--**C**	1460.13	rα1β1δε > rα1β1δγ ≈ hα3β2 >> hα7
PIC[O7] [114]	SG--**CC**KHOA**C**-GKNR--**C**	1475.11	rα1β1δε > rα1β1δγ ≈ hα3β2 >> hα7

*Table 5. Sequences and nAChR selectivity of C. purpurascens α-conotoxins. * indicates an amidated C-terminus, Z indicates pyroglutamate, O indicates hydroxyproline.[114]*

5.2.3 In vivo electrophysiology in the D. melanogaster GFS

Wild type flies (w^{1118}, fly stocks #3605 obtained from the Bloomington Drosophila Stock Center) were kept at 25 °C in vials with standard media. The α-conotoxins were prepared in 0.7% saline to a final concentration that allowed for the desired pmol of the peptide to be injected. α-Conotoxins PIA, PIC, and PIC[O7] were injected at various concentrations into the hemolymph of the fly while simultaneously recording from the GFS. Control flies were injected with 0.7% saline solution without peptide. The GFs were stimulated in the brain with 10 trains of 10 stimuli given at 100 Hz with one-second intervals between trains and the GF-DLM and GF-TTM pathways were monitored for changes in the following frequency (FF). Muscle response was monitored before and 1, 5, 10, 15, and 20 min after injection (n = 10 for all experiments). Sigma Plot (Systat Software, San Jose, CA, USA) was used to perform the statistical analysis using a nonparametric Kruskal-Wallis 1-way ANOVA and Tukey test.

5.2.4 In vitro electrophysiology in Xenopus oocytes expressing nAChRs

Oocyte preparation and nAChR subunit expression in *Xenopus* oocytes were performed as described previously [101]. Briefly, plasmids with cDNA encoding the rat (a1, b1, g and d), mouse (ε) and human (α7, α3 and β2) nAChR subunits were linearized for *in vitro* mRNA synthesis using mMESSAGE mMACHINE kit (Ambion, Foster City, CA, USA). Oocytes were injected with 5 ng cRNA two to five days before recording and kept at 18 ^{o}C in ND96 buffer (96 mM NaCl, 2 mM KCl, 1 mM $CaCl_2$, 1 mM $MgCl_2$ and 5 mM HEPES, at pH 7.4) supplemented with 5% fetal bovine serum (Bovogen Biologicals, East Keilor, VIC, Australia), 50 mg/L gentamycin (GIBCO, Grand Island, NY, USA) and 10,000 U/mL penicillin-streptomycin (GIBCO, Grand Island, NY, USA). Voltage-recording and current-injecting microelectrodes were pulled from GC150T-7.5 borosilicate glass (Harvard Apparatus Ltd., Holliston, MA, USA) giving tip resistances of 0.3e1.5 MU when filled with 3 M KCl. Two-electrode voltage clamp recordings from oocytes were conducted at room temperature (22e23 ^{o}C) using a GeneClamp 500B amplifier, Digidata 1322A interface and pClamp 9 software (Molecular Devices, Sunnyvale, CA, USA) at a holding potential of −80 mV.

Initially, oocytes in a 10 μL recording chamber were continuously perfused with ND96 solution at 2 ml/min, applied by a pump perfusion system. nAChR-mediated currents were evoked by applications of acetylcholine (ACh) at half-maximal effective concentration (EC_{50}) of 1 mM for rodent muscle, 6 mM for hα3β2 and 100 mM for hα7 nAChRs. Oocytes were preincubated with peptide for 5 min with the perfusion system turned off, followed by coapplication of ACh and peptide with flowing bath solution. Washout with bath solution occurred for 3 min between ACh applications. All peptide

solutions were prepared in ND96 0.1% bovine serum albumin. Peak ACh-evoked current amplitudes before (ACh alone) and after (ACh peptide) peptide incubation were measured using Clampfit version 10.7.0.3 software (Molecular Devices, Sunnyvale, CA, USA), where the ratio of ACh peptide-evoked current amplitude to ACh alone-evoked current amplitude was used to assess the activity of PIA, PIC, and PIC[O7] on ACh- evoked currents. All electrophysiological data were pooled and represent means ± standard error of the mean (SEM). Data sets were compared using an unpaired Student's t-test (GraphPad Prism 7, GraphPad Software, La Jolla, CA, USA). Differences were regarded statistically significant when $p < 0.05$.

5.2.5 Homology modeling of PIA and PIC bound to the Dα7 nAChR

Homology modeling of PIA and PIC bound to the Dα7 nAChR were done with Modeler v9.18 [115] using a method described previously [101]. Briefly, the X-ray crystal structure of *Aplysia californica* acetylcholine binding protein (AChBP) bound to α-conotoxin ImI (PDB ID: 2C9T) was used as a binding template [116]. Chimera v.6.1 was used for the molecular graphics analysis [117].

5.2.6 Transcriptome of the C. purpurascens venom duct

RNA was extracted from freshly dissected venom duct tissue and prepared utilizing the Illumina PolyA-Truseq preparation protocol. Samples were then sequenced on a Next-Seq 500 Illumina sequencing platform to produce four sets of paired-end sequences. All runs were concatenated to produce two single independent datasets containing 31 million forward and reverse reads. Quality metrics were obtained using FASTQC and read distribution statistics were calculated with BBMap to prove accurate group fragment pair distance (141 bp) for read assembly. The paired-end data was then assembled using De-

Bruijn graph based De Novo assembler, Trinity [118], to produce a final FASTA dataset containing 64,321 independent assembled contigs. Final assembled contigs were then converted to a BLAST database using NCBI Blast and full protein sequences were identified using local NCBI BLASTx with an E-value cutoff of e^{-7}.

5.3 Results

5.3.1 Isolation and sequencing of PIA, PIC, and PIC[O7]

The RP-HPLC profile of the injected venom from a single individual of *C. purpurascens* is shown in (Figure 21). The peaks eluted at 17 (PIC[O7]), 19 (PIC) and 57 (PIA) min were collected and MALDI-TOF mass spectrometry of the purified RP-HPLC fraction in reflector mode yielded a molecular mass of 1460.13, 1475.11and 1980.94 Da, respectively (

Table *5*). The PIC and PIC[O7] fractions were reduced, alkylated, and sequenced using Edman degradation yielding the sequences of the novel 4/4-α-conotoxins PIC and PIC[O7], respectively. The transcriptome of *C. purpurascens* venom revealed the presence of the precursor sequence for PIC and PIC[O7], whose signal sequence corresponds to the A-superfamily of conotoxins [114] (Figure 22).

PIC MGMRMMFIVFLLVVLATTVGSFTLDRVLGLASEGRNAEAIDNALDQRDPKRRTSGCCKHPACGKNRC

Figure 22. PIC precursor protein from transcriptome. The teal highlighted sequence indicates the signal sequence and the yellow highlighted sequence is the mature peptide sequence [114].

5.3.2 In vitro electrophysiology activity of PIC and PIC[O7] in the D. melanogaster GFS

α-conotoxins PIA had an inhibitory effect on the GF-DLM pathway (Figure 23a, n = 10). PIA displayed the most significant disruption of the GF-DLM responses at 88 pmol/fly (Figure 23b) compared to the 0.7% saline control injection while having

no effect on the GF-TTM pathway (Figure 23c-d). At this concentration, α-PIA decreases the probability of DLM responses to 9.8 ± 4.4% and 4.2 ± 0.2% at 10 and 20 min post-injection, respectively. To determine the effects of α-PIA at lower concentrations, 67, 44, and 21 pmol of PIA/fly were injected as well, which caused a reduced dose-dependent inhibition of the GF-DLM pathway. At the lowest concentration tested, the DLM response probability was reduced to 67.7 ± 11.8% by 10 min and 47.0 ± 8.0% by 20 min post-injection.

PIC caused the DLM response to decreased to 69.5 ± 16.5% after 20 min post-injection when compared to the 0.7% saline control, but an ANOVA analysis followed by a Tukey test showed that these measurements were not statistically significant when compared to the control. PIC[O7] at a concentration of 88 pmol/fly, exhibited no significant inhibition of the DLM response probability. Similar to α-PIA, the GF-TTM pathway was unaffected by both, PIC and PIC[O7] (Figure 23D). [114]

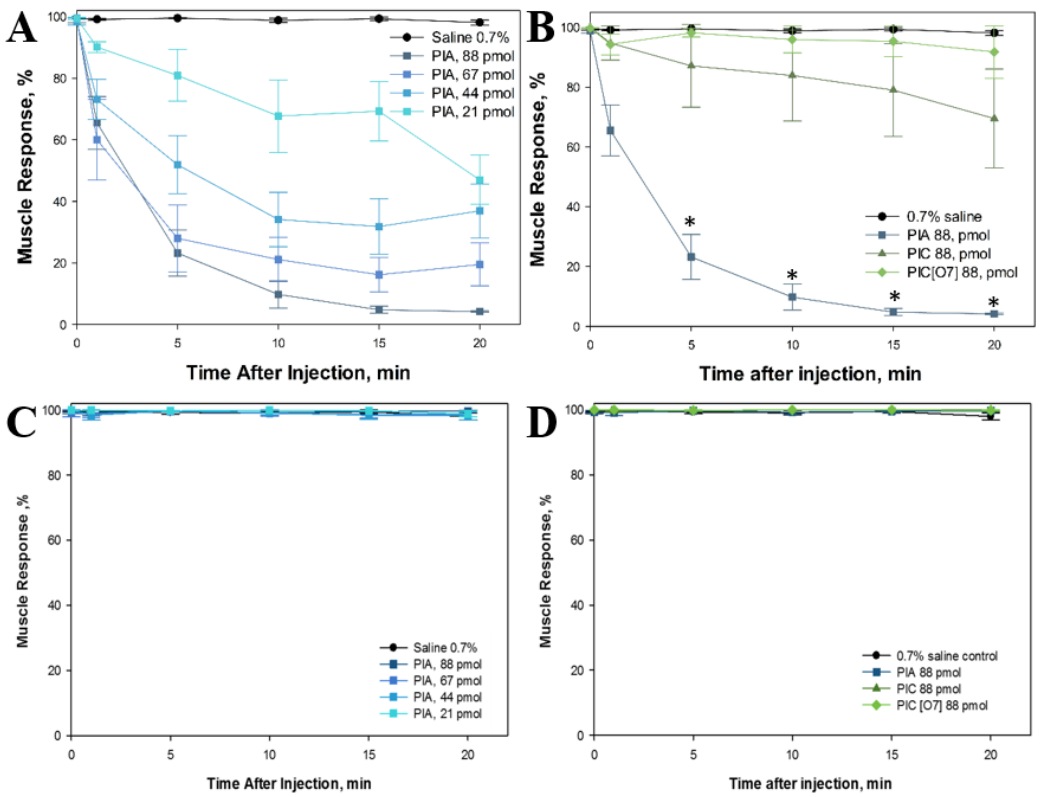

*Figure 23. Functional characterization of PIA, PIC, and PIC[O7] in the GFS. A) Effect of PIA at different concentrations on the following frequency of the GF-DLM pathway, B) Effect of PIC and PIC[O7] on the following frequency of the GF-DLM pathway C) Effect of PIA at different concentrations on the following frequency of the GF-TTM pathway D) Effect of PIC and PIC[O7] on the following frequency of the GF-TTM pathway. (mean ± SEM, n = 10, *p<0.05) [114]*

5.3.3 In vitro electrophysiology activity of PIC and PIC[O7] at the heterologously expressed nAChRs in Xenopus oocytes

α-Conotoxins PIC and PIC[O7] were tested at vertebrate human (h) hα3β2, hα7, and rodent (r) rα1β1δγ and rα1β1δε nAChR subtypes. PIA was tested at the hα7 nAChR using ImI as a positive control. We investigated the effects of the α-conotoxins on ACh-evoked currents mediated by nAChR subunit combinations expressed in *Xenopus* oocytes (Figure 24). At 1 μM, α-conotoxins PIC and PIC[O7] reversibly inhibited ACh-evoked currents mediated by α1β1δε nAChR by 59.8 ± 7.7% and 64.1 ± 4.6% (n = 3),

respectively. Both conotoxins also inhibited the hα3β2 and rα1β1δγ nAChR subtypes by ~30-45% whereas, only minimal inhibition (<10%) was observed at the hα7 nAChR subtype. At 1 μM, α-conotoxin PIA reversibly inhibited hα7 mediated ACh-evoked currents by < 10% (n = 4), whereas, α-conotoxin ImI, used as a positive control on the same oocytes and at the same concentration, reversibly inhibited > 80% (82.7 ± 2.2%, n = 4) of ACh-evoked current amplitude. In summary, PIC and PIC[O7] inhibited the muscle and neuronal nAChRs with the following selectivity sequence: α1β1δε > rα1β1δγ ≈hα3β2 >> hα7 (

Table 5). Surprisingly, PIC[O7] caused a slightly greater inhibition of α1β1δε and rα1β1δγ than PIC.

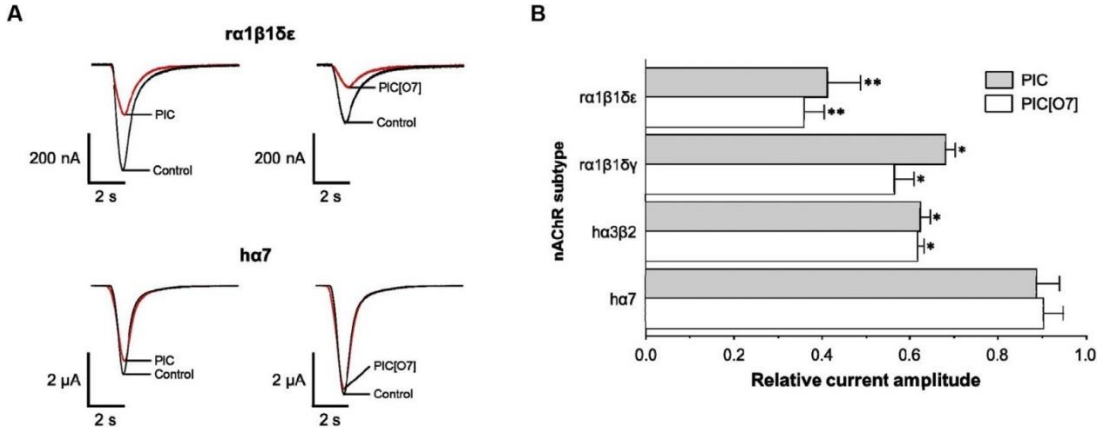

*Figure 24. Activity of PIC and PIC[O7] at rodent and human nAChR subtypes. A)Superimposed ACh-evoked currents in the absence (control) or presence of 1 μM of conotoxin (red) B) Graphical representation of the decreased evoked peak current amplitude (mean ± SEM, n = 3, *p<0.05, **p<0.0001) [114]*

5.3.4 Molecular interaction of PIA and PIC with Dα7 nAChR

The interactions between PIA, PIC and the Dα7 nAChR were further rationalized by homology modeling based upon the crystal structure of *Aplysia californica* AChBP bound to α-conotoxin ImI [116, 119], a suitable surrogate to study nAChR-conotoxin interactions. The key residues of PIA that determine

binding to Dα7 nAChR are predicted to be Asn7 and Val9 at the Dα7 principal side, and Ser6 and Val12 at the Dα7 complementary side of the binding pocket. These residues are predicted to bind to the receptor primarily through hydrogen bonding (Figure 25a-b, red) and hydrophobic interactions (Figure 25a-b, orange). This model predicts that PIA (yellow) is essentially 'glued' to the interfaces of Dα7 at the C-loop of the principal side (Figure 25a-b, light blue) and binding pocket of the complementary side (Figure 25a-b, dark blue). The homology model of PIC and Dα7 predicts fewer conotoxin-receptor interactions (Figure 25c-d), only one interaction with the C-loop of the principal side through Arg 13 in PIC. Additional residues of PIC that determine binding to Dα7 are predicted to be Pro7 at the Dα7 principal side, and Lys11 at the Dα7 complementary side of the binding pocket.

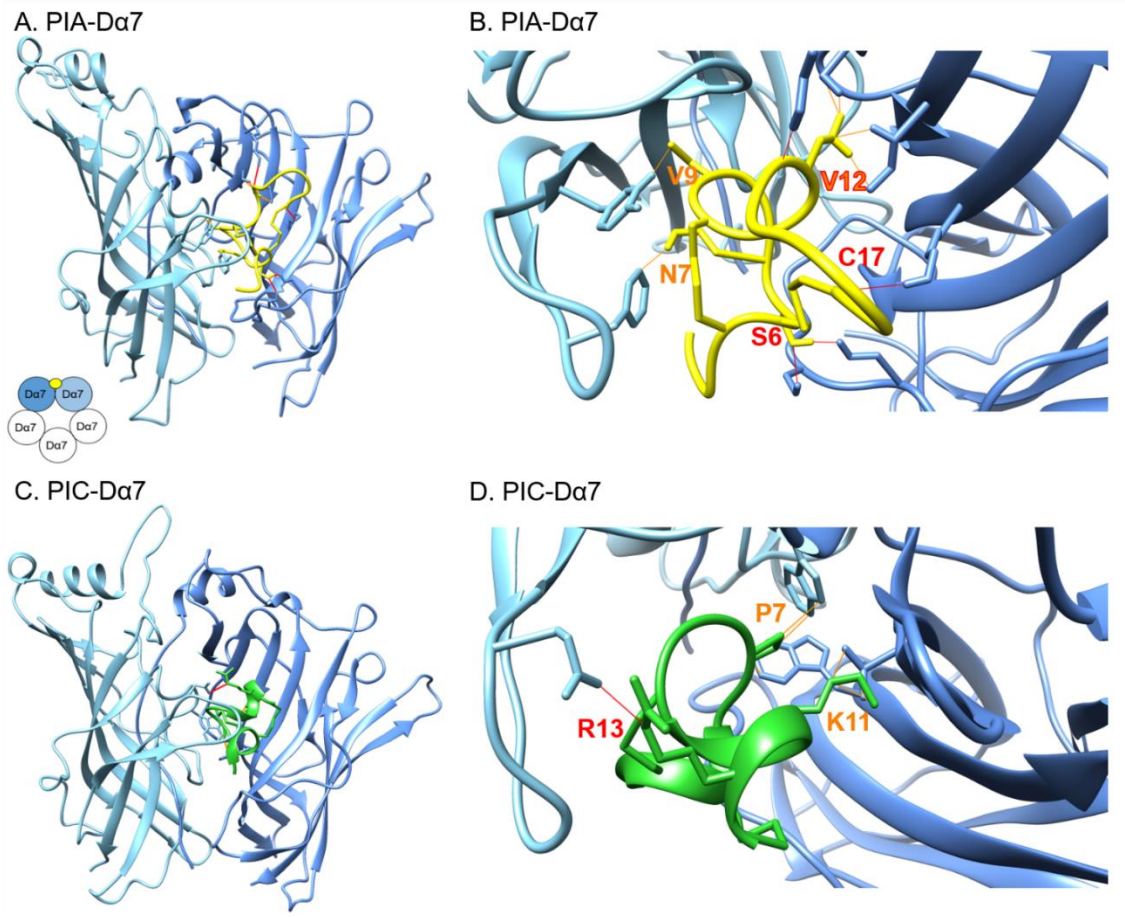

Figure 25. PIA and PIC modeled binding to the Dα7 nAChR [114]. PIA (yellow) and PIC (green) bind to the AChBP between the principal side (light blue) and the complementary side (dark blue) of the binding pocket. Hydrogen bonds (red) and hydrophobic interactions (orange) hold the peptides in the pocket preventing the subunits from changing conformation.

5.4 Discussion

The injected predatory venom of cone snails is a complex mixture of components that act synergistically to immobilize the prey. The functional characterization of such components is a major challenge, as these components are expressed in minute quantities and their direct neuropharmacological assessment, especially when using *in vivo* assays, is typically unreachable. Nevertheless, the *Drosophila*-based *in vivo* assay that permits the evaluation of picomole toxin quantities.

This assay is particularly suitable for the characterization of α-conotoxins, as the GF-DLM pathway (flight response) and not the GF-TTM (jump response) will be affected by α-conotoxins. Interestingly, not all α-conotoxins affect the *Drosophila* α7 nAChR in the same manner [43, 101, 107]. Cone snails express a variety of α-conotoxins that in turn have can have differential inhibition profiles for the nAChRs present in the prey. The particular individual of *C. purpurascens* analyzed here expresses the known α4/7-conotoxin PIA and two new ones, PIC and its hydroxylated analog PIC[O7]. PIC and PIC[O7] are α4/4-conotoxins with four amino acid residues between each cysteine loop. This is the same cysteine loop arrangement as PIB (

Table 5), a known inhibitor of muscle-subtype nAChRs located at the mammalian neuromuscular junction [113]. α-PIB was not expressed in the venom of this individual and was not tested. Sequence homology suggests that α-PIC and α-PIC[O7] may have similar selectivity to nAChRs as PIB.

Testing of the α4/4-conotoxins PIC and PIC[O7] at nAChR subtypes expressed in *Xenopus* oocytes showed that these conotoxins preferentially inhibit the rodent muscle nAChRs more than the human neuronal nAChR subtypes (Figure 24). This explains the lack of PIC and PIC[O7] activity at the neuronal nAChRs compared to α-PIA, a known neuronal nAChR subtype inhibitor. The Dα7 nAChR is a "neuronal-like" subtype, most similar to the mammalian α7 subtype [101]. However, Dα7 has been sensitive to most α-conotoxins tested to date.

These two lineages of α-conotoxins from the venom of *C. purpurascens* with varying activity between neuronal and neuromuscular nAChRs may partially explain the lower potency of PIC for the Dα7 nAChR when compared to PIA. PIA is a 4/7-α- conotoxin

with low sequence homology to the 4/4 counterparts and the longer second loop may be the cause of the difference in selectivity towards the Dα7 nAChR [120]. Synthetic α-PIA does not inhibit human α1β1δε and it has low selectivity towards rat α3β2 nAChRs when compared to α6β2β3 [111]. In this study, we show that native PIA was inactive at the human α7 nAChR. Synthetic conotoxins may exhibit different folding patterns and posttranslational modifications from the native peptide, which could account for differences in sensitivity and activity [121, 122]. It is important to note that in this study we evaluate the *in vivo* activity of conotoxins, which may differ from their activity in single cells.

The nAChR C-loop is essential in linking the conformational changes that occur when the endogenous acetylcholine ligand binds to the receptor to the open the pore. Homology models of the complex between Dα7 and PIA predict multiple interactions at the principal and complementary binding sites that resulted in locking the C-loop in a resting position hindering ACh binding and hampering the conformational changes needed for the channel to open [123]. As a result, synaptic transmission is inhibited leading to reduced DLM response. In contrast, the model of the complex between Dα7 and PIC showed diminished interactions between PIC and the C-loop, which is consistent with PIC non-inhibitory activity when compared to PIA. While these models provide a rationale for such interactions, the precise interaction of conotoxins with nAChRs can vary depending on the specific nAChR subtype and specific conotoxin in consideration.

This study accounts for the efficacious application of the GFS assay, where injected venom components of *C. purpurascens* were used to complete the *in vivo* assay. Here we

have described the isolation of picomole quantities α-conotoxins PIA, PIC, and PIC[O7] from the injected venom of a single individual of C. *purpurascens* and the corresponding *in vivo* functional characterization in a *Drosophila*-based functional assay that involves the Dα7 nAChR subtype. PIA is a known selective α6β2β3 and to a lesser extent a α3β2 nAChR inhibitor, but we have shown PIA inhibits the Dα7 nAChR. We have also shown that the novel α-conotoxin PIC and its hydroxylated counterpart PIC[O7] have no significant inhibitory activity at Dα7 nAChRs. At α1β1δε and rα1β1δγ nAChRs, PIC[O7] is a slightly more potent inhibitor than PIC suggesting that proline hydroxylation plays a delicate role in the mechanism of nAChR inhibition by α-conotoxins [124].

This demonstrates the functional characterization ability of this *in vivo* assay for minute quantities of α-conotoxins in *Drosophila*. These findings can be readily correlated with vertebrate cholinergic pathways [101, 103]. The GFS assay is an effective tool for *in vivo* screening of α-conotoxins, with the advantage of using picomole quantities of the native natural product inhibitors. Furthermore, future studies can be envisioned through genetic manipulations of the Dα7 nAChR, allowing structure-activity relationship studies for α-conotoxins and nAChR subtypes, which ultimately can be used for the evaluation of the neuropharmacology of novel α-conotoxins that can be utilized as molecular probes for diseases such as Alzheimer's, Parkinson's, and cancer.

CHAPTER 6: INTERROGATION OF TWO *CONUS BRUNNEUS* TRANSCRIPTOMES FOR P-SUPERFAMILY CONOTOXINS

6.1 Introduction

Conotoxins are weaponized peptides produced by predatory marine mollusks of the genus *Conus*, cone snails. Cone snails produce a venom for prey capture and defense. The venom is predominately comprised of peptidic toxins, conotoxins or conopeptides. The venom consists of several hundred to thousands of components [2]. Cone snail venom has been of biochemical interest thanks to its breadth of pharmacological targets, ion channels, receptors, and transporters to which the venom has high selectivity to specific subtypes [125]. Due to their specificity, conotoxins have been used as molecular probes [43, 101]. One conotoxin has been FDA approved as an analgesic, Prialt (Ziconotide) [10].

"Venomics" is a relatively new field that integrates genomics, proteomics, transcriptomic, and bioinformatics techniques to identify peptides/proteins present in venom, and it can be readily applicable to the analysis of cone snail venom. Next-generation sequencing, high-resolution mass spectrometry, and bioinformatics tools have made this task more accessible. The mRNA is extracted, amplified, reverse-transcribed, and sequenced to get the transcriptome, which represents the proteins and peptides expressed in a specific tissue. The transcriptome can then be used as a database to search tandem mass spectrometry results against to identify the components of the venom. New conotoxins, isoforms, and post-translational modification enzymes have been identified using this new approach [126, 127].

The general structure of a translated conotoxin transcript is a signal sequence followed by a pre-protein region, then the mature peptide sequence, and then a post-protein sequence (Figure 26). The pre and post protein sequences are cleaved off to reveal the mature toxin. Conotoxins are categorized into superfamilies based on their signal sequence. Then further categorized by their cysteine arrangement or their cysteine framework and finally into families by pharmacological activity [7].

Figure 26. Structure of a conotoxin precursor protein

Framework 9 conotoxins contain the cysteine arrangement of C-C-C-CXC-C where the dashed lines could be any number of amino acids between the cysteines with disulfide bonds forming between Cys (I-IV, II-V, III-VI) and a member of the P-superfamily [59]. There are currently 12 P-superfamily conotoxins on the Conoserver database from *C. gloriamaris, C. imperialis, C. litteratus, C. puliacrius, C. regius, C. textile,* and *C. victoriae* (Table 5). This chapter focuses on mining the transcriptomes of two *C. brunneus* specimens for P-superfamily conotoxins.

These cysteine knot containing conotoxins can be classified as “knottins”. These peptides are of particular interest due to their disulfide connectivity. The first two disulfides create a loop for a third disulfide to thread through and “knot” the peptide backbone. Knottins are found throughout the plant and animal kingdoms and have a variety of biological functions. The knottin structure creates an extremely stable peptide; knottins have proven stable against boiling, acidic and basic conditions, and to serum enzymatic degradation. The loops created by the disulfide bonds have been modified as stable

scaffolds that are able to carry drugs or probes to the active site. One such example of this is chlorotoxin, which is a knottin, modified with a near-IR fluorescent probe that localizes on cancer cells allowing for the visualization of tumor borders [128]. Other knottin peptides could also prove to be ideal scaffolds. Conotoxin knottins have activity towards several ion channels and due to their stability, any new conotoxin knottins should be evaluated for activity.

Next-generation sequencing and RNA-seq was used to sequence the transcriptomes of two *C. brunneus* specimens, one adult and one juvenile. The transcriptomes were assembled and translated into amino acids. They were then interrogated for P-superfamily conotoxins. Thirty-nine unique P-superfamily signal sequence containing precursor proteins were found within the transcriptomes, 21 from the adult and 19 from the juvenile. All P-superfamily conotoxins from the two individuals contained six cysteine residues within the mature peptide region. They are also all classified as framework IX conotoxins. Thirty-seven of the identified P-superfamily precursor proteins have not yet been identified in the crude venom of *C. brunneus.*

6.2 Materials and Methods

6.2.1 Specimen collection

C. brunneus specimens were collected from the Pacific coast of Costa Rica in October 2016 and transported to the lab alive. The specimens were kept alive in aquaria until sacrificed for their venom ducts.

6.2.2 RNA preparation and sequencing

One adult and one juvenile *C. brunneus* specimen were sacrificed and the venom duct of each was dissected and individually placed into RNAlater solution (Qiagen). RNA

was prepared using the Illumina PolyA-Truseq preparation protocol. Illumina Next-Seq 500 platform was used to sequence the samples, which resulted in two sets of paired-end sequences. All runs were combined to form two single independent datasets of forward and reverse reads. FASTQC [129] was used to produce quality sequence data and BBMap [129] was used to show accurate fragment pair distance (141 bp) for read assembly. The *de novo* assembler Trinity [130] was used to assemble the paired-end data. The contigs were translated using Emboss get open reading frame(getORF) tool on the Galaxy platform using the settings of 120 minimum nucleotide open reading frame size, translate only between start and stop codons, finding ORFs in the reverse complement, and that all codons start with methionine [131, 132].

6.2.3 Mining the transcriptome

The translated transcriptome of both the adult and juvenile specimen were interrogated for their coding of P-superfamily conotoxins. Protein precursors of the *Conus* P-superfamily signal sequences were obtained from the Conoserver database [54, 133] (Table 6). The signal sequence was used to perform a blastx search in Geneoius 10.1 (Biomatters, Ltd., UK). The blast hits were compiled and the duplicate and non-framework IX containing precursor proteins were removed. An E value of one was used to get the most possible matches, but only the high scoring hits were included as results.

A manual mature sequence search had to be done for bru9a, as it was not one of the transcriptome hits to the Conoserver signal sequences. Once found, the signal sequence of bru9a was extracted from the protein precursor and a separate blastx was performed on both the adult and juvenile transcriptomes.

The ConoPrec [7, 54, 133] tool on Conoserver was used to predict the signal sequences, pre/post peptide regions, and the mature peptide region. ConoPrec predicted that the last four residues of bru9b to be cleaved off as a post-peptide sequence, but we know from Edman Degradation sequencing that these residues are indeed present in the isolated peptide. This discrepancy led us to disregard the “post-peptide” designation from ConoPrec and include those residues as part of the mature peptide.

Name	Precursor Protein Sequence
GmIXA	**MHLSLARSAVLMLLLLFALGNFVVVQS**GLITRDVDNGQLTDNRRNLQTEWNPLSLFMSRRSCNNS--CQSHSDCASH-CICTFRG--CGAVNG [32, 59]
Im9.12	**MHLSLASSAVLMLLLLFALGNFVGVQP**GQITRDADNLRNLRSQWKKRGLFKSLDKR---TNCEAHS-CSPS--CPDE-CYCDTNEDTCHPERRGH[134]
Lt9a	**MTLTKSAVLILVLLLAFDNFA**DVQPGLITMGGGRLSNLLSKR----------VRIWFCASRT-CSAPADCNP--CTCESGV--CVDWL [135]
Lt9a v2	**MTLTKSAVLILVLLLAFDNFA**DVQPGLITMGGGRLSNLLSKR----------VSIWFCASRT-CSTPADCNP--CTCESGV--CVDWL [135]
Lt9a v1	**MTLTKSAVLILVLLLAFDNFA**DVQPGLITMGGGRLSNLLSKR----------VSIWFCASRT-CSAPADCNP--CTCESGV--CVDWL [135]
Pu9.1	**MHLSLARPAVLMLLLLFALGNFNGVQP**GQITRDVDNSVRNLQSRWEPMSLLKSLNKPR--SCTGS--CSSSSFCPPG-CDCFHAE--CT [136]
Pu9.2	**MHPSLARSALVMLLLLFALGVQS**GQITRDVDSADLKSLRKPMTLLGSLYKR--------VGCGDH--CLSNAHCPPV-CRDCTYDSGCQM [136]
Rg9.1	**MHLSLARSAVLILLLLFALG**NFVGVQPGQITRDADHGINLRSLRKQMSRSPLVKGA----FCGQA--CSSVK-CPKK-CFCHPEEKVCYREMRTKERD
TxIXA	**MHLSLARSAVLMLLLLFALGNFVVVQS**GQITRDVDNGQLTDNRRNLQSKWKPVSLYMSRRGCNNS--CQEHSDCESH-CICTFRG--CGAVNG [32, 59]
Vc9.1	**MHQSLARSAVLMLLLLFALG**NFVVVQSGLITRDVDNGQLTDNRRNLQSEWKPVSLFMSRRTCHKP--CQRHSECASH-CICLIDT--CDDAG [89]
Vc9.2	**MHQSLTRSAVLMLLLLFALGNFVVVQS**GLITRDVDNGQLTDNRRNLQTEWNPLSLFMSRRSCNNS--CQNHSDCASH-CICTFRG--CGAVNG [89]
Vc14.5	**MHLSLARSAVLMLLLLYALG**NFVGVQPEQITRDVDNGQLTDNRRNLQSEWKPVSLFKSLYKRQPRFESCQQDSDCDFQFFCWNNECHRIILI [89]

Table 6. P-superfamily conotoxins on Conoserver. The signal sequence (bold), pre-peptide and post-peptide sequences (not bold or underlined), and mature conotoxin (underlined) of the P-superfamily precursor proteins from Conoserver [54, 133]. All except Vc14.5 are framework IX conotoxins consisting of six cysteines (red).

6.2.4 Dissected venom extraction

Dissected venom was extracted using the same procedure as in section 2.3.2. The extracted ducts were dissected from previous specimens and the age of the animals was not documented. It was assumed that the extracted ducts came from the adult and the juvenile specimens.

6.2.5 Size-exclusion HPLC of the dissected venom

Dried dissected venom extract was reconstituted in 0.1M ammonium bicarbonate (NH_4HCO_3) (~2.5mg/0.5mL) and separated via size-exclusion high-performance liquid chromatography (SE-HPLC) on a Superdex Peptide HR 10/30 column with 0.1M NH_4HCO_3 at 0.5mL/min (Agilent Technologies 1200 Binary Pump). Chromatographic fractions were UV-detection (Agilent Technologies 1200 DAD Detector) monitored at λ= 220 nm and collected manually over 60 min. Fractions were lyophilized and stored at -20°C until further use.

6.2.6 Reduction/alkylation and trypsin digest of fractions

Fractions were divided into either protein (early eluting) or peptide (late eluting) fractions. The protein fractions (1-5) were reduced/alkylated and trypsinized. The peptide fractions (6-11) were reduced/alkylated. Peptide and protein fractions were brought up in 25 µl of 50 mM ammonium bicarbonate, reduced with one µL of 500 mM of Tris (2-carboxyethyl) phosphine (TCEP), and incubated at 60°C for 1 hour. Then the free thiols were modified with 1.5 µL of 375 mM iodoacetamide in the dark at room temperature for 1 hour. The peptide fractions were zip-tipped and dried. The protein fraction then underwent trypsin digestion using a 1:50 protein to enzyme ratio. The protein fractions were incubated at 37°C for 16 hours while shaking. Trypsin was quenched by adding

acidifying the same with 3% trifluoroacetic acid (TFA), incubated at 37°C for 45 minutes, and then centrifuged at 13,000 rpm for 10 minutes. The protein fractions were then zip-tipped and dried.

6.2.7 Identification of P-superfamily conotoxins using high-resolution mass spectrometry

Dried fractions were reconstituted in 50 µL of 0.1% TFA in water and transferred to autosampler vials for analysis on the Orbitrap Fusion Lumos Tribrid Mass Spectrometer. An 85 min gradient was used with solution A (0.1% formic acid (FA) in 5% acetonitrile (ACN) and water) and solution B (0.1% FA in 80% ACN and water) on an Acclaim PepMap 2µm C18 Column (75 µm x 25 cm). A flow rate of 0.3 µl/min was used with the following gradient steps: 0 min at 0% B, 10 min at 5% B, 53 min at 27.5% B, 60 min at 40% B, 65 min at 95% B, 76 min at 5% B, and end at 85 min.

The spectra were collected using positive mode higher-energy collision dissociation (HCD). The MS1 scan was collected using an Orbitrap resolution of 120K, quadrupole isolation; scan range 200-2000, RF lens 30%, automatic gain control (AGC) target 4.0e5, and a 50 ms injection time. The MS2 scan was done with a peptide filter on parent ions with a 2-6 charge state. A dynamic exclusion after 10 MS2 collections in 30 sec the parent ion is placed on an exclusion list for 60 sec. An intensity threshold of 2.5e4 was used and ddMS^2 settings of quadrupole isolation, HCD energy 32% were collected in the Orbitrap using a resolution of 30K, and an AGC target 5.4e4 or 54 ms injection time.

Spectra were matched to transcriptome sequences using Thermo Proteome Discoverer 2.0.0.802. A Basic Consensus workflow was used, and the processing workflow consisted of a precursor ion spectra selection, Sequest HT with Percolator. The

following amino acid modification were used in the search: Met and Pro oxidation, Glu carboxylation, N-terminal pyro-glutamate, C-terminal amidation, and Cys carbamidomethyl.

6.3 Results

6.3.1 RNA preparation and sequencing

The venom duct had preserved mRNA of high enough quality to evaluate. The Trinity assembly resulted in 60,818 and 88,798 contigs sequences for the adult and juvenile specimen, respectively.

6.3.2 Mining the transcriptome

Twenty-one adult and 18 juvenile P-superfamily precursor proteins were found from the mRNA of the two dissected *C. brunneus* specimens *(*Table 7). Twenty-five unique Framework IX conotoxins were coded for within the two transcriptomes (Table 8). A distinct signal sequence is not conserved among the P-superfamily conotoxins, but there is a conserved patch within the signal sequence (Table 9*).*

Name	Precursor Protein Sequence
bru_a9.1	**MHLSGSAVLMLLLLFSLGVQS**GDVVNGQLTDNRRNLRSQWNQMSLFKSLDKR----------SCGGS-CFGG--CWPG--CSCYART--CFRD
bru_a9.2	**MHLSLASSAVLMLLLLFALGNFVGVQP**GQITRDADNHINLRSQRKQMSR---------SLDKGSNCGQD-CSSDN-CPSG--CFCYPRDNVCYVERRKN
bru_a9.3	**MHLSGSAVLMLLLLFTLGNFIGIQS**GDVDNRRNLESQWQRRSLFKTLAKR----------ACHLP-CYDG--CGSG--CHCHTRTYHCHRSY
bru_a9.4	**MHLSLAGSAVFMLLLLFALGNFVGVHP**GQITRDTDNGQFTDNRRNLRPLWKPMSLSKSADKR--TCEGT-CFVDDQCHSH--CHCHTDNT-CSYPD
bru_a9.5	**MHLSLAGSAVLILLLLFAFGNFVGVQP**GDVDNGQLSDNSHNLRSWVKPSSFFRSLERK----RELCPGE-CDPDRGCPSG--CYCRWLR--CWRP
bru_a9.6	**MHLSLAGSAVLMLLLLFALGNFVGVQP**GKITRNVDNGQLTDNRRNLRSRGKPMSLLRSLDRR--HCWGGACSNESQCPHY--CHCGNEQH-CHRDV
bru_a9.7	**MHLSLAGSAVLMLLLLFALGNFVGVQP**GQITRDVDNGQLTDNRRDLQPHWQERGLFKTLAKR--ACHLP-CYDG--CGSG--CHCHTRTYHCHRSY
bru_a9.8	**MHLSLAGSAVLMLLLLFALGNFVGVQP**GQITRDVDNGQLTDNRRNLQSLRKPMRLFKSLAKR--WCVAP-CAGDPQCNIG--CSCNENGV-CEYNDVAW
bru_a9.9	**MHLSLAGSAVLMLLLLFALGNFVGVQP**GQITRDVDNGQLTDNRRNPQSLWKPMSLFKLLNK--RMCGAT-CYPFDDCPAN--CPCAPNGH-CARS
bru_a9.10	**MHLSLAGSAVLMLLLLFALGNFVGVQS**GQVTRDVDNGQLTDNRRNLQSQWNRLSLFKSLHKR-GTCGA--CGLG--CPRG--CSCAYRI--CWTS
bru_a9.11	**MHLSLAGSAVLMLLLLFALGNFVGVQS**GQVTRDVDNGQLTDNRRNLQSQWNRLSLFKSLHKR-GTCGT--CAFG--CPGG--CTCAYRI--CWTS
bru_a9.12	**MHLSLAGSAVLMLLLLFALGNFVGVQS**GQVTRDVDNGQLTDNRRNLRSRGKPMSLLRSLDRR--HCWGGACSNESQCPHY--CHCGNEQH-CHRDV
bru_a9.13	**MHLSLAGSAVLMLLLPFALG**NVVGVQPGQTTRDVDNGQLTDNRRDLQPHWQERGLFKTLAKR--ACHLP-CYDG--CGSG--CHCHTRTYHCHRSY
bru_a9.14	**MHLSLAGSAVLMLLLPFALG**NVVGVQPGQTTRDVDNGQLTDNRRNLQSQWQQSSLFKLLAKRR-MCPLL-CRGT--CPPG--CICRHGH--CYDSDF
bru_a9.15	**MHVSLAGSAVLILLLLFALDNFVGVQP**GPITMDNGQLTDNHRNLRSLQKPVNLLTKR-------SCPGGWCIRPAHCAGT--CSCNRGF--CG
bru_a9.16	**MHAVLMLLLLFALGNFVGVQP**GKITRNVDNGQLTDNRRNLRSRGKPMSLLRSLDRR--------HCWGGACSNESQCPHY--CHCGNEQH-CHRDV
bru_a9.17	**MHAVLMLLLLFALGNFVGVQP**GQITRDVDNGQLTDNRRNLQSQWQQSSLFKLLAKRR-------MCPLL-CRGT--CPPG--CICRHGH--CYDSDF
bru_a9.18	**MHAVLMLLLLFAMGNFIGIQS**GDVDNRRNLESQWQRRSLFKTLAKR----------GVCKVH-CVGG--CPMG--CHCHHGH--CHHPDDESNHHPDGVHK
bru_a9.19	**MRLSTMHSVILMLLLMFVFDNVDG**DDPGQTARDVDNRKLMSSLRSKGKPAAFFMPREKR----TVCSRKRCPTP--CHGR--CYCGPGNF-CIPWDYPGK
bru_a9.20	**MRLSTMHSVVLMLLLVFAFDNVDG**DEPGQTARDVDNGKFMSSLRSEGEAAPFFMAVEKR----KSCYERLCYED--CSGD--CACDLDGL-CYEFDEPWK
bru_a9.21	**MRLSTMHSVVLMLLLVFAFDNVDG**DEPGQTARDVDNGKFMSSLRSEGKPAPFFTPGEKR----HICSEGSCPND--CPSDR-CWCYSDTL-CGRWLPV
bru_j9.22	**MHLSGSAVLMLLLLFSLGVQS**GDVVNGQLTDNRRNLRSQWNQMSLFKSLDKR----------SCGGS-CFGG--CWPG--CSCYART--CFRD
bru_j9.23	**MHLSLAGSAVWMLLLLFALGNFVGVQP**GQITRDADNHINLRSQRKQVSR---------SLDKGSYCGQD-CSSDN-CPSG--CFCYPRDNVCYVERRKN
bru_j9.24	**MHLSLAGSAILMLLLLFTLSNFIGVQP**GQITGDVDNGQLTDNRRNLRSRWQPKALSKLFAIR--YCQQVPCRSDGGCGTG--CSCSSGS--CW
bru_j9.25	**MHLSLAGSAVLILLLLFAFGNFVGVQP**GDVDNGQLSDNSRNLRSWVKPSSFFRSLERK----RVLCPGE-CDPDRGCPSG--CYCYSLK--CWR
bru_j9.26	**MHLSLAGSAVLMLLLLFALGNFIGIQS**GDVDNRRNLESQWQRRSLFKTLAKR----------GVCKVH-CVGG--CPMG--CHCHHGH--CHHPDDESNHHPDGVHK
bru_j9.27	**MHLSLAGSAVLMLLLLFALGNFIGIQS**GDVDNRRNLQSLRKPMRLFKSLAKR----------WCVAP-CAGDPQCNIG--CSCNENGV-CEYNDVAW
bru_j9.28	**MHLSLAGSAVLMLLLLFALGNFIGIQS**GDVDNRRNLQSLRKPMSLFKSAGKR----------NPCTSYKCKGNGDCEPN--CVCRQS---CGDP
bru_j9.29	**MHLSLAGSAVLMLLLLFALGNFVGVQP**GQITRDVDNGQLTDNRRNLRSQWKQVSLFKSLDKK-TKCGQS-CASSA-CPSS--CSCSSKKI-CIRIWG
bru_j9.30	**MHLSLAGSAVWMLLLLFALGNFVGVQP**GQITRDADNHINLRSQRKQTSR---------SLYKGSNCGQD-CSSDN-CPSG--CFCYPAVGICFRKA
bru_j9.31	**MHLSPAGSAVLMFLLLCALG**DFIGVKPGQITRDVDNGQLTDNRRNLRSQWKQVSLFKSLDKK-TKCGQS-CASSA-CPSS--CSCSSKKI-CIRIWG
bru_j9.32	**----------MLLLLFALGNFVGVQS**GQITRDVDNGQLTDNRRNLQSQWQQSSLFKLLAKRR-MCPLL-CRGT--CPPG--CICRHGH--CYDSDF
bru_j9.33	**----------MLLLLFALGNFVGVQS**GQVTRDVDNGQLTDNRRNLQSQWNRLSLFKSLHKR-GTCGA--CGLG--CPRG--CSCAYRI--CWTS
bru_j9.34	**----------MLLLLFALGNFVGVQS**GQVTRDVDNGQLTDNRRNLRSQWNQMSLSKSLDKR-TLCGYS-CFSG--CPKG--CYCSVILL-CMVRHG
bru_j9.35	-----**MHSVILMLLLMFVFDNVDG**DEPGQTARDVDNRKLMSSLRSKGKPAAFFMPREKR----TVCSGKRCPTP--CHGR--CYCGPGNF-CIPWDYPGK
bru_j9.36	-----**MHSVILMVPLMFAFDNVDG**DEPGQTARDADNGKLMSILRSEGKPAPFFTPREKR----FDCTKIACSDA--CSYSNGCRCHFSKF-CGSWSGK
bru_j9.37	-----**MHSVILMVPLMFAFDNVDG**DEPGQTARDVDNGKFMSSLRSEGEAAPFFMAVEKR----KSCYERLCYED--CSGD--CACDLDGL-CYEIDEPWK

bruj9.38 -----**MHVSLAGSAVWMLLLLFALGNFVGVQP**GQITRDVDNGQLTDNHRNLRSLQKPVNLLTKRSCPGGWCIMPAHCAGT--CSCNWGF--CG
bruj9.39 **MRLSTMHSVILMLLLMFVFDNVDG**DDPGQTARDVDNRKLMSSLRSKGKPAAFFMPREKR----TVCSGKRCPTP--CHGR--CYCGPGNF-CIPWDYPGK

Table 7. P-superfamily precursor protein sequence mined from the transcriptomes of an adult and a juvenile C. brunneus specimen. Precursors from the adult and juvenile are denoted by a subscript "a" and "j", respectively. The precursor protein sequence contains the signal sequence (bold), pre-peptide sequence (not bold or underlined), and mature peptide sequence (underlined). The cysteines (red) are aligned to show the conserved cysteine framework IX among the P-superfamily precursor proteins found. Seven of the juvenile sequences are missing a portion of the signal sequence and therefore, incomplete due to the assembly.

Conotoxin	Monoisotopic Mass (Da) Experimental	Precursor	Mature Peptide
bru9a*ϕ	2531.865	bru_a9.1, bru_j9.22	------SCGGS-CFGG--CWOG--CSCYART--CFRD
bru9bϕ	4128.634	bru_a9.2	SLDKGSNCGQD-CSSDN-COSG--CFCYPRDNVCYVERRKN
bru9.3ϕ		bru_a9.3, bru_a9.7, bru_a9.13	------ACHLP-CYDG--CGSG--CHCHTRTYHCHRSY
bru9.4ϕ		bru_a9.4	------TCEGT-CFVDDQCHSH--CHCHTDNT-CSYPD
bru9.5ϕ		bru_a9.5	----RELCPGE-CDPDRGCPSG--CYCRWLR--CWRP
bru9.6		bru_a9.6, bru_a9.12, bru_a9.16	------HCWGGACSNESQCPHY--CHCGNEQH-CHRDV
bru9.7*		bru_a9.8, bru_j9.27	------WCVAP-CAGDPQCNIG--CSCNENGV-CEYNDVAW
bru9.8ϕ		bru_a9.9	-----RMCGAT-CYPFDDCPAN--CPCAPNGH-CARS
bru9.9*ϕ		bru_a9.10, bru_j9.33	-----GTCGA--CGLG--CPRG--CSCAYRI--CWTS
bru9.10		bru_a9.11	-----GTCGT--CAFG--CPGG--CTCAYRI--CWTS
bru9.11*		bru_a9.14, bru_a9.17, bru_j9.32	------MCPLL-CRGT--CPPG--CICRHGH--CYDSDF
bru9.12ϕ		bru_a9.15	------SCPGGWCIRPAHCAGT--CSCNRGF--CG
bru9.13*		bru_a9.18, bru_j9.26	-----GVCKVH-CVGG--CPMG--CHCHHGH--CHHPDDESNHHPDGVHK
bru9.14*		bru_a9.19, bru_j9.35, bru_j9.39	-----TVCSRKRCPTP--CHGR--CYCGPGNF-CIPWDYPGK
bru9.15		bru_a9.20	-----KSCYERLCYED--CSGD--CACDLDGL-CYEFDEPWK
bru9.16		bru_a9.21	-----HICSEGSCPND--CPSDR-CWCYSDTL-CGRWLPV
bru9.17ϕ		bru_j9.23	SLDKGSYCGQD-CSSDN-CPSG--CFCYPRDNVCYVERRKN
bru9.18ϕ		bru_j9.24	------YCQQVPCRSDGGCGTG--CSCSSGS--CW
bru9.19ϕ		bru_j9.25	----RVLCPGE-CDPDRGCPSG--CYCYSLK--CWR
bru9.20		bru_j9.28	-----NPCTSYKCKGNGDCEPN--CVCRQS---CGDP
bru9.21ϕ		bru_j9.29, bru_j9.31	-----TKCGQS-CASSA-CPSS--CSCSSKKI-CIRIWG
bru9.22ϕ		bru_j9.30	SLYKGSNCGQD-CSSDN-CPSG--CFCYPAVGICFRKA
bru9.23		bru_j9.36	-----FDCTKIACSDA--CSYSNGCRCHFSKF-CGSWSGK
bru9.24		bru_j9.37	-----KSCYERLCYED--CSGD--CACDLDGL-CYEIDEPWK
bru9.25ϕ		bru_j9.38	------SCPGGWCIMPAHCAGT--CSCNWGF--CG

*Table 8. Mature conotoxin sequences of the P-superfamily precursor proteins. All 25 sequences contain the cysteine framework IX cysteine arrangement. Six mature peptides were coded for in both the adult and the juvenile denoted by a superscript *. Sequence found in the MS/MS of the crude venom is indicated by ϕ several mature peptides were associated with multiple signal sequences as indicated in the "precursor" column*

Name	Precursor Signal Sequence
bru$_a$9.9	MHLSLAGSAVLMLLLLFALGNFVGVQP
bru$_j$9.29	MHLSLAGSAVLMLLLLFALGNFVGVQP
bru$_a$9.8	MHLSLAGSAVLMLLLLFALGNFVGVQP
bru$_a$9.7	MHLSLAGSAVLMLLLLFALGNFVGVQP
bru$_a$9.6	MHLSLAGSAVLMLLLLFALGNFVGVQP
bru$_a$9.2	MHLSLASSAVLMLLLLFALGNFVGVQP
bru$_j$9.23	MHLSLAGSAVWMLLLLFALGNFVGVQP
bru$_j$9.30	MHLSLAGSAVWMLLLLFALGNFVGVQP
bru$_j$9.38	MHVSLAGSAVWMLLLLFALGNFVGVQP
bru$_a$9.4	MHLSLAGSAVFMLLLLFALGNFVGVHP
bru$_a$9.5	MHLSLAGSAVLILLLLFAFGNFVGVQP
bru$_j$9.25	MHLSLAGSAVLILLLLFAFGNFVGVQP
bru$_a$9.15	MHVSLAGSAVLILLLLFALDNFVGVQP
bru$_a$9.10	MHLSLAGSAVLMLLLLFALGNFVGVQS
bru$_a$9.12	MHLSLAGSAVLMLLLLFALGNFVGVQS
bru$_a$9.11	MHLSLAGSAVLMLLLLFALGNFVGVQS
bru$_a$9.1	MHLS--GSAVLMLLLLFSLG----VQS
bru$_j$9.22	MHLS--GSAVLMLLLLFSLG----VQS
bru$_a$9.3	MHLS--GSAVLMLLLLFTLGNFIGIQS
bru$_a$9.16	MHAVL------MLLLLFALGNFVGVQ-
bru$_a$9.17	MHAVL------MLLLLFALGNFVGVQ-
bru$_a$9.18	MHAVL------MLLLLFAMGNFIGIQS
bru$_j$9.32	----------MLLLLFALGNFVGVQS
bru$_j$9.33	----------MLLLLFALGNFVGVQS
bru$_j$9.34	----------MLLLLFALGNFVGVQS
bru$_a$9.13	MHLSLAGSAVLMLLLPFALG-------
bru$_a$9.14	MHLSLAGSAVLMLLLPFALG-------
bru$_j$9.26	MHLSLAGSAVLMLLLLFALGNFIGIQS
bru$_j$9.27	MHLSLAGSAVLMLLLLFALGNFIGIQS
bru$_j$9.28	MHLSLAGSAVLMLLLLFALGNFIGIQS
bru$_j$9.31	MHLSPAGSAVLMFLLLCALG-------
bru$_j$9.24	MHLSLAGSAILMLLLLFTLSNFIGVQP
bru$_a$9.19	MRLSTMHSVILMLLLMFVFDNVDG---
bru$_j$9.39	MRLSTMHSVILMLLLMFVFDNVD----
bru$_a$9.20	MRLSTMHSVVLMLLLVFAFDNVD----
bru$_a$9.21	MRLSTMHSVVLMLLLVFAFDNVDGD--
bru$_j$9.35	----------MHSVILMLLLMFVFDNVDG---
bru$_j$9.36	----------MHSVILMVPLMFAFDNVD----
bru$_j$9.37	----------MHSVILMVPLMFAFDNVDG---

Table 9. Signal sequence homology among the P-superfamily precursor proteins. The signal sequences have been aligned to show the conserved residues (highlighted aqua and gray).

6.3.3 Size-exclusion HPLC of crude venom

Eleven fractions were collected over 60 minutes. Most of the P-superfamily conotoxins eluted in fraction 6-8 (Figure 27). The fractions were reduced, modified, and digested based on the fraction elution time. Fractions 1-5 were considered the higher

molecular weight containing fractions and 6-11 were considered the lower molecular weight containing fractions.

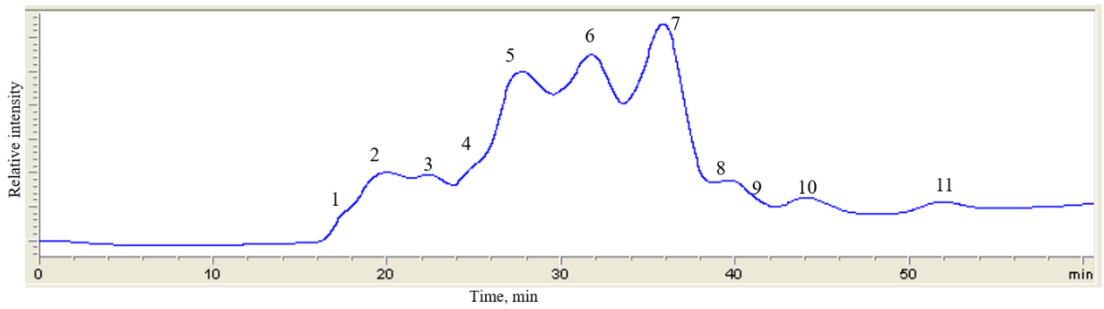

Figure 27. Size-exclusion HPLC of crude C. brunneus venom. P-superfamily conotoxins bru9a and bru9b elute in peaks seven and six, respectively.

6.3.4 LC-MS/MS of size exclusion fractions

The MS/MS spectra from the LC-MS/MS (Figure 28) of the peptide fractions were collected and are summarized in

Table 10. Each fraction's spectra were compared to both the Adult and Juvenile specimen's transcriptome for matches. The number of precursor hits represents the number of transcripts that had at least one spectra sequence match. The peptide spectral matches were used to match the spectra sequence matches to the precursor protein.

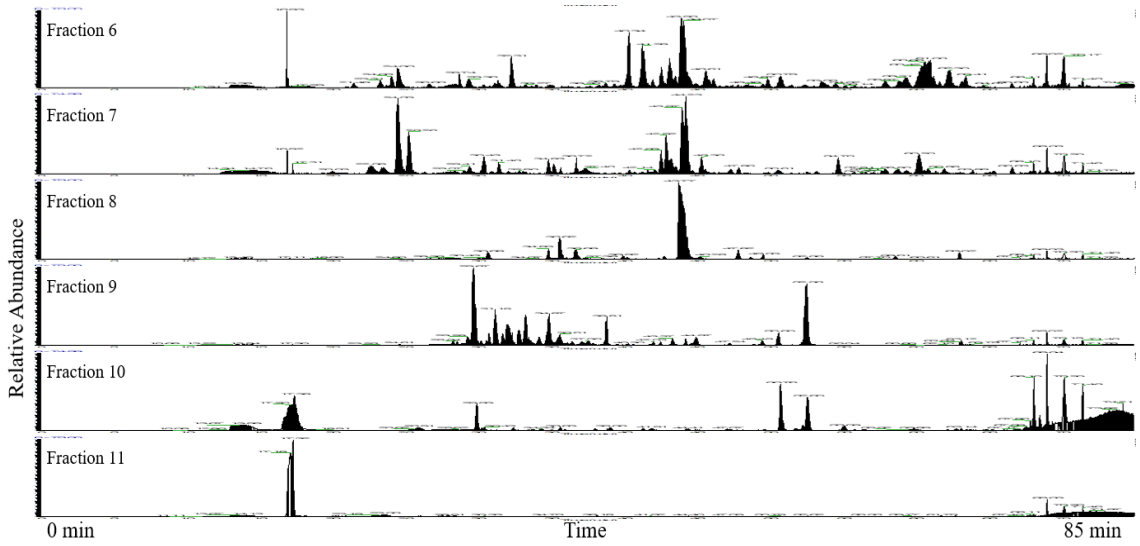

Figure 28. LC-MS/MS chromatograms of the SE-HPLC peptide fractions of C. brunneus.

			Adult	Juvenile	
Fraction	MS/MS Spectra	Precursor Hits	Peptide Spectral Matches	Precursor Hits	Peptide Spectral Matches
6	35209	37	141	39	897
7	32983	25	120	16	129
8	26567	29	84	18	55
9	30055	21	41	9	612
10	20149	16	26	12	38
11	18793	15	40	8	14

Table 10. LC-MS/MS results for reduced and alkylated peptide fractions against the two transcriptomes.

6.3.5 Identification of P-superfamily conotoxins in the crude venom

Of the 39 P-superfamily transcripts found within the two transcriptomes, 18 had MS/MS sequence hits in Proteome Discoverer (PD). The 17 transcript hits corresponded to 11 mature conotoxin sequences, two sequences (bru9a and bru9.9) were found in both the adult and juvenile in the PD hits. The other mature conotoxins that were found in the crude venom extract were bru9b, bru9.3, bru9.8, bru9.12, bru9.17, bru9.18, bru9.19, bru9.21, and bru9.25 (

Table 10 and Table 11).

Accession number	Precursor	Conotoxin	Confirmed mature peptide sequence
TRINITY_DN33088_c4_g1_i1_2	bru_a9.1	bru9a	------SCGGS-CFGG--CWOG--CSCYART--CFRD
TRINITY_DN49783_c7_g2_i1_4	bru_j9.22	bru9a	------SCGGS-CFGG--CWOG--CSCYART--CFRD
TRINITY_DN36669_c4_g12_i1_4	bru_a9.2	bru9b	SLDKGSNCGQD-CSSDN-COSG--CFCYORDNVCYVERRKN
TRINITY_DN36851_c9_g6_i20_1	bru_a9.3	bru9.3	------ACHLO-CYDG--CGSG--CHCHTRTYHCHRSY
TRINITY_DN36851_c9_g6_i4_1	bru_a9.13	bru9.3	------ACHLO-CYDG--CGSG--CHCHTRTYHCHRSY
TRINITY_DN36851_c9_g6_i7_1	bru_a9.7	bru9.3	------ACHLO-CYDG--CGSG--CHCHTRTYHCHRSY
TRINITY_DN36851_c9_g6_i21_1	bru_a9.9	bru9.8	-----RMCGAT-CYOFDDCOAN--COCAONGH-CARS
TRINITY_DN36851_c9_g6_i17_1	bru_a9.10	bru9.9	-----GTCGA--CGLG--CPRG--CSCAYRI--CWTS
TRINITY_DN45319_c2_g1_i1_2	bru_j9.33	bru9.9	-----GTCGA--CGLG--CPRG--CSCAYRI--CWTS
TRINITY_DN33088_c0_g1_i1_3	bru_a9.15	bru9.12	------SCPGGWCIROAHCAGT--CSCNRGF--C*
TRINITY_DN49325_c7_g1_i8_1	bru_j9.23	bru9.17	SLDKGSYCGQD-CSSDN-COSG--CFCYORDNVCYVERRKN
TRINITY_DN41173_c2_g1_i1_1	bru_j9.24	bru9.18	------YCQQVOCRSDGGCGTG--CSCSSGS--CW
TRINITY_DN49325_c7_g1_i2_1	bru_j9.25	bru9.19	----RVLCOGE-CDODRGCOSG--CYCYSLK--CWR
TRINITY_DN49325_c7_g1_i12_1	bru_j9.29	bru9.21	-----TKCGQS-CASSA-COSS--CSCSSKKI-CIRIW*
TRINITY_DN49325_c7_g1_i17_1	bru_j9.31	bru9.21	-----TKCGQS-CASSA-COSS--CSCSSKKI-CIRIW*
TRINITY_DN49325_c7_g1_i9_1	bru_j9.38	bru9.21	-----TKCGQS-CASSA-COSS--CSCSSKKI-CIRIW*
TRINITY_DN49325_c7_g1_i10_1	bru_j9.38	bru9.25	------SCOGGWCIMOAHCAGT--CSCNWGF--CG

*Table 11. Confirmed P-superfamily conotoxins present in C. brunneus crude venom. O indicates hydroxyproline and *indicates amidated C-terminal*

6.4 Discussion

Thirty-nine P-superfamily precursor proteins were found within the two *C. brunneus* transcriptomes. Two of the 39 have been isolated and sequenced using Edman degradation, bru9a[69] and bru9b[70]. Six of the unique mature conotoxins were present in both the adult and the juvenile: bru9a, bru9.7, bru9.9, bru9.11, bru9.13, and bru9.14. The discrepancy between the number of total precursor proteins and mature conotoxins is due to several different signal sequences signaling for the same mature conotoxin. This could be an evolutional advantage to the cone snail. If more than one gene encodes for an important venom component, then a single genetic mutation would not have catastrophic effects for the snail.

Although there does not appear to be a defined and distinct signal sequence for all of the P-superfamily conotoxins, there are some residues that are conserved throughout. The aligned signal sequences (Table 9) show a conserved block of Met and Leu in the center of the sequence. The first several residues of the sequence also have a high homology among the protein precursors. Six of the juvenile precursor proteins are missing several of the first coding residues of the signal sequence that is denoted by the dashes in

Table *7* and Table 8, this appears to be a shortcoming of the assembly process.

Only two of these P-superfamily conotoxins had been isolated in large enough quantitates to sequence by Edman degradation. These data suggest that either our previous isolation methods selected against P-superfamily conotoxins, or that the snails possess the ability to synthesize many different conotoxins and do so based on selective regulation. Through high-resolution MS/MS, we were able to confirm the presence of 17 P-superfamily transcripts containing the mature sequence of 11 conotoxins in the crude venom of *C. brunneus*. Two of these sequences were previously described in the Marí lab, but nine of these sequences are novel P-superfamily framework IX conotoxins.

P-superfamily conotoxins are interesting because they often contain a cysteine knot that has the same covalent arrangement as the plant cyclotides discussed previously. Cysteine knot containing peptides have been shown to resist degradation from both thermal and enzymatic means. Due to their increased stability, cysteine knot containing peptides are attractive leads to use as a scaffold or for grafting a biologically active sequence or compound to the backbone. Regardless of their biological activity, the discovery of novel cysteine knot containing peptides is beneficial to the field of peptide modification for drug delivery by providing more knottin options.

CHAPTER 7: CONCLUSIONS

This work presented the isolation and *in vivo* characterization of six conotoxins and three cyclotides in *D. melanogaster*, the *in vitro* functional characterization of two new α-conotoxins in *Xenopus* oocytes, the assembly of two new *Conus* transcriptomes, and the discovery of nine new P-superfamily conotoxins.

Peptides are desirable for their ability to mimic endogenous pathways. Insulin, one of the first therapeutic peptides, has been used as a treatment for diabetes patients since the 1920s. Since then, other therapeutic peptides such as oxytocin and vasopressin have been used clinically. Peptides are superior to small molecules in their binding potency and selective modulation of their targets. Small molecules often have side effects due to non-specific binding and drug counter interactions. Peptides have some challenges to overcome in order to compete with traditionally small molecule drugs. They have relatively poor plasma stability and low oral availability due to peptidases and they are quickly excreted from the system.

Animal venoms are a relatively unexplored repertoire of biologically active peptides. Venoms consist of a complex cocktail of proteins, peptides, and small molecules. The components have targeted specificity towards ion channels and receptors creating a disruption in the nervous, cardiovascular, and neuromuscular systems. The high specificity of the venom components for their target has increased the interest to use them as pharmacological tools and in drug development.

Venom peptides are often disulfide constrained. Disulfide bonds are covalent bonds that aid in the structure and function of a peptide or protein. Reducing existing disulfide bonds and blocking them from reforming can decrease stability [137] and affect ligand-binding abilities [138]. In theory, having more disulfide linkages would increase a folded peptide's stability. A disulfide bond can contribute 2.5-3.5 kcal/mol towards structural stabilization [56]. Conotoxins, by definition, are disulfide-rich peptides in the venom of cone snails. The structural stability of conotoxins, as well as their functional selectivity are two of their properties that have aided in their popularity as drugs, drug leads, and molecular probes.

Cysteine knot containing peptides are highly resistant to degradation from both high temperatures and proteolytic enzymes. Some conotoxins contain a cysteine knot, but all cyclotides have the three disulfide bonds need to form the knot. The structural stability of both conotoxins and cyclotides have made them interesting as scaffolds for designing functional peptides [25, 35, 139]. Synthetic peptides can be designed to incorporate non-natural amino acids or add modifications onto the backbone to increase bioavailability. Peptide drug development is most popular in some of man's most prevalent diseases: cancer, cardiovascular, metabolic, and pain disorders. Sixty-eight peptide therapeutics have been approved worldwide and there are 155 peptide drugs in clinical development. The market for peptide drugs is expected to grow from $21.5 billion in 2016 to $48.1 billion globally in the next decade.

The traditional method of bioactivity-guided fractionation to discover conotoxins is time-consuming and requires large quantities of venom. There were also issues related to dynamic range and number of venom components that made identification of venom

components difficult. The application of venom proteomics to cone snails has increased the number of identifiable conotoxins by ten-fold per species [140]. The integration of transcriptomics, genomics, and bioinformatics has improved venom studies by decreasing the amount of sample required while also the time and money invested in the discovery of new conotoxins. Omics can be used to identify peptides with unusual or multiple PTMs. It has been shown that up to 75% of the amino acids within a conotoxin may be modified [57].Genomics has also aided in the identification and characterization of ion channels and receptors which has given researchers a better idea of how the peptide and biological target are interacting.

This work included both *in vivo* and *in vitro* experiments. Both approaches have their benefits and drawbacks. Generally, *in vivo* experiments are preferred because a complete system is used, but that is also a drawback. The exact effect can be difficult to isolate. The dosing amount may also vary between specimens due to size and variation in metabolism. *In vitro* experiments can be designed to be extremely targeted and to be high-throughput, but it is an isolated system that may not behave the same as it would in its natural environment. Here, using an *in vitro* assay allowed us to evaluate vertebrate nAChRs without the difficulties and ethical issues associated with working with live animals or humans.

D. melanogaster is a model organism used in drug screening. It is attractive to scientists for its small size, rapid reproduction, ease of care, well-mapped genetics, and short life cycle. However, there are issues with performing experiments on an invertebrate, even as a model organism, and drawing conclusions that will transfer to humans. Often the absorption, distribution, metabolism, excretion, and toxicity of a drug in a non-human

model do not transfer to humans causing the high failure rate of clinical trials. There is variation in the types of channels and receptors expressed in vertebrates versus invertebrates. One example of this are the subunits of the nAChR. There are 10 types of subunits in vertebrates that are activated by acetylcholine, α2-7, α9, α10, and β2-4 [141]. The invertebrate *D. melanogaster* also has 10 subunits Dα1-7 and Dβ1-3 [142]. The Dα5-7 subunits have the greatest homology to the vertebrate α7 nAChR [143]. Even though *Drosophila* possesses similar basic physiological processes found in humans, it has been determined that there can be variation in the sequences of the binding pockets, as is the case for the nAChRs between vertebrates and invertebrates as shown by Heghinian et al. [101]. Considering that the fly has an open nervous system, blood-brain barrier permeability may pose issues later down the development line when tested in mammals. Due to the issues discussed above, the fly is a fantastic model organism for initial drug screening, but these effects might not be directly transferred to humans or even other model organisms; the appropriate correlations have to be made and supported with experimental evidence.

It is possible that the reason the P-superfamily conotoxins were not active in the *D. melanogaster* GFS is due to the absence of their biological target in the fly nervous system. For this reason, it is suggested that these conotoxins be evaluated in other types of assays. Some areas to consider for activity would be the immune and hemostasis systems. The P-superfamily conotoxins may be affecting the clotting abilities of their prey to facilitate the distribution of the venom throughout the body. To the best of our knowledge, there have not been any hemolysis or clotting experiments done with P-superfamily conotoxins.

Another member of the Marí lab has recently discovered that conotoxins from the venom duct of *Conus nux* have anti-malarial activities. It would be interesting to test both the P-superfamily conotoxins of *C. brunneus* and the cyclotides of *V. tricolor* in this assay to evaluate their possible anti-malarial activities.

It has been shown that some cyclotides may have surfactant-like activity on lipid membranes causing an increase in membrane conduction and capacitance [144]. This type of activity may better explain the disruption seen in the GFS by *V. tricolor* cyclotides. For this reason, it would be advantageous to perform electrical impedance spectroscopy experiments to determine if the same activity applies to the cyclotides of *V. tricolor*. That data combined with the neurological data from the GFS could help determine the target of cyclotides or if their activity is simply due to their association with membranes. Due to the increase in membrane resistance caused by the conotoxin gm9a, it would also be interesting to evaluate gm9a in this assay as well.

Cysteine-knot containing peptides, like P-superfamily conotoxins and cyclotides (Chapters 2-4 and 6), are remarkable peptidic natural products as these scaffolds are well suited for drug design and delivery. While their native targets remain elusive, it is important to recognize that using peptide engineering, new non-intended applications of these compounds can be devised. The chemical and biological characterization of conotoxins remains an expanding field. Several assays were described in their ability to identify biological targets and specificity of conotoxins (Chapters 2-5). This work also highlights the importance of high-resolution tandem mass spectrometry in the venomics studies as seen by the results in Chapter 6. The integration of LC-MS/MS coupled to transcriptomic analysis and bioinformatics workflows will aid in the elucidation of the complex cone snail

venom. It is hoped that his work has helped emphasize the important role of disulfide-constrained peptides, as well as the venom of a unique specimen, the cone snail, for the discovery of molecular probes and novel therapeutic treatments.

REFERENCES

1. Puillandre, N., et al., *Molecular phylogeny and evolution of the cone snails (Gastropoda, Conoidea).* Mol Phylogenet Evol, 2014. **78**: p. 290-303.
2. Rodriguez, A.M., et al., *Intraspecific variations in Conus purpurascens injected venom using LC/MALDI-TOF-MS and LC-ESI-TripleTOF-MS.* Anal Bioanal Chem, 2015. **407**(20): p. 6105-16.
3. Olivera, B.M., et al., *Prey-Capture Strategies of Fish-Hunting Cone Snails: Behavior, Neurobiology and Evolution.* Brain Behav Evol, 2015. **86**(1): p. 58-74.
4. Gray, W.R., et al., *Peptide toxins from Conus geographus venom.* J Biol Chem, 1981. **256**(10): p. 4734-40.
5. Robinson, S.D. and R.S. Norton, *Conotoxin gene superfamilies.* Mar Drugs, 2014. **12**(12): p. 6058-101.
6. Woodward, S.R., et al., *Constant and hypervariable regions in conotoxin propeptides.* Embo j, 1990. **9**(4): p. 1015-20.
7. Kaas, Q., J.C. Westermann, and D.J. Craik, *Conopeptide characterization and classifications: an analysis using ConoServer.* Toxicon, 2010. **55**(8): p. 1491-509.
8. Kerr, L.M. and D. Yoshikami, *A venom peptide with a novel presynaptic blocking action.* Nature, 1984. **308**(5956): p. 282-4.
9. McGivern, J.G., *Targeting N-type and T-type calcium channels for the treatment of pain.* Drug Discov Today, 2006. **11**(5-6): p. 245-53.

10. Miljanich, G.P., *Ziconotide: neuronal calcium channel blocker for treating severe chronic pain.* Curr Med Chem, 2004. **11**(23): p. 3029-40.

11. Wang, Y.X., et al., *Interactions of intrathecally administered ziconotide, a selective blocker of neuronal N-type voltage-sensitive calcium channels, with morphine on nociception in rats.* Pain, 2000. **84**(2-3): p. 271-81.

12. Gran, L., *Oxytocic principles of Oldenlandia affinis.* Lloydia, 1973. **36**(2): p. 174-8.

13. Gran, L., K. Sletten, and L. Skjeldal, *Cyclic peptides from Oldenlandia affinis DC. Molecular and biological properties.* Chem Biodivers, 2008. **5**(10): p. 2014-22.

14. Gruber, C.W., et al., *Distribution and evolution of circular miniproteins in flowering plants.* Plant Cell, 2008. **20**(9): p. 2471-83.

15. Colgrave, M.L. and D.J. Craik, *Thermal, chemical, and enzymatic stability of the cyclotide kalata B1: the importance of the cyclic cystine knot.* Biochemistry, 2004. **43**(20): p. 5965-75.

16. Jennings, C., et al., *Biosynthesis and insecticidal properties of plant cyclotides: the cyclic knotted proteins from Oldenlandia affinis.* Proc Natl Acad Sci U S A, 2001. **98**(19): p. 10614-9.

17. Gillon, A.D., et al., *Biosynthesis of circular proteins in plants.* Plant J, 2008. **53**(3): p. 505-15.

18. Serra, A., et al., *A high-throughput peptidomic strategy to decipher the molecular diversity of cyclic cysteine-rich peptides.* Sci Rep, 2016. **6**: p. 23005.

19. Hellinger, R., et al., *Peptidomics of Circular Cysteine-Rich Plant Peptides: Analysis of the Diversity of Cyclotides from Viola tricolor by Transcriptome and Proteome Mining.* J Proteome Res, 2015. **14**(11): p. 4851-62.

20. Barbeta, B.L., et al., *Plant cyclotides disrupt epithelial cells in the midgut of lepidopteran larvae.* Proc Natl Acad Sci U S A, 2008. **105**(4): p. 1221-5.

21. Cascales, L., et al., *Identification and characterization of a new family of cell-penetrating peptides: cyclic cell-penetrating peptides.* J Biol Chem, 2011. **286**(42): p. 36932-43.

22. Huang, Y.H., et al., *The biological activity of the prototypic cyclotide kalata b1 is modulated by the formation of multimeric pores.* J Biol Chem, 2009. **284**(31): p. 20699-707.

23. Mulvenna, J.P., C. Wang, and D.J. Craik, *CyBase: a database of cyclic protein sequence and structure.* Nucleic Acids Res, 2006. **34**(Database issue): p. D192-4.

24. Wang, C.K., et al., *CyBase: a database of cyclic protein sequences and structures, with applications in protein discovery and engineering.* Nucleic Acids Res, 2008. **36**(Database issue): p. D206-10.

25. Wong, C.T., et al., *Orally active peptidic bradykinin B1 receptor antagonists engineered from a cyclotide scaffold for inflammatory pain treatment.* Angew Chem Int Ed Engl, 2012. **51**(23): p. 5620-4.

26. Jones, R.M. and G. Bulaj, *Conotoxins - new vistas for peptide therapeutics.* Curr Pharm Des, 2000. **6**(12): p. 1249-85.

27. Mir, R., et al., *Conotoxins: Structure, Therapeutic Potential and Pharmacological Applications.* Curr Pharm Des, 2016. **22**(5): p. 582-9.

28. Grand View Research, I., *Peptide Therapeutics Market By Application (Cancer, Cardiovascular Disorder, Metabolic Disorder, Respiratory Disorder, Pain, Dermatology), By Type (Generic, Innovative) By Type of Manufacturers (In-house, Outsourced), And Segment Forecasts, 2014 - 2025*. 2017. p. 85.

29. Lau, J.L. and M.K. Dunn, *Therapeutic peptides: Historical perspectives, current development trends, and future directions.* Bioorg Med Chem, 2017.

30. King, G.F., *Venoms as a platform for human drugs: translating toxins into therapeutics.* Expert Opin Biol Ther, 2011. **11**(11): p. 1469-84.

31. Terlau, H. and B.M. Olivera, *Conus venoms: a rich source of novel ion channel-targeted peptides.* Physiol Rev, 2004. **84**(1): p. 41-68.

32. Miles, L.A., et al., *Structure of a novel P-superfamily spasmodic conotoxin reveals an inhibitory cystine knot motif.* J Biol Chem, 2002. **277**(45): p. 43033-40.

33. Conibear, A.C., et al., *Approaches to the stabilization of bioactive epitopes by grafting and peptide cyclization.* Biopolymers, 2016. **106**(1): p. 89-100.

34. D'Souza, C., et al., *Using the MCoTI-II Cyclotide Scaffold To Design a Stable Cyclic Peptide Antagonist of SET, a Protein Overexpressed in Human Cancer.* Biochemistry, 2016. **55**(2): p. 396-405.

35. Akcan, M., et al., *Transforming conotoxins into cyclotides: Backbone cyclization of P-superfamily conotoxins.* Biopolymers, 2015. **104**(6): p. 682-92.

36. Adams, M.D., et al., *The genome sequence of Drosophila melanogaster.* Science, 2000. **287**(5461): p. 2185-95.

37. Bier, E., *Drosophila, the golden bug, emerges as a tool for human genetics.* Nat Rev Genet, 2005. **6**(1): p. 9-23.

38. Reiter, L.T., et al., *A systematic analysis of human disease-associated gene sequences in Drosophila melanogaster.* Genome Res, 2001. **11**(6): p. 1114-25.

39. Dzitoyeva, S., N. Dimitrijevic, and H. Manev, *Gamma-aminobutyric acid B receptor 1 mediates behavior-impairing actions of alcohol in Drosophila: adult RNA interference and pharmacological evidence.* Proc Natl Acad Sci U S A, 2003. **100**(9): p. 5485-90.

40. McClung, C. and J. Hirsh, *Stereotypic behavioral responses to free-base cocaine and the development of behavioral sensitization in Drosophila.* Curr Biol, 1998. **8**(2): p. 109-12.

41. Nichols, C.D. and E. Sanders-Bush, *A single dose of lysergic acid diethylamide influences gene expression patterns within the mammalian brain.* Neuropsychopharmacology, 2002. **26**(5): p. 634-42.

42. Torres, G. and J.M. Horowitz, *Activating properties of cocaine and cocaethylene in a behavioral preparation of Drosophila melanogaster.* Synapse, 1998. **29**(2): p. 148-61.

43. Mejia, M., et al., *A novel approach for in vivo screening of toxins using the Drosophila Giant Fiber circuit.* Toxicon, 2010. **56**(8): p. 1398-407.

44. Finelli, A., et al., *A model for studying Alzheimer's Abeta42-induced toxicity in Drosophila melanogaster.* Mol Cell Neurosci, 2004. **26**(3): p. 365-75.

45. Feany, M.B. and W.W. Bender, *A Drosophila model of Parkinson's disease.* Nature, 2000. **404**(6776): p. 394-8.

46. Gunawardena, S., et al., *Disruption of axonal transport by loss of huntingtin or expression of pathogenic polyQ proteins in Drosophila.* Neuron, 2003. **40**(1): p. 25-40.

47. Quinn, W.G., W.A. Harris, and S. Benzer, *Conditioned behavior in Drosophila melanogaster.* Proc Natl Acad Sci U S A, 1974. **71**(3): p. 708-12.

48. Tully, T. and W.G. Quinn, *Classical conditioning and retention in normal and mutant Drosophila melanogaster.* J Comp Physiol A, 1985. **157**(2): p. 263-77.

49. Nestler, E.J. and S.E. Hyman, *Animal models of neuropsychiatric disorders.* Nat Neurosci, 2010. **13**(10): p. 1161-9.

50. Allen, M.J. and T.A. Godenschwege, *Electrophysiological recordings from the Drosophila giant fiber system (GFS).* Cold Spring Harb Protoc, 2010. **2010**(7): p. pdb.prot5453.

51. Allen, M.J., et al., *Making an escape: development and function of the Drosophila giant fibre system.* Semin Cell Dev Biol, 2006. **17**(1): p. 31-41.

52. Mejia, M., et al., *Paired nanoinjection and electrophysiology assay to screen for bioactivity of compounds using the Drosophila melanogaster giant fiber system.* J Vis Exp, 2012(62).

53. Resing, K.A. and N.G. Ahn, *Proteomics strategies for protein identification.* FEBS Letters, 2005. **579**(4): p. 885-889.

54. Kaas, Q., et al., *ConoServer, a database for conopeptide sequences and structures.* Bioinformatics, 2008. **24**(3): p. 445-6.

55. Liang, K.-H., *3 - Transcriptomics*, in *Bioinformatics for Biomedical Science and Clinical Applications*. 2013, Woodhead Publishing. p. 49-82.

56. Calvete, J.J., *Venomics: integrative venom proteomics and beyond.* Biochem J, 2017. **474**(5): p. 611-634.

57. Gerwig, G.J., et al., *Glycosylation of conotoxins.* Mar Drugs, 2013. **11**(3): p. 623-42.

58. Buczek, O., G. Bulaj, and B.M. Olivera, *Conotoxins and the posttranslational modification of secreted gene products.* Cell Mol Life Sci, 2005. **62**(24): p. 3067-79.

59. Lirazan, M.B., et al., *The spasmodic peptide defines a new conotoxin superfamily.* Biochemistry, 2000. **39**(7): p. 1583-8.

60. Fainzilber, M., et al., *gamma-Conotoxin-PnVIIA, a gamma-carboxyglutamate-containing peptide agonist of neuronal pacemaker cation currents.* Biochemistry, 1998. **37**(6): p. 1470-7.

61. Fainzilber, M., et al., *Mollusc-specific toxins from the venom of Conus textile neovicarius.* Eur J Biochem, 1991. **202**(2): p. 589-95.

62. Rigby, A.C., et al., *A conotoxin from Conus textile with unusual posttranslational modifications reduces presynaptic Ca2+ influx.* Proc Natl Acad Sci U S A, 1999. **96**(10): p. 5758-63.

63. Buczek, O., et al., *Structure and sodium channel activity of an excitatory I1-superfamily conotoxin.* Biochemistry, 2007. **46**(35): p. 9929-40.

64. Terlau, H., et al., *Strategy for rapid immobilization of prey by a fish-hunting marine snail.* Nature, 1996. **381**(6578): p. 148-51.

65. Cruz, L.J., et al., *Conus geographus toxins that discriminate between neuronal and muscle sodium channels.* J Biol Chem, 1985. **260**(16): p. 9280-8.

66. Sharpe, I.A., et al., *Two new classes of conopeptides inhibit the alpha1-adrenoceptor and noradrenaline transporter.* Nat Neurosci, 2001. **4**(9): p. 902-7.

67. England, L.J., et al., *Inactivation of a serotonin-gated ion channel by a polypeptide toxin from marine snails.* Science, 1998. **281**(5376): p. 575-8.

68. Petrel, C., et al., *Identification, structural and pharmacological characterization of tau-CnVA, a conopeptide that selectively interacts with somatostatin sst3 receptor.* Biochem Pharmacol, 2013. **85**(11): p. 1663-71.

69. Pflueger, F.C., *Isolation and characterization of novel conopeptides from the marine cone snail Conus brunneus*, in *Chemistry and Biochemistry* 2008, Florida Atantic University Boca Raton, FL.

70. Bushman, M.M., *Isolation and Characterization of Novel Conopeptides from the Venom of Conus brunneus*, in *Chemistry and Biochemistry*. 2010, Florida Atlantic University Boca Raton, FL p. 76.

71. Wilkins, M.R., et al., *Protein identification and analysis tools in the ExPASy server.* Methods Mol Biol, 1999. **112**: p. 531-52.

72. Augustin, H., M.J. Allen, and L. Partridge, *Electrophysiological recordings from the giant fiber pathway of D. melanogaster.* J Vis Exp, 2011(47).

73. Lee, D. and D.K. O'Dowd, *Fast excitatory synaptic transmission mediated by nicotinic acetylcholine receptors in Drosophila neurons.* J Neurosci, 1999. **19**(13): p. 5311-21.

74. Puttamadappa, S.S., et al., *Backbone dynamics of cyclotide MCoTI-I free and complexed with trypsin.* Angew Chem Int Ed Engl, 2010. **49**(39): p. 7030-4.

75. Gustafson, K.R., et al., *Circulins A and B. Novel human immunodeficiency virus (HIV)-inhibitory macrocyclic peptides from the tropical tree Chassalia parvifolia.* Journal of the American Chemical Society, 1994. **116**(20): p. 9337-9338.

76. Tam, J.P., et al., *An unusual structural motif of antimicrobial peptides containing end-to-end macrocycle and cystine-knot disulfides.* Proc Natl Acad Sci U S A, 1999. **96**(16): p. 8913-8.

77. Lindholm, P., et al., *Cyclotides: a novel type of cytotoxic agents.* Mol Cancer Ther, 2002. **1**(6): p. 365-9.

78. Jennings, C.V., et al., *Isolation, solution structure, and insecticidal activity of kalata B2, a circular protein with a twist: do Mobius strips exist in nature?* Biochemistry, 2005. **44**(3): p. 851-60.

79. Colgrave, M.L., et al., *Cyclotides: natural, circular plant peptides that possess significant activity against gastrointestinal nematode parasites of sheep.* Biochemistry, 2008. **47**(20): p. 5581-9.

80. Colgrave, M.L., et al., *The anthelmintic activity of the cyclotides: natural variants with enhanced activity.* Chembiochem, 2008. **9**(12): p. 1939-45.

81. Craik, D.J., et al., *Plant cyclotides: A unique family of cyclic and knotted proteins that defines the cyclic cystine knot structural motif.* J Mol Biol, 1999. **294**(5): p. 1327-36.

82. Heghinian, M., *Discovery and biological characterization of conotoxins from the venom of Conus brunneus in Drosophila melanogaster*, in *Chemistry and Biochemistry*. 2014, Florida Atlantic University: Boca Raton, FL, USA.

83. MacMillan, H.A. and B.N. Hughson, *A high-throughput method of hemolymph extraction from adult Drosophila without anesthesia.* J Insect Physiol, 2014. **63**: p. 27-31.

84. Pinto, M.F., et al., *Identification and structural characterization of novel cyclotide with activity against an insect pest of sugar cane.* J Biol Chem, 2012. **287**(1): p. 134-47.

85. Claeson, P., et al., *Fractionation Protocol for the Isolation of Polypeptides from Plant Biomass.* J Nat Prod, 1998. **61**(1): p. 77-81.

86. Stromstedt, A.A., et al., *Selective membrane disruption by the cyclotide kalata B7: complex ions and essential functional groups in the phosphatidylethanolamine binding pocket.* Biochim Biophys Acta, 2016. **1858**(6): p. 1317-27.

87. Robinson, S.D., et al., *The Venom Repertoire of Conus gloriamaris (Chemnitz, 1777), the Glory of the Sea.* Mar Drugs, 2017. **15**(5).

88. Hasson, A., et al., *Alterations of voltage-activated sodium current by a novel conotoxin from the venom of Conus gloriamaris.* J Neurophysiol, 1995. **73**(3): p. 1295-301.

89. Robinson, S.D., et al., *Diversity of conotoxin gene superfamilies in the venomous snail, Conus victoriae.* PLoS One, 2014. **9**(2): p. e87648.

90. von Reyn, C.R., et al., *A spike-timing mechanism for action selection.* Nat Neurosci, 2014. **17**(7): p. 962-70.

91. Maimon, G., A.D. Straw, and M.H. Dickinson, *Active flight increases the gain of visual motion processing in Drosophila.* Nat Neurosci, 2010. **13**(3): p. 393-9.

92. Anthis, N.J. and G.M. Clore, *Sequence-specific determination of protein and peptide concentrations by absorbance at 205 nm.* Protein Sci, 2013. **22**(6): p. 851-8.

93. Gouwens, N.W. and R.I. Wilson, *Signal propagation in Drosophila central neurons.* J Neurosci, 2009. **29**(19): p. 6239-49.

94. Akondi, K.B., et al., *Discovery, synthesis, and structure-activity relationships of conotoxins.* Chem Rev, 2014. **114**(11): p. 5815-47.

95. Lewis, R.J., et al., *Conus venom peptide pharmacology.* Pharmacol Rev, 2012. **64**(2): p. 259-98.

96. Marí, F. and J. Tytgat, *2.15 - Natural Peptide Toxins*, in *Comprehensive Natural Products II*. 2010, Elsevier: Oxford. p. 511-538.

97. Biass, D., et al., *Comparative proteomic study of the venom of the piscivorous cone snail Conus consors.* J Proteomics, 2009. **72**(2): p. 210-8.

98. Lebbe, E.K., et al., *Conotoxins targeting nicotinic acetylcholine receptors: an overview.* Mar Drugs, 2014. **12**(5): p. 2970-3004.

99. McIntosh, J.M., A.D. Santos, and B.M. Olivera, *Conus peptides targeted to specific nicotinic acetylcholine receptor subtypes.* Annu Rev Biochem, 1999. **68**: p. 59-88.

100. Cuny, H., et al., *alpha-Conotoxins active at alpha3-containing nicotinic acetylcholine receptors and their molecular determinants for selective inhibition.* Br J Pharmacol, 2017.

101. Heghinian, M.D., et al., *Inhibition of cholinergic pathways in Drosophila melanogaster by alpha-conotoxins.* Faseb j, 2015. **29**(3): p. 1011-8.

102. Quik, M., et al., *Alpha7 nicotinic receptors as therapeutic targets for Parkinson's disease.* Biochem Pharmacol, 2015. **97**(4): p. 399-407.

103. Taly, A. and S. Charon, *alpha7 nicotinic acetylcholine receptors: a therapeutic target in the structure era.* Curr Drug Targets, 2012. **13**(5): p. 695-706.

104. Valles, A.S. and F.J. Barrantes, *Chaperoning alpha7 neuronal nicotinic acetylcholine receptors.* Biochim Biophys Acta, 2012. **1818**(3): p. 718-29.

105. Castro, J., et al., *alpha-Conotoxin Vc1.1 inhibits human dorsal root ganglion neuroexcitability and mouse colonic nociception via GABAB receptors.* Gut, 2016.

106. Livett, B.G., et al., *Therapeutic applications of conotoxins that target the neuronal nicotinic acetylcholine receptor.* Toxicon, 2006. **48**(7): p. 810-29.

107. Mejia, M., et al., *New tools for targeted disruption of cholinergic synaptic transmission in Drosophila melanogaster.* PLoS One, 2013. **8**(5): p. e64685.

108. Fayyazuddin, A., et al., *The nicotinic acetylcholine receptor Dalpha7 is required for an escape behavior in Drosophila.* PLoS Biol, 2006. **4**(3): p. e63.

109. Hopkins, C., et al., *A New Family of Conus Peptides Targeted to the Nicotinic Acetylcholine Receptor*. Journal of Biological Chemistry, 1995. **270**(38): p. 22361-22367.

110. Cano, H., *Isolation and characterization of neuroactive peptides from the venom of cone snail species*, in *Chemistry and Biochemistry*. 2005, Florida Atlantic University

111. Dowell, C., et al., *Alpha-conotoxin PIA is selective for alpha6 subunit-containing nicotinic acetylcholine receptors.* J Neurosci, 2003. **23**(24): p. 8445-52.

112. Chi, S.-W., et al., *Solution structure of α-conotoxin PIA, a novel antagonist of α6 subunit containing nicotinic acetylcholine receptors.* Biochem. Biophys. Res. Commun., 2005. **338**(4): p. 1990-1997.

113. Lopez-Vera, E., et al., *A novel alpha conotoxin (alpha-PIB) isolated from C. purpurascens is selective for skeletal muscle nicotinic acetylcholine receptors.* Toxicon, 2007. **49**(8): p. 1193-9.

114. Hoggard, M.F., et al., *In vivo and in vitro testing of native alpha-conotoxins from the injected venom of Conus purpurascens.* Neuropharmacology, 2017.

115. Webb, B. and A. Sali, *Protein structure modeling with MODELLER.* Methods Mol Biol, 2014. **1137**: p. 1-15.

116. Ulens, C., et al., *Structural determinants of selective alpha-conotoxin binding to a nicotinic acetylcholine receptor homolog AChBP.* Proc Natl Acad Sci U S A, 2006. **103**(10): p. 3615-20.

117. Yang, Z., et al., *UCSF Chimera, MODELLER, and IMP: an integrated modeling system.* J Struct Biol, 2012. **179**(3): p. 269-78.

118. Grabherr, M.G., et al., *Full-length transcriptome assembly from RNA-Seq data without a reference genome.* Nat Biotech, 2011. **29**(7): p. 644-652.

119. Brejc, K., et al., *Crystal structure of an ACh-binding protein reveals the ligand-binding domain of nicotinic receptors.* Nature, 2001. **411**(6835): p. 269-76.

120. Cuny, H., et al., *Key Structural Determinants in the Agonist Binding Loops of Human beta2 and beta4 Nicotinic Acetylcholine Receptor Subunits Contribute to alpha3beta4 Subtype Selectivity of alpha-Conotoxins.* J Biol Chem, 2016. **291**(45): p. 23779-23792.

121. Kang, T.S., et al., *Protein folding determinants: structural features determining alternative disulfide pairing in alpha- and chi/lambda-conotoxins.* Biochemistry, 2007. **46**(11): p. 3338-55.

122. Khoo, K.K., et al., *Distinct disulfide isomers of mu-conotoxins KIIIA and KIIIB block voltage-gated sodium channels.* Biochemistry, 2012. **51**(49): p. 9826-35.

123. Celie, P.H., et al., *Crystal structure of nicotinic acetylcholine receptor homolog AChBP in complex with an alpha-conotoxin PnIA variant.* Nat Struct Mol Biol, 2005. **12**(7): p. 582-8.

124. Franco, A., et al., *Hyperhydroxylation: a new strategy for neuronal targeting by venomous marine molluscs.* Prog Mol Subcell Biol, 2006. **43**: p. 83-103.

125. Olivera, B.M., *E.E. Just Lecture, 1996. Conus venom peptides, receptor and ion channel targets, and drug design: 50 million years of neuropharmacology.* Mol Biol Cell, 1997. **8**(11): p. 2101-9.

126. Hu, H., et al., *Characterization of the Conus bullatus genome and its venom-duct transcriptome.* BMC Genomics, 2011. **12**: p. 60.

127. Terrat, Y., et al., *High-resolution picture of a venom gland transcriptome: case study with the marine snail Conus consors.* Toxicon, 2012. **59**(1): p. 34-46.

128. Veiseh, M., et al., *Tumor paint: a chlorotoxin:Cy5.5 bioconjugate for intraoperative visualization of cancer foci.* Cancer Res, 2007. **67**(14): p. 6882-8.

129. D'Antonio, M., et al., *RAP: RNA-Seq Analysis Pipeline, a new cloud-based NGS web application.* BMC Genomics, 2015. **16**: p. S3.

130. Haas, B.J., et al., *De novo transcript sequence reconstruction from RNA-seq using the Trinity platform for reference generation and analysis.* Nat Protoc, 2013. **8**(8): p. 1494-512.

131. Blankenberg, D., et al., *A framework for collaborative analysis of ENCODE data: making large-scale analyses biologist-friendly.* Genome Res, 2007. **17**(6): p. 960-4.

132. Rice, P., I. Longden, and A. Bleasby, *EMBOSS: the European Molecular Biology Open Software Suite.* Trends Genet, 2000. **16**(6): p. 276-7.

133. Kaas, Q., et al., *ConoServer: updated content, knowledge, and discovery tools in the conopeptide database.* Nucleic Acids Res, 2012. **40**(Database issue): p. D325-30.

134. Liu, Z., et al., *Diversity and evolution of conotoxins in Conus virgo, Conus eburneus, Conus imperialis and Conus marmoreus from the South China Sea.* Toxicon, 2012. **60**(6): p. 982-9.

135. Pi, C., et al., *Diversity and evolution of conotoxins based on gene expression profiling of Conus litteratus.* Genomics, 2006. **88**(6): p. 809-819.

136. Lluisma, A.O., et al., *Novel venom peptides from the cone snail Conus pulicarius discovered through next-generation sequencing of its venom duct transcriptome.* Mar Genomics, 2012. **5**: p. 43-51.

137. Baskakov, I.V. and D.W. Bolen, *The paradox between m values and deltaCp's for denaturation of ribonuclease T1 with disulfide bonds intact and broken.* Protein Sci, 1999. **8**(6): p. 1314-9.

138. Glasgow, B.J., et al., *A conserved disulfide motif in human tear lipocalins influences ligand binding.* Biochemistry, 1998. **37**(8): p. 2215-25.

139. Barba, M., et al., *Cupricyclins, novel redox-active metallopeptides based on conotoxins scaffold.* PLoS One, 2012. **7**(2): p. e30739.

140. Davis, J., A. Jones, and R.J. Lewis, *Remarkable inter- and intra-species complexity of conotoxins revealed by LC/MS.* Peptides, 2009. **30**(7): p. 1222-7.

141. Jones, C.K., N. Byun, and M. Bubser, *Muscarinic and nicotinic acetylcholine receptor agonists and allosteric modulators for the treatment of schizophrenia.* Neuropsychopharmacology, 2012. **37**(1): p. 16-42.

142. Dupuis, J., et al., *Insights from honeybee (Apis mellifera) and fly (Drosophila melanogaster) nicotinic acetylcholine receptors: from genes to behavioral functions.* Neurosci Biobehav Rev, 2012. **36**(6): p. 1553-64.

143. Sattelle, D.B., et al., *Edit, cut and paste in the nicotinic acetylcholine receptor gene family of Drosophila melanogaster.* Bioessays, 2005. **27**(4): p. 366-76.

144. Cranfield, C.G., et al., *Kalata B1 and Kalata B2 Have a Surfactant-Like Activity in Phosphatidylethanolomine-Containing Lipid Membranes.* Langmuir, 2017. **33**(26): p. 6630-6637.